PART I: EXTRACELLULAR HYDROGEN IONS ACTIVATE TYROSINE HYDROXYLASE IN CATECHOLAMINERGIC CELLS

PART II: IDENTIFICATION OF NOVEL MECHANISM(S) OF PARKINSON'S DISEASE CAUSING 1-METHYL-4-PHENYLPYRIDINIUM NEUROTOXICITY

A Dissertation by

Viet Quang Le

Bachelor of Science, Wichita State University, May 2006

Submitted to the College of Liberal Arts and Sciences
and the faculty of the Graduate School of
Wichita State University
in partial fulfillment of
the requirements for the degree of
Doctor of Philosophy

May 2015

PART I: EXTRACELLULAR HYDROGEN IONS ACTIVATE TYROSINE HYDROXYLASE IN CATECHOLAMINERGIC CELLS

PART II: IDENTIFICATION OF NOVEL MECHANISM(S) OF PARKINSON'S DISEASE CAUSING 1-METHYL-4-PHENYLPYRIDINIUM NEUROTOXICITY

The following faculty members have examined the final copy of this dissertation for form and content, and recommend that it be accepted in partial fulfillment of the requirement for the degree of Doctor of Philosophy with a major in Chemistry.

Kandatege Wimalasena, Committee Chair

We have read this dissertation and recommend its acceptance:

James G. Bann, Committee Member

Paul Rillema, Committee Member

David Eichhorn, Committee Member

David McDonald, Committee Member

Accepted for the College of Liberal Arts and Sciences

Ron Matson, Dean

Accepted for the Graduate School

Abu S.M. Masud, Interim Dean

DEDICATION

To my loving Parents

ACKNOWLEDGEMENTS

I would like to offer my boundless gratitude to my supervisor Prof. K. Wimalasena, for his guidance and wisdom during the course of my research work. He encouraged me to develop my critical thinking and research skills and greatly assisted me with scientific writing. Without his enthusiasm and persistent help this dissertation would not have been possible.

I wish to express my appreciation to the members of dissertation committee, Profs. Jim Bann, David Eichhorn, Paul Rillema, and David McDonald for serving in my committee and for their support and advice. In addition, I would like to thank Profs. Francis D' Souza and Jeffrey May who were in my committee for their guidance throughout my time at Wichita State University.

My sincere thanks go to Dr. Warren Samms, Dr. Inoka Hewawithrana, Dr. Yamuna Kollalpitiya, Chamila Kadigamuwa, and Mapa Sumudu for their help and support in my research works. I would like to thank my family and friends for helping me keep my life in proper balance.

With my hearing loss, I would like to extend my gratitude to Katie Stewart, Debbie McCain, Kimberly Smith, and the disability office for their continuing support throughout my academic years.

Finally I wish to express my gratitude to the faculty and staff of the WSU Chemistry department and friends for assisting me in numerous ways.

ABSTRACT

Tyrosine hydroxylase (TH) is the rate-limiting step of the catecholamine biosynthetic pathway, thus, in theory, modulating the TH activity could be a target for therapeutic purposes. Despite extensive studies, there are significant deficiencies in the current model of *in vivo* TH activation. In the present study, we report the discovery that the $[H^+]_o$ stimulate the TH activity in MN9D and PC12 cells under physiologically attainable concentrations. The $[H^+]_o$-dependent activation of TH requires $[Cl^-]_o$, but not Na^+ or Ca^{2+}. In addition, while the Cl^-/HCO_3^- transporter inhibitor, 4,4'-Diisothiocyano-2,2'-stilbenedisulfonic acid, inhibits TH activation, the Na^+/H^+ exchanger inhibitor, amiloride, potentiates it. $[H^+]_o$ increases the $[H^+]_i$, $[Ca^{2+}]_i$ and phosphorylation of Ser 40, the regulatory domain of TH. Based on these and other findings, we propose that the increase of $[H^+]_o$ and/or intracellular alkalinity during the exocytotic release of acidic content from the synaptic vesicles may signal *in vivo* TH activation.

Part II of my research is focused on Parkinson's disease causing N-methyl-4-phenylpyridinium (MPP^+). Although selective dopaminergic toxicity of MPP^+ is due to the specific uptake through the dopamine transporter (DAT), recent studies show that MPP^+ is taken through multiple pathways in dopaminergic cells and other cells. Here we show that a previously unidentified Na^+/Cl^--independent, Ca^{2+}-sensitive MPP^+ uptake pathway is present specifically in dopaminergic cells but not in other cell types. We further show that the toxicity of MPP^+ may be associated with the unidentified Na^+/Cl^--independent, Ca^{2+}-sensitive MPP^+ uptake pathway. Therefore, we propose that the specific dopaminergic toxicity of MPP^+ could be a consequence of its interference with the physiological function(s) of this transporter and a better understanding of its physiological role may provide clues to the etiology of sporadic PD.

TABLE OF CONTENTS

PART I: EXTRACELLULAR HYDROGEN IONS ACTIVATE TYROSINE HYDROXYLASE IN CATECHOLAMINERGIC CELLS

TABLE OF CONTENTS (continued)

TABLE OF CONTENTS (continued)

PART II: IDENTIFICATION OF NOVEL MECHANISM(S) OF PARKINSON'S DISEASE CAUSING 1-METHYL-4-PHENYLPYRIDINIUM NEUROTOXICITY

TABLE OF CONTENTS (continued)

TABLE OF CONTENTS (continued)

LIST OF TABLES

PART II

LIST OF FIGURES

PART I

PART II

LIST OF FIGURES (continued)

LIST OF FIGURES (continued)

LIST OF SCHEMES

PART I

PART II

LIST OF ABBREVIATIONS

Abbreviation	Systematic Name
2-APB	2-Aminoethoxydiphenylborane
5-HTP	5-Hydroxyl-L-Tytophan
6-OHDA	6-Hydroxydopamine
µL	Microliter
µM	Micromolar
AA	Amino Acid
AAADC	L-Aromatic Amino Acid Decarboxylase
AD	Alzheimer's Disease
AD	Aldehyde Dehydrogenase
ADP	Adenosine Diphosphate
AE	Na+-Independent Cl-/HCO3- Exchanger
AMP	Adenosine Monophosphate
Asc	Ascorbic Acid
ASIC	Acid-Sensing Ion Channel
ATP	Adenosine Triphosphate
BCECF-AM	7'-Bis(Carboxyethyl)-5,6-Carboxyfluorescein Acetoxy-Methyl Ester
BH_4	Tetrahydrobiopterin
Bp	Base Pairs
BSA	Bovine Serum Albumin
CICR	"Ca^{2+}"-Induced Ca^{2+} Release
CNS	Central Nervous System
COMT	Catechol-O-Methyltransferase

LIST OF ABBREVIATIONS (continued)

DβM	Dopamine-β-Monooxygenase
DA	Dopamine
Da	Dalton
DAT	Dopamine Transporter
DIDS	4,4'-Diisothiocyano-2,2'stilbenedisulfonic acid
DMEM	Dulbecco's Modified Eagle's Medium
DMF	N,N-Dimethylformamide
DMSO	Dimethyl Sulfoxide
DNA	Deoxyribonucleic Acid
DOPAC	3,4-dihydroxyphenylacetic acid
DOPAldehyde	Dihydroxyphenylacetaldehyde
E	Epinephrine
EGTA	Ethylene Glycol-bis(beta-aminoethyl ether)-N,N,N',N'-tetracetic Acid
ER	Endoplasmic Reticulum
FBS	Fetal Bovine Serum
h	Hour
H_2O_2	Perioxide
HEPES	2-[4-(2-hydroxyethyl) piperazin-1-yl]ethanesulfonic acid
HPLC	High-Performance Liquid Chromatography
HPLC-EC	HPLC with Electrochemical Detection
HPLC-UV	HPLC with Ultraviolet
HPMP	4-hydroxyl-4-phenyl-N-methylpiperidine
HS	Horse Serum

LIST OF ABBREVIATIONS (continued)

HRP	Horseradish Peroxidase
HVA	Homovanilic
HVA	High Voltage-Active
HVAldehyde	Homovanilic Aldehyde
IC_{50}	Half-Maximal Inhibitory Concentration
IP_3	Inositol 1,4,5-Triphosphate
K_d	Dissociation Constant
K_i	Inhibition Constant
K_m	Michaelis Constant
kDa	Kilodalton
KRB	Krebs-Ringer Buffer
LB	Lewy Bodies
LC_{50}	Half-Maximal Lethal concentration
L-DOPA	3,4-Dihydroxy-L-phenylalanine
LVA	Low Voltage-Active
MAO	Monoamine Oxidase
mDβM	Membrane-bound DβM
MES	2-(N-morpholino)ethanesulfonic acid
mg	Milligram
min	Minutes
mL	Milliliter
mm	Millimeter
mM	Millimolar
MP	1-methyl-4-piperidone

$MPDP^+$	1-methyl-4-phenyl-1, 2-dihydropyridinium
MPP^+	1-methyl-phenylpyridium
MPPP	1-Methyl-4-phenyl-4-propionoxypiperidine
MPTP	1-Methyl-4-phenyl-1,2,3,6-tetrahydropyridine
MTT	3-(4,5-dimethylthiazol-2-yl)-2,5-diphenyltetrazolium bromide)
mV	Millivolt
NBC	Na+/HCO3- Co-Transporter
NCBE	Na+-driven Cl-/HCO3- Exchanger
NAD	Nicotinamide Adenine Dinucleotide (oxidized form)
NADH	Nicotinamide Adenine Dinucleotide (reduced form)
NCX	Na^+/Ca^{2+} Exchanger
NE	Norepinephrine
NET	Norepinephrine transporter
ng	Nanogram
NHE	Na+/H+ Exchanger
nmole	Nanomole
nm	Nanometer
$NO^\bullet$	Nitric Oxide
$^\bullet NO_2$	Nitrogen Dioxide
N_2O_3	Dinitrogen Trioxide
N_2O_4	Dinitrogen tetroxide
L-DOPA	L-dihydroxyphenylalanine
$O_2^{\bullet-}$	Superoxide

LIST OF ABBREVIATIONS (continued)

OCT	Organic Cation Transporter
$OH^{\bullet}$	Hydroxyl radical
$ONOO^{-}$	Peroxinitrite
Pmole	Picomole
PBS	Phosphate Buffered Saline
PD	Parkinson's Disease
PDF	Parkinson's Disease Foundation
PKU	Phenylketonuria
PLP	Pyridoxal Phosphate
PMAT	Plasma Monoamine Transporter
PMCA	Plasma Membrane Ca^{2+} ATPase
PNMT	Phenylethanolamine-N-Methyltransferase
PNS	Peripheral Nervous System
PQ	Paraquat
RMT	Rostral Mesencephalictegmentum
RNS	Reactive Nitrogen Species
ROS	Reactive Oxygen Species
sDβM	Soluble DβM
S.D.	Standard Deviation
SDS	Sodium Dodecyl Sulfate
Ser	Serine
SOCE	Store Operated Ca^{2+} Entry
SOD	Superoxide Dismutase
TBS	Tris-Buffered Saline

TTBS	Mixture of Tris-Buffered Saline and Tween 20%
TH	Tyrosine Hydroxylase
TRP	Transient Receptor Potential
TRPA	Transient Receptor Potential Ankyrin
TRPC	Transient Receptor Potential Canonical
TRPM	Transient Receptor Potential Melastatin
TRPML	Transient Receptor Potential Mucolipin
TRPP	Transient Receptor Potential Polycystin
TRPV	Transient Receptor Potential Vanilloid
Tyr	L-Tyrosine
UV	Ultraviolet
VGCC	Voltage-gated Calcium Channel
Vmax	Maximum Velocity

PART I: EXTRACELLULAR HYDROGEN IONS ACTIVATE TYROSINE HYDROXYLASE IN CATECHOLAMINERGIC CELLS

CHAPTER I

INTRODUCTION

Tyrosine hydroxylase (TH) [EC 1.14.16.2; tyrosine 3-monooxygenase; L-tyrosine, tetrahydropteridine: oxygen oxidoreductase (3-hydroxylating)] catalyzes the conversion of L-tyrosine to DOPA, which is the initial and rate-limiting step in the biosynthesis of catecholamine DA, NE, and E. Alterations in catecholamine metabolism in the central and peripheral nervous system are implicated in numerous clinical disorders including Parkinson's Disease. Thus, studies on the properties of this key enzyme are of importance for understanding the mechanisms by how its activity is regulated.

TH activity is increased by phosphorylation at Ser residues Ser 8, Ser 19, Ser 31, and Ser 40 by a range of protein kinases. When the action potential reaches the nerve terminal, voltage-gated Ca^{2+} channels mediate Ca^{2+} influx in response to membrane depolarization leading to the increase in TH phosphorylation through Ca^{2+}-dependent protein kinases. However, it is not known whether the extracellular Ca^{2+} is involved in TH phosphorylation in this process. There is a non-heme iron atom in the active site of TH. In the presence of molecular oxygen, the ferrous iron (Fe^{2+}) can be oxidized to the ferric form (Fe^{3+}) causing the enzyme TH to be inactive. Conversely, the reductant tetrahydrobiopterin (BH_4) can reduce Fe^{3+} to Fe^{2+} for L-tyrosine to DOPA conversion. The oxidation of the ferrous enzyme to the ferric form results in an enzyme with high affinity for catecholamines. In order for TH to regain its activity, this bound catecholamine must be released. However, the catecholamines are constantly stored and released from cytosolic vesicles into the synaptic cleft. Therefore, the catecholamine levels in the cytosol

must increase with respect to the basal due to the reuptake through plasma membrane transporters. In theory, the increase in the catecholamine levels in the cytosol should compete against BH_4 and inhibit rather than activate TH. There are inconsistencies in the proposals of phosphorylation/catecholamine-dissociation model of TH activation. In the present study, we report the accidental discovery that extracellular H^+ ions ($[H^+]_o$) efficiently stimulate the TH activity in dopaminergic MN9D and adrenergic PC12 cells under physiological conditions.

The specific aims of this research were (I) to evaluate the mechanism of TH activation due to cellular pH in time and H^+ concentration manner, (II) to determine if $[H^+]_o$-mediated activation of TH is Na^+, Cl^-, K^+, or Ca^{2+}-dependent, (III) to determine the intracellular H^+ and Ca^{2+} levels in respect to increasing $[H^+]_o$, and (IV) to determine the role of Ser40 in $[H^+]_o$-mediated activation of TH using catecholaminergic MN9D and PC12 cells.

CHAPTER II

BACKGROUND AND SIGNIFICANCE

2.1 Regulation of Catecholamines

Catecholamines are stored in the synaptic vesicles in catecholaminergic neurons. During nerve firing, catecholamines are released from the synaptic vesicles into the synaptic cleft which may be taken up again through plasma membrane monoamine transporters. While most of these catecholamines are recycled into vesicles for re-release, the remainder is being metabolized. In the course of repeated synaptic release, tyrosine hydroxylase (TH) that catalyzes the rate-limiting step of the catecholamine biosynthesis pathway must be activated in order to restore the synaptic catecholamine levels. However, the exact nature of the physiological stimulus responsible for the activation of TH has not been unequivocally established. The catecholamine biosynthesis pathway as well as catabolism of catecholamines is further discussed below to aid understanding the regulation of catecholamine biosynthesis.

2.1.1 Catecholamine Neurotransmitter Biosynthesis

Monoamines contain one amino group that is connected to an aromatic ring by a two-carbon chain (-CH_2-CH_2-). Catechol has hydroxyl side groups on the $3^{rd}$and 4^{th} positions of the benzene ring. Thus, a monoamine with a catechol and a side-chain amine is called catecholamine (1). Catecholamines are neurotransmitters that are derived from the amino acids tyrosine or phenylalanine. Dopamine (DA), norepinephrine (NE), and epinephrine (E), shown in Scheme 1, are the neurotransmitters in both peripheral (PNS) and central (CNS) nervous systems and they are believed to regulate many physiological processes. These neurotransmitters are also

implicated in the development of a large number of neurological, psychiatric, endocrine, and cardiovascular diseases under certain physiological conditions (2).

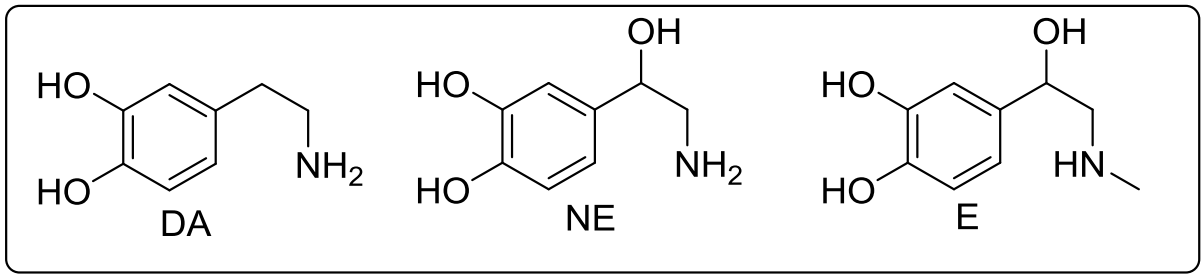

Scheme 1 : Catecholamine Neurotransmitters. Dopamine (DA), Norepinephrine (NE), and Epinephrine (E).

All the catecholamines are biosynthesized from the amino acid L-tyrosine through a number of enzymatic transformations as shown in Scheme 2.

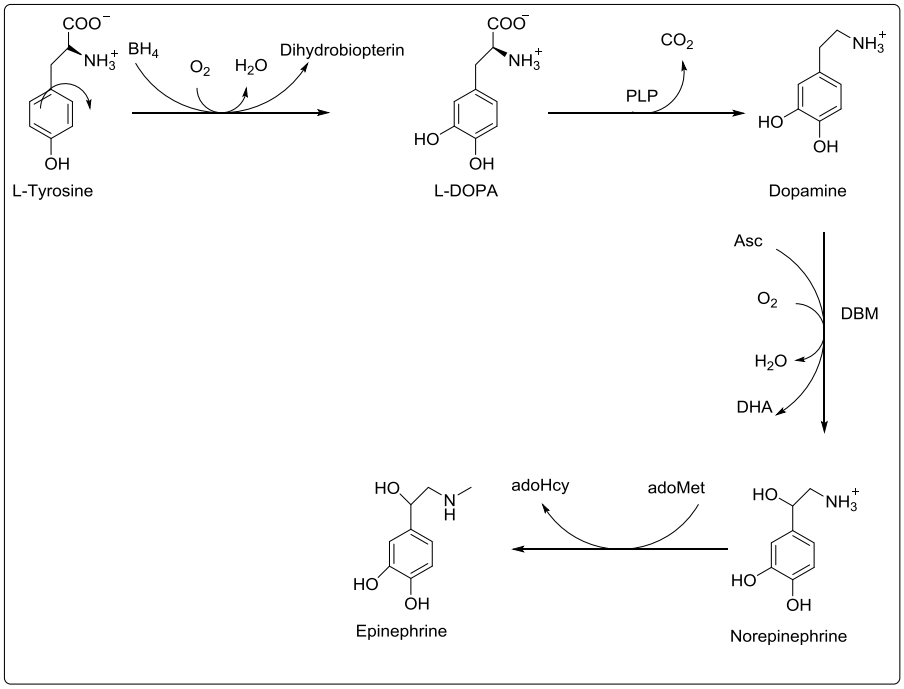

Scheme 2: Catecholamine Biosynthesis Pathway. AAADC- L-aromatic amino acid decarboxylase, adoHcy- S-adenosylhomocysteine, adoMet- S-adenosylmethionine, Asc- ascorbate, BH_4- tetrahydrobiopterin, DβM- dopamine-β-monooxygenase, PLP- pyridoxal phosphate, PNMT- phenylethanolamine-N-methyltransferase.

2.1.2 Tyrosine Hydroxylase (TH)

Tyrosine hydroxylase is an iron containing monooxygenase (TH; tyrosine 3-monooxygenase 1.14.16.2) present in the cytosol of catecholaminergic cells which catalyzes the rate limiting step of the catecholamine biosynthesis pathway. TH catalyzes the meta hydroxylation of the aromatic ring of L-tyrosine (Tyr) to produce 3,4-dihydroxy-L-phenylalanine (L-DOPA) in the presence of the cofactor, tetrahydrobiopterine (BH_4), and molecular oxygen. TH has a high degree of specificity for Tyr with the K_m value in the micromolar range (1) and does not accept analogous aromatic side chains such as the indole group of tryptophan. The active form of TH contains Fe^{2+}, but may becomes inactive when Fe^{2+} is oxidized to Fe^{3+} by molecular oxygen under certain physiological conditions. This inactive form of the enzyme can be reactivated by the reduction of Fe^{3+} to Fe^{2+} by the co-factor BH_4 (3,4). However, catecholamines compete with BH_4 for the Fe^{3+} enzyme to produce a tightly catechol-bound dead-end complex [K_d ~1 nM (5,6)]. TH can also be inhibited by the substrate L-tyrosine and BH_4 at higher concentrations (7,8). α-methyl-ρ-tyrosine, analog of Tyr, is a commonly used competitive inhibitor of TH (1).

TH is a homotetramer with four identical subunits, and each monomer contains a catalytic domain near the C-terminus and a regulatory domain near the N-terminus (9,10). The catalytic domain contains residues that are necessary for catalysis and substrate specificity and the regulatory domain is thought to regulate the catalytic activity of the enzyme (9,11,12). The molecular structure of the catalytic domain of TH has been reported (13), but the structure of the regulatory domain has not been determined. In humans, there are four isoforms of TH due to four different types of the regulatory domain and these isoforms are derived from a single gene by alternate-splicing (14-16), although their crystal structures have not yet been determined. TH

activity is mediated by medium- to long-term by gene expression and by short-term mechanisms which is a combination of protein phosphorylation, feedback inhibition by catecholamines, and allosteric regulation by substrates and products (14). The regulatory domain of TH contains Ser 8, 19, 31, and 40 which can be phosphorylated by protein kinases and then it modulates the TH activity (9,17).

2.1.3 Aromatic L-Amino Acid Decarboxylase (AADC)/ Dopa Decarboxylase

Aromatic L-amino acid decarboxylase (AADC; E.C.4.1.1.28) is a homodimeric enzyme in complex with the cofactor pyridoxal-5'-phosphate, the active form of vitamin B6, that catalyzes the conversion of L-dihydroxyphenylalanine (L-DOPA) to DA. This enzyme is also commonly known as DOPA decarboxylase. AADC also catalyzes the conversion of 5-hydroxy-L-trytophan (5-HTP) to 5-hydroxytryptamine (serotonine)(18). It has a low K_m and high V_{max} for L-DOPA and thus, endogenous L-DOPA is rapidly converted to DA in comparison to 5-HTP. Carbidopa and methyldopa are commonly used competitive inhibitors for AADC (1).

2.1.4 Dopamine- β- Monooxygenase (DβM)

Dopamine-β-monooxygenase (DβM; E.C. 1.14.17.1) is a copper-containing monooxygenase which catalyzes the conversion of DA to NE in catecholamine-containing cells. It is localized in the synaptic vesicles of noradrenergic and adrenergic cells and is known to exist in soluble (sDβM) and membrane bound (mDβM) forms in approximately equal amounts. These two forms are similar in their immunoreactivities, carbohydrate content, and binding affinities of various substrates (19). It has been reported that mDβM has two subunits of 70 kDa and 75 kDa whereas sDβM has four identical subunits (72 kDa) (20). However, SDS- polyacrylamide gel electrophoresis demonstrated that the subunits of sDβM are non-identical; 75 kDa, 72 kDa, and

69 kDa (21,22). The molecular difference of these subunits is not clearly understood at present. DβM can be inhibited by the competitive inhibitors nepicastat (23)and disulfiram (24).

2.1.5 Phenylethanolamine-N-Methyltransferase (PNMT)

Phenylethanolamine-N-methyltransferase (PNMT; E.C 2.1.1.280) catalyzes the conversion of NE to E as the last step of the catecholamine biosynthesis. This enzyme transfers a methyl group from the cofactor S-adenosyl-L-methionine to the amine functional group of NE to produce E in the cytosol. PNMT is found in cells in the brainstream and chromaffin cells of the adrenal medulla that synthesize and secret E as the neurotransmitter. PNMT activity is regulated by corticosteroids such as cortisol which is produced in the adrenal cortex (25). The commonly used PNMT inhibitors are LY 78335 and LY 134046 (26).

2.2 Catabolism of Catecholamines

Catecholamines or neurotransmitters are released from synaptic vesicles through exocytosis and diffuse across the synaptic cleft to bind to a post-synaptic receptor to stimulate the post-synaptic neurons. At the end of the signaling process, the signal is no longer needed to be deactivated in order to regulate the stimulation. Several mechanisms contribute to the deactivation of the neurotransmitters, including diffusion away from the synapse, reuptake followed by metabolic degradation of the neurotransmitter by specific enzymes, and reuptake followed by storage in presynaptic vesicles. When catecholamines are not properly stored in synaptic vesicles and remain in the cytosolic catecholamine pool, they are subject to metabolic degradation by monoamine oxidase (MAO) and catechol-O-methyltransferase (COMT) (Scheme 3). DA can be degraded by either MAO followed by COMT, or *vice versa* (1). These catcholamines are initially converted to the unstable catabolic intermediates 3,4-

dihydroxyphenylacetaldehyde (DOPAldehyde), 3-O-methyldopamine, and homovanillicaldehyde and then to more stable metabolites 3,4-dihydroxyphenylacetic acid (DOPAC) and/or homovanilic acid (HVA) by aldehyde dehydrogenase (27) as shown in Scheme 3.

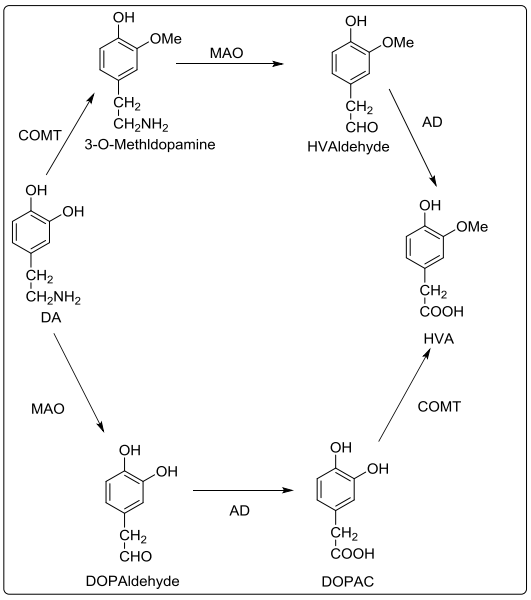

Scheme 3: Oxidation Degradation Pathways of DA. AD- aldehyde dehydrogenase, COMT- catechol-O-methyltransferase, DOPAC- 3,4-diihydroxy-L-phenylalanine, DOPAldehyde- 3,4-dihydroxyphenylacetaldehyde, HVAldehyde- homovanilic aldehyde, HVA- homovanilic acid, MAO- monoamine oxidase.

2.2.1 Monoamine Oxidase (MAO)

Monoamine Oxidase (MAO; E.C. 1.4.3.4.) is a flavin-containing enzyme located in the outer membrane of the mitochondria and catalyzes oxidative deamination of monoamines into their corresponding aldehydes in the presence of molecular oxygen (Scheme 3). There are two isoforms of MAO with distinct substrate specificities: MAO-A and MAO-B. Both isoforms share about 70% amino acid sequence identity (28). In the human brain, MAO-A is primarily expressed in catecholaminergic neurons and preferentially deaminates NE whereas MAO-B is

primarily expressed in actrocytes and deaminates serotonin (1,29). However, both isoforms can deaminate DA. Clorgyline and parglyline are selective inhibitors for brain MAO-A and MAO-B, respectively.

2.2.2. Catechol-O-Methyltransferase (COMT)

Catechol-O-Methyltransferase (COMT, E.C 2.1.1.6) is present in all cells and catalyzes the conversion of DOPAC to HVA by transferring a methyl group from S-adenosylmethionine to the 3-OH group of the catechol moiety. Talcopone is a known inhibitor of COMT.

2.3 Roles of cellular Ca^{2+} and pH

Calcium has a very large concentration gradient across the plasma membrane of all cells and plays a major role in neurons such as triggering the release of neurotransmitters from the synaptic vesicles. In addition, many other aspects of neuronal function are regulated by changes in intracellular free Ca^{2+} concentration. On the other hand, intracellular pH also plays a critical role in the function of all cells (30). The extracellular pH under normal conditions is approximately 7.4, whereas the intracellular pH is maintained close to pH 7 to keep the biomolecules in their optimal ionic state for their functions (31). In addition, cellular pH has been shown to modulate the cytosolic calcium level causing the release or storage of calcium through the intracellular organelles or the efflux or influx of calcium through a transporter/channel. Several channels, transporters, and exchangers that are responsible for the regulation of pH will be discussed.

2.3.1 Na^+/H^+ Exchanger (NHE)

Na^+/H^+ exchanger (NHE) is an integral membrane protein that transports one extracellular Na^+ ion across the membrane in exchange for one intracellular proton H^+ (32). NHE is critical for the regulation of intracellular pH and cell volume to promote the physiological change of cells (33). To date, nine isoforms (NHE-1 to NHE-9) have been identified (34,35) and they share approximately 25-75% sequence homology with the calculated molecular weights in the range of 74 kDa to 93 kDa (34,36). These isoforms are predicted to consist of 12 transmembrane segments with N- and C- termini on the cytoplasmic face. The NHE-1 isoform is the most characterized of the NHE family and it is highly expressed in the plasma membrane of nearly all tissues (34). The NHE-2 and NHE-3 isoforms are mainly expressed in the kidney and intestine (37,38). NHE-4 is widely present in the stomach, but also expressed in the intestine, kidney, brain, uterus, and skeletal muscle (37). NHE-5 is predominately expressed in the brain, but is also present in other non-epithelial cells at low levels (39,40). NHE-6 is expressed in the heart, brain, and skeletal muscle in high levels (35,41). NHE-7 and NHE-8 isoforms are mainly localized on the trans-Golgi network (35,42) and NHE-9 is in late recycyling endosomes (35). Amiloride and its analogs are the most commonly used inhibitors for NHE (43).

2.3.2 Na^+/HCO_3^- Co-Transporter (NBC)

Na^+/HCO_3^- co-transporter (NBC) mediates both the influx of one Na^+ ion and two HCO_3^- ions and the efflux of one Na^+ ion and three HCO_3^- ions. NBCs are found in many mammalian tissues including the kidney, pancreas, and brain (44). Three NBC isoforms have been identified based on their N- and C-terminal sequences (2 N-terminus and one C-terminus isoforms). Despite the difference in sequence, those isoforms share identical physiological function. These

isoforms consist of 12 transmembranes with N- and C- termini facing on the cytoplasmic side. The bicarbonate ion that was transported into the cell interacts with secreted H^+ ions (mostly from NHE) to form CO_2 and H_2O. NBC can be effectively inhibited by 4,4'-diisothiocyano-2,2'stilbenedisulfonic acid (DIDS).

2.3.3 Na^+-Driven Cl^-/HCO_3^- Exchanger (NCBE)

Na^+-driven Cl^-/HCO_3^- exchanger (NCBE) is an intracellular pH regulator that mediates the influx of one Na^+ ion and two HCO_3^- ions in exchange for one Cl^- ion (45,46). NCBE was first discovered in invertebrate neurons (47) and was found later in vertebrate neurons and non-neuronal cells (45). NCBE is predicted to consist of 10 transmembrane domains with N- and C-termini facing on the cytoplasmic side (48). NCBE can also be inhibited by 4,4'-diisothiocyano-2,2'stilbenedisulfonic acid (DIDS).

2.3.4 Na^+-Independent Cl^-/HCO_3^- (AE)

Na^+-independent Cl^-/HCO_3^-exchanger (AE) is an intracellular pH regulator like NCBE, but mediates the influx of one Cl^- ion in exchange for one HCO_3^- ion (49). To date, three isoforms of AE have been identified; AE-1, AE-2, and AE-3 and they are widely expressed in numerous cell types (49,50). Each isoform contains a N-terminal cytoplasmic domain, a C-terminal membrane-spanning domain of 500 amino acids comprising 14 helices, and an acidic, short C-terminal domain in the cytoplasm. However, they differ in the N- and C- terminal sequence, but share a similar function of anion translocation through the plasma membrane (50,51).

2.3.5 Acid-Sensing Ion Channel (ASIC)

The acid-sensing ion channel (ASIC) is a voltage-independent proton channel that is activated by the extracellular proton (52). ASIC channels are also permeable to Na^+ ions, and are expressed in both the peripheral and central nervous system (53,54). So far six isoforms of ASIC have been identified; ASIC-1a, 1b, 2a, 2b, 3, and 4. ASIC-1a, 1b, and 2a, 2b are splice variants (55). These isoforms are trimeric that consist of two transmembranes with N- and C-termini on the cytoplasmic side (56). In addition, Yermolaieva *et al.* (57) proposed that the activation of ASIC-1a by extracellular acidosis can lead to an increase of cytosolic Ca^{2+}in neurons. ASIC can be inhibited by Amiloride and its analogs (58).

2.4 Mechanisms of Tyrosine Hydroxylase Activation

Several mechanisms for the activation of TH have been proposed, but the exact nature of the physiological stimulus responsible for the activation of TH has not been clearly established. As mentioned above, modulation of TH activity *in vivo* occurs through the phosphorylation of the regulatory domains, Ser 19, 31, and 40. However, mutant TH lacking the regulatory domain is fully active (59), suggesting that the phosphorylation alone does not directly activate TH. These inconsistencies suggest that the phosphorylation/catecholamine-dissociation model of TH activation needs further clarification. Furthermore, the initial extracellular or intracellular signal(s) for TH activation has not been unequivocally identified.

In response to physiological stimuli, synaptic vesicles release highly buffered acidic content into the synaptic cleft *in vivo*. For example, bovine adrenal chromaffin vesicles (a well characterized catecholaminergic model) releases up to ~500 mM protonated catecholamine, ~125 mM ATP, large amounts of acidic chromagranins and other proteins and [H^+] equivalent to a pH

5.4 acidic environment (60). Although the extracellular and intracellular [H^+] of neuronal and other cells are tightly regulated under normal physiological conditions, high frequency synaptic release could exceed the buffering capacity and the rate of diffusion of H^+, leading to a transient synaptic cleft acidification in catecholaminergic and other neurons. Therefore, we proposed that the acidification of the synaptic cleft area during repeated synaptic acidic release could be the initial signal for in vivo TH activation in catecholaminergic neurons.

2.5 MN9D and PC12 Cells as Catecholamine Models

MN9D cells are a fused cell line derived from the mouse embryonic ventral mesencephalic cells (rostral mesencephalictegmentum –RMT) and neuroblastoma cells (N18TG2) (61). This cell line is extensively used as a dopaminergic cell model because it synthesizes, stores, and releases catecholamines. MN9D cells contain high amounts of DOPA and dopamine with a low NE level (61). Nonetheless, undifferentiated MN9D cells appear not to fully exhibit some of the characteristic electrophysiological properties (62). On the other hand, differentiation of MN9D cells with the treatment of butyric acid closely resembles that of dissociated matured CNS DA neurons (63).

PC12 cells, established by Greene and Tischler in 1976, are derived from pheochromocytoma cells of the rat adrenal medulla (64). Because of their ability to respond to nerve growth factor and show gene expression profiles similar to that of adrenergic neurons (65), they became one of the most widely studied and useful neuronal cell models. These cells, when treated with nerve growth factor, undergo partial growth arrest and differentiate to a phenotype with characteristics of sympathetic neurons. PC12 cells synthesize and store catecholamine

neurotransmitters, DA and NE but do not synthesize E due to the inability to express the enzyme PNMT (64). PC12 cells also synthesize, store and release acetylcholine (66).

CHAPTER III

EXPERIMENTAL METHODS

3.1 Materials

Standard chemicals and reagents were purchased from Sigma-Aldrich (St. Louis, MO, USA) or Fisher Scientific (Pittsburgh, PA, USA), unless otherwise noted. All cell culture media and reagents were purchased from Sigma-Aldrich. Fetal bovine serum (FBS) was from Valley biomedical (Winchester, VA, USA). F-12K medium and horse serum (HS) were from American Type Culture Collection, ATCC (Manassas, VA, USA). Protein assay reagents, bovine serum albumin (BSA) standards, and HRP color developing kits were obtained from Bio-Rad (Hercules, CA, USA). Rabbit polyclonal anti-TH (Millipore Corporation, Temecula, CA, USA), rabbit polyclonal anti-P-TH-Ser 40 (Millipore Corporation, Temecula, CA, USA), and HRP-conjugated secondary antibodies (Bio-Rad, Hercules, CA, USA) were purchased and aliquots were stored at appropriate temperatures. 35 mm glass bottom dishes for fluorescent measurement were purchased from MatTek Coporation. All buffers and cell culture media were prepared in Milli Q-deionized water (Millipore, Billerica, MA, USA). When DMSO was used as co-solvent, final DMSO concentration was kept to a minimum usually <0.5% volume. KRB-HEPES contained 125 mM NaCl, 4.8 mM KCl, 1.2 mM $MgSO_4$, 1.2 mM $CaCl_2$, 25 mM HEPES and 5.6 mM glucose, pH 7.4. Dulbecco's Modified Eagles Medium (DMEM/HCO_3^-) contained 109.5 mM NaCl, 5.34 mM KCl, 0.81 mM $MgSO_4$, 1.8 mM $CaCl_2$, 0.77 mM NaH_2PO_4, 44 mM $NaHCO_3$ and 5.55 mM glucose. In experiments where Cl^- free incubations were necessary, NaCl, KCl, and $CaCl_2$ in the incubation media were replaced with equimolar concentrations of the corresponding Na^+, K^+, and Ca^{2+} gluconates, respectively.

3.2 Instrumentation

Catecholamines levels were analyzed by reversed-phrase HPLC with electrochemical detection (HPLC-EC) on a C_{18} reversed-phase column and catecholamines were quantified using a coulochem-II electrochemical detector with ESA 501 chromatographic software (Chelmsford, MA, USA). Intracellular pH and Ca^{2+} levels are measured using a Nikon ECLIPS-Ti microscope equipped with a Nikon S FLURO 40X lens.

3.3 Methods

3.3.1 Cell Culture of MN9D and PC12 cells

The mouse hybridoma cell line MN9D was graciously provided by Dr. Alfred Heller, University of Chicago. MN9D cells were cultured in 100 mm^2 Falcon tissue culture plates and grown to near confluence in DMEM with high glucose (4500 mg/L) supplemented with 10% FBS, 50 μg/ml streptomycin and 50 IU/ml penicillin at 37 ^oC and 5 % CO_2.

The rat adrenal medulla cell line PC12, obtained from ATCC, were cultured in 100 mm^2 Biocoat tissue culture plates coated with rat tail collagen type-I and grown to near confluence in F-12K medium supplemented with 2.5% FBS and 15% horse serum at 37 ^oC and 5% CO_2. Cells were fed every two days.

3.3.2 Differentiation of MN9D Cells

Differentiation of MN9D cells were carried out using *n*-butyrate according to the published procedure of Choi *et al* .(67). Briefly, MN9D cells were seeded at a density of 1.0 x 10^5 cells/well in 6-well culture plates and were treated with 1 mM *n*-butyrate for 3 days in DMEM media, at which time the media was replaced with fresh 1 mM *n*-butyrate containing

media and incubated for an additional 3 days. All differentiated cells were used in appropriate experiments after the 6th day of differentiation. TH activation experiments with differentiated MN9D cells were carried out using the same protocol outlined above for undifferentiated cells.

3.3.3 Protein Determination

Protein contents of various cell preparations were determined by the method of Bradford (68) using BSA as the standard. Samples of cell suspensions (50 µL) in KRB-HEPES were incubated with 950 µL of Bradford protein reagents for 10 min and absorbance at 595 nm was measured.

3.3.4 Intracellular Catecholamine Analysis

Cells grown to 70%-80% confluence in 12 well-plates and were washed several times with warm KRB-HEPES. The washed cells were incubated with various agents at various pH values (pH 5.5, 6.0, 6.5, 7.0, 7.5, 8.0, and 8.5) which was adjusted with 1 M HCl or 1 M NaOH in KRB-HEPES for 1 h, or for a desired period of time. After the incubation, cells were rinsed two times with cold KRB-HEPES and suspended in 1 mL of the same buffer and 50 µL was withdrawn for protein analysis. The cell suspensions were centrifuged at 6,000 rpm for 3 min and the cell pellet was treated with 75 µL of 0.1 M $HClO_4$ to extract catecholamines. The cell extract were then centrifuged at 12.5 x G for 8 min. A 20 µL sample of cell extract was analyzed by HPLC-EC as previously described (69,70). All the catecholamines from cell extracts were separated on a C_{18} reversed phase column (ESA, HR-80) using a mobile phase composed of 90 mM NaH_2PO_4, 50 mM citric acid, 0.05 mM Na_2EDTA, 1.7 mM 1-octanesulfonic acid sodium salt, pH 3.0, with 10% CH_3CN at a flow rate of 1.0 mL/minutes and 300 mV. However, only the DOPA and/or DA levels are reported depending on the nature of the experiment. All the

catecholamine levels were normalized for the protein content of each sample and expressed as nmoles/mg of protein based on calibration curves constructed using commercial standards. The individual experiments were carried out in triplicates. The error bars indicate the standard deviations of the experimental data.

3.3.5 Effect of Extracellular Hydrogen Concentration ($[H^+]_o$) on Intracellular pH ($[H^+]_i$)and Ca^{2+} ($[Ca^{2+}]_i$)

The pH sensitive membrane permeable pH probe 7'-bis(carboxyethyl)-5,6-carboxyfluorescein acetoxy-methyl ester (BCECF-AM) was used to determined the effect of $[H^+]_o$ on the $[H^+]_i$ of MN9D cells (71-74). Cells were grown in 35 mm glass bottomed culture plates to about 70-80% confluence, washed two times with KRB-HEPES, and were loaded with 5 μM FURA-2AM for 20 min at 37 °C in the same buffer, in the dark. Cells were washed with KRB-HEPES, pH 7.4 three times and incubated in the same buffer for an additional 20 min at room temperature in the dark to facilitate the complete hydrolysis of the acetoxy-methyl ester. Dye-loaded cells were placed on the stage of a Nikon ECLIPS-Ti microscope equipped with a Nikon S FLURO 40X lens. The regions of interests (ROI) were selected (20-30 regions) based on the uniformity of fluorescence emission at 520 nm for 440 nm and 495 nm excitation wavelengths. The baseline 520 nm emission intensity ratio at 440 nm and 495 nm excitations (I_{495}/I_{440}) were simultaneously recorded for 3 min. Then, the pH of the media was quickly changed from 7.8 to 6.02 (pre-determined) by the addition of five volumes of MES-KRB (125 mM NaCl, 2 mM KCl, 1.4 mM $MgSO_4$, 1.2 mM $CaCl_2$, 1.2 mM KH_2PO_4, 25 mM MES and 5 mM glucose, pH 5.8) and was continually measured the I_{495}/I_{440} ratio. Raw intensity data at each excitation wavelength were corrected for background and the background-corrected I_{495}/I_{440} ratios were used to estimate the change in $[H^+]_I$.

The effect of $[H^+]_o$ on the intracellular Ca^{2+} levels ($[Ca^{2+}]_i$) was determined using the Ca^{2+} sensitive cell permeable fluorescence probe, acetoxy-methyl ester of FURA-2 (Fura-2AM; K_D 0.14 μM) using the same protocol described above for BCECF-AM, except that the fluorescence emission at 540 nm was measured for both 340 nm and 380 nm excitation wavelengths (71-74). Note that the data were not corrected for the change in K_d of FURA-2 for Ca^{2+} due to the change in the $[H^+]_i$ and the absolute changes in the concentrations of intracellular Ca^{2+} were not calculated.

3.3.6 Effect of $[H^+]_o$ on the Serine-40 Phosphorylation of TH in MN9D Cells using Western Blot

The content of the Ser 40 phosphorylated and total TH in MN9D cells were determined by quantitative Western blotting experiments using commercial antibodies specific for TH and Ser 40 phosphorylated TH. Briefly, MN9D cells were grown in multi-well plates to 70-80% confluence under standard growth conditions. Cells were incubated in KRB-HEPES buffer at the desired pH and time and washed with cold phosphate-buffered saline, harvested, and centrifuged at low speed. The pellets were solubilized with 50 mM Tris, 150 mM NaCl, 1% Triton X-100, and 2.5% protein inhibitor cocktail (Sigma), pH 7.5, for 30 min at 4 ^oC. After the incubation, the samples were centrifuged for 10 min at 1200 g and the supernatants were used for the Western blotting experiments.

Samples of solubilized proteins (100 μg) were boiled in Laemmli buffer for 5 min and subjected to 8.5% SDS gel electrophoresis under standard conditions. Protein bands were transferred onto 0.2 μm PVDF membranes (Bio-Rad, Hercules, CA) using standard protocols. After blocking the protein binding sites of PVDF membranes with 5% nonfat dried milk in TBS

(Invitrogen, CA) containing 1% Tween 20, they were incubated with rabbit polyclonal anti-TH (Millipore Corporation, Temecula, CA, USA) or rabbit polyclonal anti-P-TH-Serine-40 (Millipore Corporation, Temecula, CA, USA) in an antibody buffer (TTBS, 0.05% Tween-20, 10% nonfat dried milk). Hybridized membranes were washed with TBS, 0.05% Tween 20 (TTBS, Invitrogen, CA), and incubated with the appropriate HRP-conjugated secondary antibodies (Bio-Rad, Hercules, CA, USA) in a hybridizing buffer (TBS, 1% Tween-20, 1% nonfat dried milk). After washing the membranes, the protein bands were visualized using the HRP color development reagent kit (Bio-Rad, Hercules, CA, USA). The intensities of bands were quantified by using a Gel Logic 100 imaging system. The protein contents of the cell preparations were determined by the method of Bradford using the Bio-Rad protein assay with BSA as the standard.

CHAPTER IV

RESULTS

4.1 Effect of $[H^+]_o$ on Intracellular DOPA Levels in MN9D Cells

MN9D cells were seeded and grown to nearly confluence in 12-well plates containing DMEM media supplemented with 10% FBS, 50 μg/mL streptomycin, and 50 IU/mL penicillin. MN9D cells were initially incubated with regular KRB-HEPES for 1 h in the pH range of 7.5 to 5.5 as described in "Experimental Methods" in order to evaluate the intracellular DOPA levels. Data in Fig. 1 demonstrate that decreases in extracellular pH increases intracellular DOPA levels significantly. At pH 6.0, DOPA increase was approximately 6-7 fold from the basal level and at the pH range of 6.5-7.5, DOPA increases were about 2-3 fold increased in under standard incubation conditions.

4.1.1 Effect of Extracellular Na^+, K^+, Ca^{2+} and Cl^- on Intracellular DOPA Levels in MN9D Cells in a $[H^+]_o$ Dependent Manner

To investigate whether the Na^+ ion has any effect on the intracellular DOPA in a $[H^+]_o$ dependent manner, the Na^+ in the incubation buffer was replaced with an equimolar concentration of choline or Li^+. According to Fig. 1, Na^+ has no significant effect on the DOPA production. Under similar conditions, high concentration of K^+ (i.e. depolarizing conditions) in the incubation buffer did not affect the DOPA production (Fig. 2). However, replacement of Cl^- in the incubation medium with the corresponding Na^+ and K^+ gluconates almost completely halted the increased production of intracellular DOPA in a $[H^+]_o$ dependent manner (Fig. 1). In

addition, extracellular Ca^{2+} did not affect the DOPA production (Fig. 3). These results suggest that not Na^{+}, K^{+}, or Ca^{2+} but Cl^{-} is required for induced-increase of DOPA production.

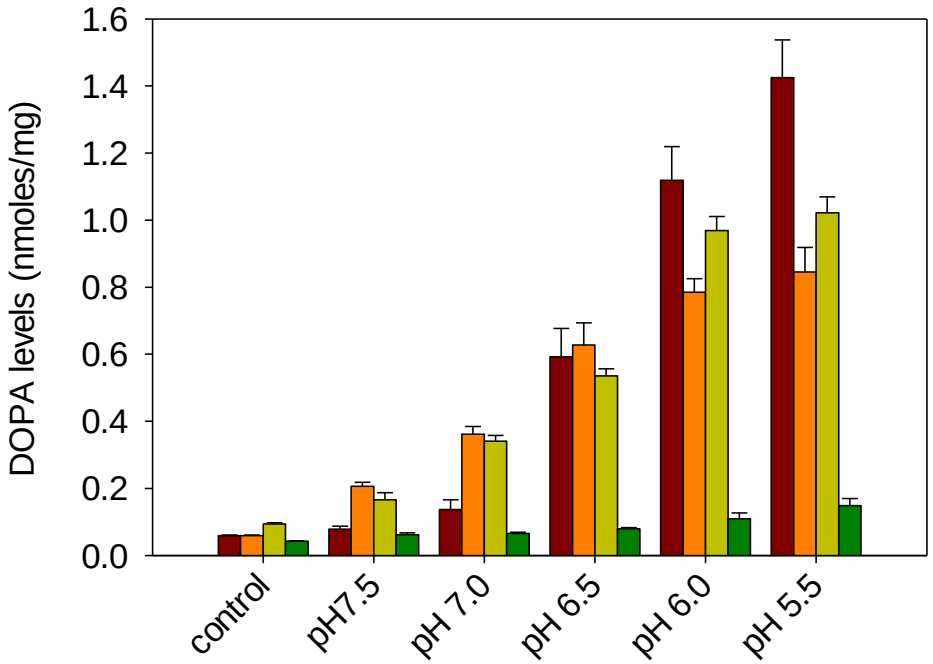

Figure 1- Effect of $[H^{+}]_o$, $[Na^{+}]_o$, and $[Cl^{-}]_o$ on Intracellular DOPA Levels in MN9D Cells. MN9D Cells were grown to near confluence in 12-wells plate and incubated with regular KRB-HEPES for 1 h in the pH range of 7.5 to 5.5. Cells were washed, collected and intracellular DOPA levels were quantified and determined by reversed-phase HPLC-EC and normalized to respective cellular protein concentrations. DOPA levels are expressed as nmoles/mg. Data represent mean ± S.D. of three samples. Brown, Regular KRB-HEPES; Orange, Lithium (Na^{+}-free); Yellow, Choline (Na^{+}-free); Green, Gluconate (Cl^{-}-free).

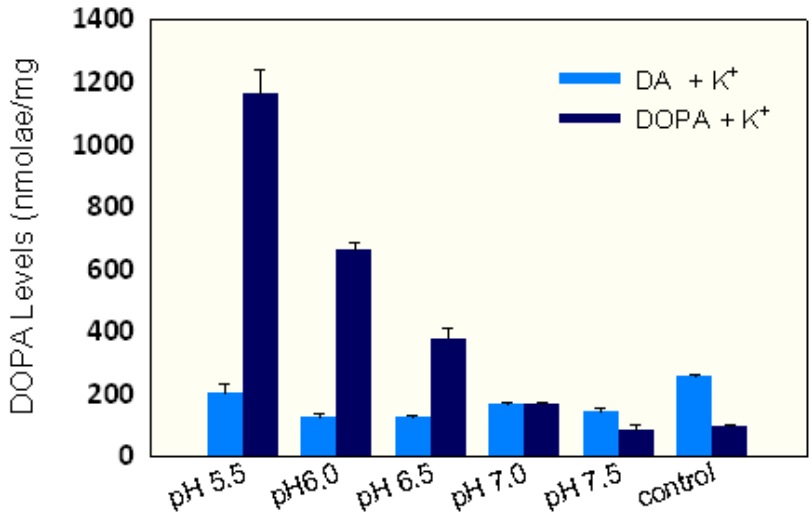

Figure 2- Effect of $[H^+]_o$ and $[K^+]_o$ on Intracellular DOPA and DA Levels in MN9D Cells. MN9D Cells were grown to near confluence in 12-wells plate and incubated with regular KRB-HEPES for 1 h in the pH range of 7.5 to 5.5. Cells were washed, collected and intracellular DOPA levels were quantified and determined by reversed-phase HPLC-EC and normalized to respective cellular protein concentrations. DOPA and DA levels are expressed as nmoles/mg. Data represent mean ± S.D. of three samples. Blue, DA and Purple, DOPA.

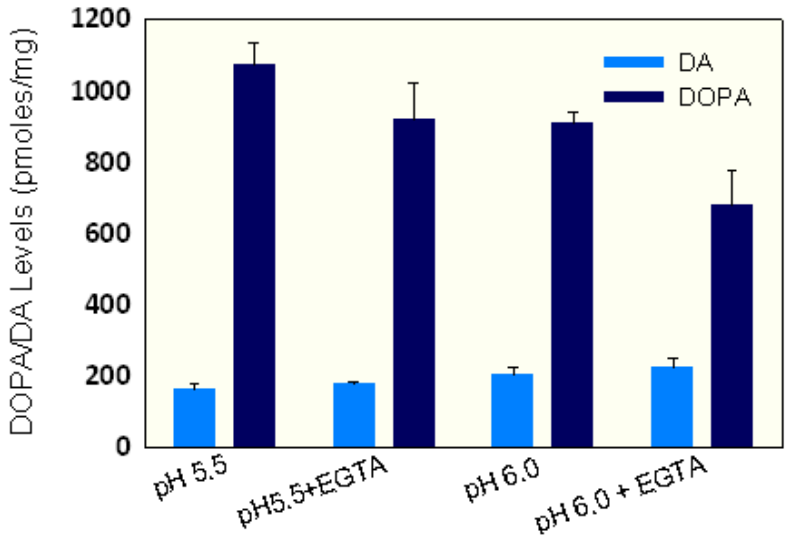

Figure 3- Effect of $[H^+]_o$ and $[Ca^{2+}]_o$ on Intracellular DOPA and DA Levels in MN9D Cells. MN9D Cells were grown to near confluence in 12-wells plate and incubated with regular KRB-HEPES for 1 h in the pH range of 7.5 to 5.5. Cells were washed, collected and intracellular DOPA levels were quantified and determined by reversed-phase HPLC-EC and normalized to respective cellular protein concentrations. DOPA and DA levels are expressed as nmoles/mg. Data represent mean ± S.D. of three samples. Blue, DA and Purple, DOPA.

4.1.2 Effect of TH Inhibitor, α-Methyl Tyrosine, on Intracellular DOPA Levels in MN9D Cells in a $[H^+]_o$ Dependent Manner

MN9D cells were pre-incubated with 1 mM TH inhibitor, α-methyl tyrosine, for 24 h in a normal growth condition, and then washed several times with KRB-HEPES. MN9D cells were incubated with KRB-HEPES at pH 5.5 or 6.0 for 1 h as described in Experimental Methods. Compared to a treated control without the TH inhibitor, α-methyl tyrosine, DOPA levels slightly increase in the cells pre-treated with TH inhibitor (Fig. 4B). These results show that the $[H^+]_o$-dependent increase of intracellular DOPA is due to the increased turnover of intracellular TH in MN9D cells.

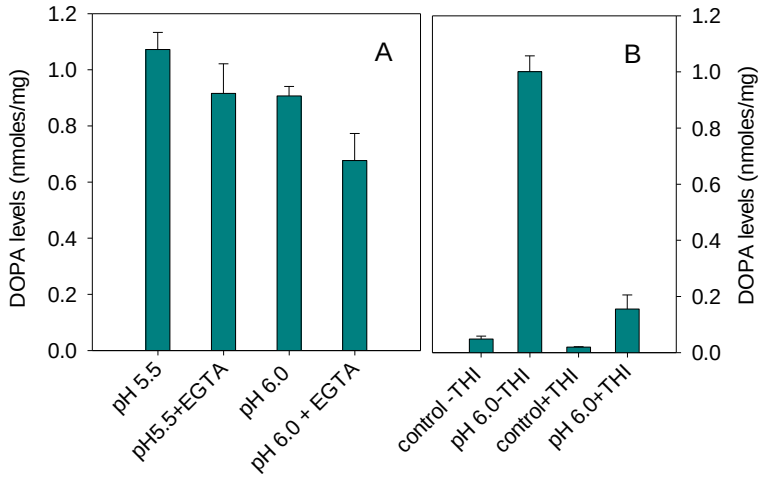

Figure 4- Effect of $[H^+]_o$ on Intracellular DOPA Levels in MN9D Cells. Panel A. MN9D Cells were grown to near confluence in 12-well plates and incubated with regular KRB-HEPES or Ca-free (2 mM EGTA) KRB-HEPES for 1 h in the pH range of 5.5 and 6.0. Cells were washed, collected and intracellular DOPA levels were quantified and determined by reversed-phase HPLC-EC and normalized to respective cellular protein concentrations. DOPA levels are expressed as nmoles/mg. Data represent mean ± S.D. of three samples. Panel B. MN9D Cells were pre-incubated without (control) or with 1 mM TH inhibitor, α-methyl-tyrosine, for 24 h in DMEM media supplemented with 10% FBS 50 µg/mL streptomycin and 50 IU/mL penicillin and grown to near confluence in 12-wells plate. Cells were washed several times in KRB-

HEPES and incubate with KRB-HEPES at pH 6.0 for 1 h. Cells were washed, collected and intracellular DOPA levels were quantified and determined by reversed-phase HPLC-EC and normalized to respective cellular protein concentrations. DOPA levels are expressed as nmoles/mg. Data represent mean ± S.D. of three samples.

4.1.3 Time Course Study on DOPA Production in MN9D Cells

The time dependence of DOPA production in response to $[H^+]_o$ was examined at pH 6.0 in KRB-HEPES. During the first 20 min of incubation, the intracellular DOPA levels have increased moderately (Fig. 5). Then after 20 min of incubation, the increase was significant and reached a plateau at about 60 min. The average rate of DOPA was estimated to increase approximately 5 pmoles/mg/min during the first 20 min and it rapidly rose to ~20-40 pmoles/mg/min between 20-50 min. These kinetic data appear to suggest that the activation of TH by $[H^+]_o$ is not a direct or single step kinetic process, but involves at least two or more kinetically distinct steps.

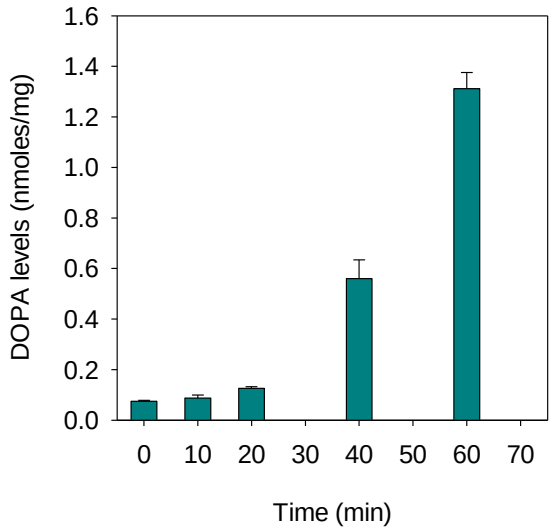

Figure 5- Time Dependence of the DOPA Production in Response to $[H^+]_o$. MN9D Cells were grown to near confluence in 12-well plates and incubated with regular KRB-HEPES for 0, 10, 20, 40, and 60 min at pH 6.0. Cells were washed, collected and intracellular DOPA levels were

quantified and determined by reversed-phase HPLC-EC and normalized to respective cellular protein concentrations. DOPA levels are expressed as nmoles/mg. Data represent mean ± S.D. of three samples.

4.1.4 Effect of DIDS and Amiloride on Intracellular DOPA Levels in MN9D Cells at pH 6.5

The non-specific Cl^-/HCO_3^- transporter inhibitor, DIDS , inhibits the $[H^+]_o$-mediated increase of DOPA levels in MN9D cells with an apparent IC_{50} in the range of 100-250 μM at pH 6.0 (Fig. 6A). On the other hand, the Na^+/H^+ exchanger and the acid-sensing ion channel (ASIC) inhibitor, amiloride, increases the intracellular DOPA levels at pH 6.5 in the concentration range of 10-100 μM (Fig. 6B).These results indicate that Cl^-/HCO_3^-, H^+/Na^+ and/or ASIC may play a role in $[H^+]_o$-mediated activation of TH in MN9D cells.

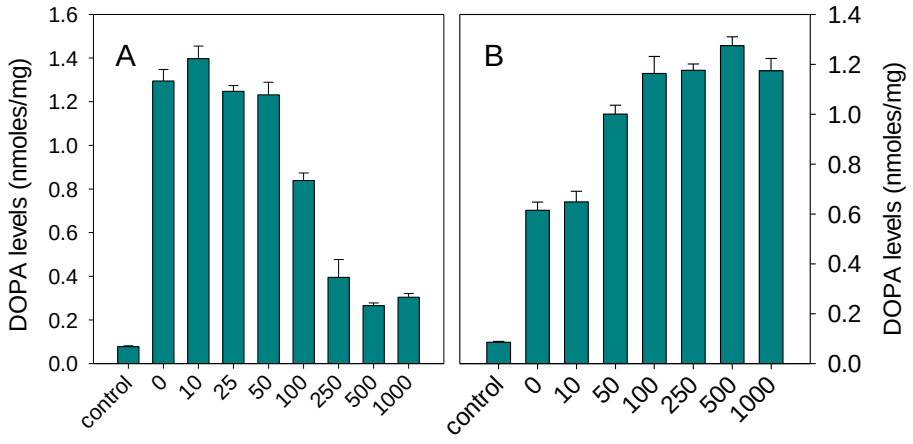

Figure 6- Inhibitory Effect of DIDS and Amiloride on Intracellular DOPA Production at pH 6.0 in MN9D Cells. MN9D Cells were grown to near confluence in 12-well plates and incubated with regular KRB-HEPES for 1 h at pH 6.0 in presence of DIDS (Panel A) and Amiloride (Panel B) at the concentration of 0-1000 μM. Cells were washed, collected and intracellular DOPA levels were quantified and determined by reversed-phase HPLC-EC and normalized to respective cellular protein concentrations. DOPA levels are expressed as nmoles/mg. Data represent mean ± S.D. of three samples.

4.2 Effect of $[H^+]_o$ on Intracellular DOPA and DA Levels in Differentiated MN9D and PC12 Cells

Incubation of differentiated MN9D cells in regular KRB-HEPES for 1 h show a substantial increase of DA level in a $[H^+]_o$ dependent manner (Fig. 7). Between pH 8.5-6.5, the increase of DA level is about 2 -3 fold. This increase of DA levels is more pronounced in comparison to undifferentiated cells (data not shown). On the other hand, the increase of DOPA levels in a $[H^+]_o$ dependent manner were less pronounced in comparison to undifferentiated cells (data not shown). Interestingly, the increase of DA and DOPA levels in a $[H^+]_o$ dependent manner in undifferentiated PC12 cells were similar to that of the differentiated MN9D cells (Fig. 7). Therefore, the activation of TH in response to $[H^+]_o$ is common to catecholaminergic cells.

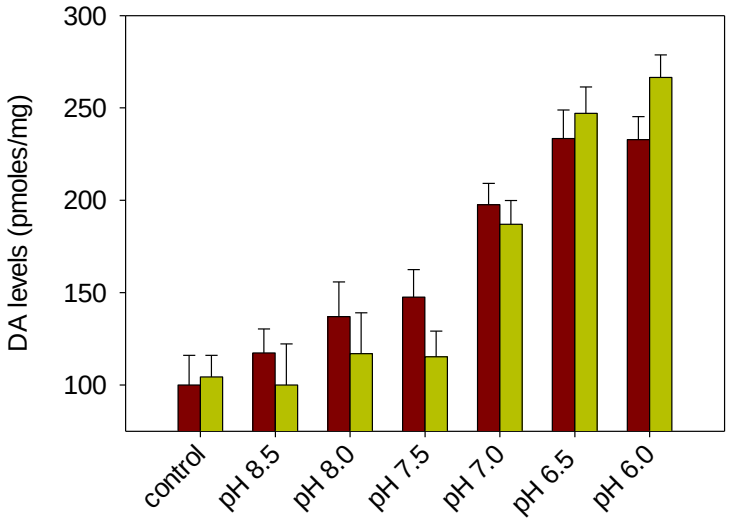

Figure 7- Effect of $[H^+]_o$ on Intracellular DOPA and DA Levels in Differentiated MN9D and PC12 Cells. MN9D cells were differentiated with 1 mM *n*-butyrate in 6-well plates as detailed in Experimental Methods. PC12 cells were grown in 12-well plates coated with rat tail collagen type I. When cells were nearly confluent, they were washed several times and incubated with regular KRB-HEPES for 1 h in the pH range of 8.5 to 6.0. Cells were washed, collected and

intracellular DOPA levels were quantified and determined by reversed-phase HPLC-EC and normalized to respective cellular protein concentrations. DOPA levels are expressed as nmoles/mg. Data represent mean ± S.D. of three samples.

4.3 Investigation of intracellular pH and Ca^{2+} Levels of MN9D Cells

To investigate whether $[H^+]_o$ has an effect on the intracellular pH and Ca^{2+} level in MN9D cells, Ca^{2+} and pH sensitive membrane permeable fluorescence probes FURA-2AM and BCECF-AM, respectively, were used on the Nikon ECLIPS-Ti microscope equipped with a Nikon S FLURO 40X lens. According to Fig. 8, the increase of $[H^+]_o$ (abrupt change of extracellular pH from 7.8 to 6.02) causes an increase of both $[H^+]_i$ and $[Ca^{2+}]_i$ in the presence of extracellular Cl^- through time. However, the increase $[H^+]_i$ and $[Ca^{2+}]_i$ were comparatively smaller in the absence of extracellular Cl^- under similar experimental conditions (Fig. 8).

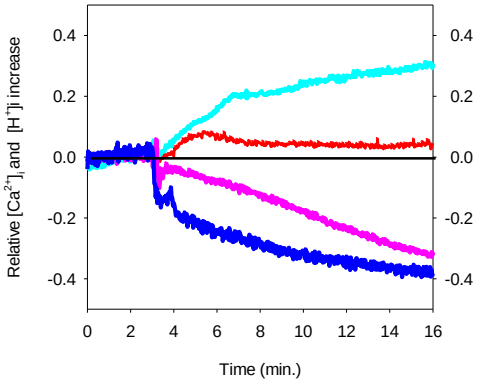

Figure 8- The Effect of $[H^+]_o$ on the Intracellular Ca^{2+} and pH Levels. The effect of $[H^+]_o$ on the intracellular Ca^{2+} levels ($[Ca^{2+}]_i$) were determined using Fura-2-AM and on intracellular pH using BCECF-AM in MN9D cells. Cells were grown in 35 mm glass bottomed culture plates to about 70-80% confluence, washed two times with KRB-HEPES, and were loaded with 5 µM BCECF-AM or Fura-2-AM for 20 min at 37°C in the same buffer, in the dark. Cells were washed with KRB-HEPES, pH 7.4 three times and incubated in the same buffer for an additional 20 min at room temperature in the dark to facilitate the complete hydrolysis of the methyl ester. Dye loaded cells were placed on the stage of a Nikon ECLIPS-Ti microscope equipped with a Nikon S FLURO 40X lens. The intracellular pH or Ca^{2+} was measured as detailed in Experimental Methods. The pH of the media was quickly changed from 7.8 to 6.02 (pre-

determined) by the addition of five volumes of MES-KRB (125 mM NaCl, 2 mM KCl, 1.4 mM $MgSO_4$, 1.2 mM $CaCl_2$, 1.2 mM KH_2PO_4, 25 mM MES and 5 mM glucose, pH 5.8).

4.4 The Effects of $[H^+]_o$ on the Phosphorylation Levels of the Regulatory Domain Serine-40 of TH

The effects of $[H^+]_o$ on the phosphorylation levels of the regulatory domain Ser 40 of TH were determined using a western blotting. The initial control experiments were carried out to measure the total TH in MN9D cells and about 20% of total TH was Ser 40 phosphorylated under normal growth conditions. As shown in Fig. 9, the fraction of Ser 40 phosphorylated increased significantly as $[H^+]_o$ increased in the incubation buffer of MN9D cells. At the same time, the total concentration of TH remains unaffected. Therefore, a decrease in extracellular pH increases the ratio of Ser 40 phoshorylated to the total enzyme; i.e. from pH 7.5 to 6.5, the ratio of Ser 40 phosphorylated to total enzyme increases by about 300%.

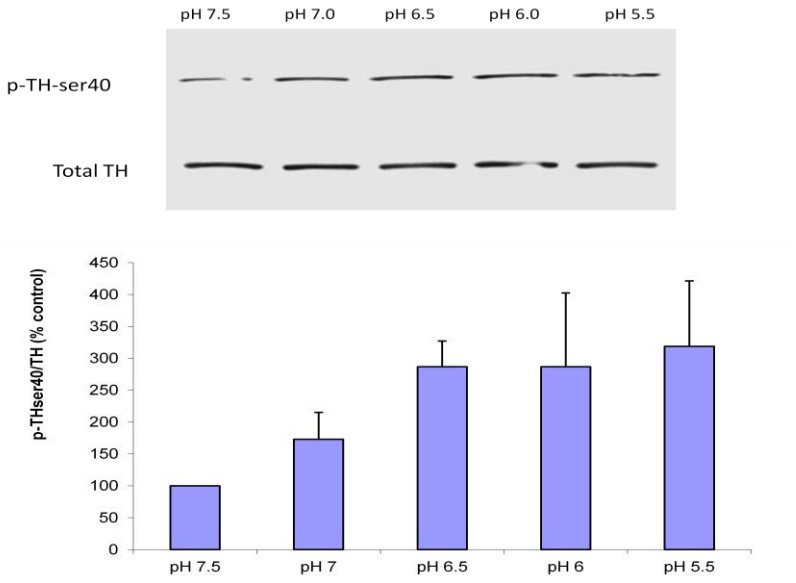

Figure 9- The Effects of $[H^+]_o$ on the Phosphorylation Levels of the Regulatory Domain Serine-40 of TH. The effects of $[H^+]_o$ on the phosphorylation levels of the regulatory domain Ser 40 of TH were determined using western blotting experiment as detailed in Experimental Methods.

CHAPTER V

DISCUSSION

The intracellular TH activity of MN9D cells is stimulated by the $[H^+]_o$ through concentration and time course which does not require extracellular Na^+ or Ca^{2+} under normal conditions. However, the extracellular Cl^- is required to stimulate the $[H^+]_o$-mediated activation of TH. In addition, Cl^-/HCO_3^- exchanger inhibitor ,DIDS, inhibits while the Na^+/H^+ exchanger inhibitor ,amiloride, potentiates the $[H^+]_o$-mediated activation of TH which may suggest that the intracellular $H^+([H^+]_i)$ is involved in this process. The $[H^+]_i$ is increased in response to the increased $[H^+]_o$ in the presence of extracellular Cl^- whereas the $[H^+]_i$ is slowly increased in the absence of extracellular Cl^-. In addition, the $[Ca^{2+}]_i$ and the phosphorylation of Ser40 of the regulatory domain of TH also increases in response to the increase of $[H^+]_o$. Therefore, these results may suggest that the Cl^--dependent intracellular acidification, possibly through the Cl^-/HCO_3^- exchanger, in response to $[H^+]_o$, causes an increase of $[Ca^{2+}]_i$ and phosphorylation of Ser 40 which appears to be responsible for the $[H^+]_o$-mediated activation of TH in MN9D cells.

The $[H^+]_o$-mediated TH activation is observed in differentiated cells similar to undifferentiated MN9D cells under normal conditions. However in the comparison to undifferentiated cells, the increase in DA levels in response to $[H^+]_o$ is significantly more pronounced, while the increase in DOPA levels were less pronounced in differentiated cells. This difference may be due to higher expression of TH in the undifferentiated MN9D cells, which is significantly reduced during differentiation. In addition, TH activation in response to $[H^+]_o$ in undifferentiated PC12 cells is similar to differentiated MN9D cells. Thus, these findings suggest

that the activation of TH in response to increase in $[H^+]_o$ may be true for any catecholaminergic cells.

It is still not clear which physiological stimulus is responsible for the activation of TH. There are at least three proposed trans-membrane signaling systems for the TH activation. First, the depolarization of the membrane followed by Ca^{2+} entry through voltage gated calcium channels during synaptic release leads to the increase in TH phosphorylation through Ca^{2+}-dependent protein kinases. However, it is not known whether the extracellular Ca^{2+} is involved in TH phosphorylation. Secondly, as mentioned earlier, the current model for catecholamine-dissociation proposed that TH activation by phosphorylation is due to the alteration of the kinetics of interaction of substrates and modulators with the enzyme. This hypothesis was demonstrated by showing that the rate of dissociation of Fe^{3+}-bound catecholamines from the inhibitory complex is increased by ~500 fold increase by the phosphorylation of Ser 40 of the purified enzyme compared to the non-phosphorylated enzyme (75,76). Thus, the dissociation of the Fe^{3+} bound catecholamines by the phosphorylation of Ser 40 allows the efficient reduction of the enzyme by BH_4 (5,77,78). While the *in vitro* dissociation constant (K_d) for phosphorylated catecholamine-TH (Fe^{3+}) complex is lower, in the range of 500 nM, the K_m of DA for synaptic vesicle membrane vesicular monoamine transporter is higher, in low micromolar range [5-10 μM for bovine chromaffin granule vesicular monoamine transporter-2 (69,70)]. Therefore, this suggests that the basal cytosolic catecholamine levels in catecholaminergic cells could be in the range of low micromolar at pH 7.4 and favor association of rather than dissociation of. Lastly, during repeated synaptic release, the catecholamine levels must increase with respect to the basal level due to the reuptake through respective plasma membrane amine transporters which leads to

increased inhibition rather than activation of TH. Overall, there are inconsistencies in the proposed of phosphorylation/catecholamine-dissociation model of TH activation.

When synaptic vesicles fuse with the presynaptic membrane, they release highly buffered acidic content into the synaptic cleft. Accordingly, several studies described below have observed acidification during synaptic transmission; for example, bovine adrenal chromaffin vesicle (a well characterized catecholaminergic model) releases up to ~500 mM protonated catecholamine, ~125 mM ATP, large amounts of acidic chromagranins, other proteins and [H^+] equivalent to a pH 5.4 acidic environment (60). Although the neuronal and cellular pH are tightly regulated under normal physiological conditions, high frequency synaptic release could exceed the buffering capacity and the rate of diffusion of H^+ leads to a transient synaptic cleft acidification. Krishtah, *et al.*, the electrical stimulation of presynaptic pathways in rat hippocampal slices produced a rapid acidic shift in the synaptic cleft area followed by a long-lasting alkaline one (79). Shuba, *et al.*, showed secretory vesicles released from differentiated PC12 cells caused local elevations in [H and proposed that the signal alteration in confined micro-domains of synapses is caused by co-released of H^+ concentration (80). DeVries has showed that the vesicular [H^+] is released during exocytosis allowing the feedback to suppress the Ca^{2+} released from the nearby calcium channels in mammalian cone receptors (81). Furthermore, Palmer, *et al.*, demonstrated the transient change of synaptic cleft pH from 7.5 to ~6.9 in the retinal bipolar cells is observed during the exocytosis (82). In cultured rat cerebellar granule cells, the enhancement of $GABA_A$ signaling due to the exocytotic synaptic acidification has also been observed (83). In addition, the association of synaptic transmission with the acidification of the synaptic cleft area is demonstrated in numerous studies (57,84).

Based on our findings and literature evidence, these may suggest that the acidity of synaptic release also plays a role in *in vivo* activation of TH in catecholaminergic neurons. It is likely that during repeated synaptic acidic release, the acidification of the synaptic area could be the initial signal for in vivo TH activation. The increase of $[H^+]_o$ is parallel with the increase in intracellular acidification and cytosolic Ca^{2+} leading to a significant increase of the phosphorylation of the regulatory domain Ser 40 and activation of TH. Intracellular acidification also depends on extracellular Cl^- and the observation of DIDS inhibiting and amiloride promoting TH activation suggesting that intracellular acidification in response to $[H^+]_o$ occurs most likely through a sodium independent Cl^-/HCO_3^- exchanger, as previously shown in avian osteoblasts (85). In addition, some studies have shown that the pH optima for catecholamine-bound and catecholamine-free purified TH are ~6 and ~7, respectively and, TH bound catecholamine freely dissociates at pH 6 (86,87). Therefore, Ser 40 phosphorylation increased and the intracellular acidification could induce the dissociation of the Fe^{3+}-bound catecholamine from the inhibitory complex causing TH to fully activate. This would not only activate TH for increased catecholamine synthesis, but also restore $[H^+]$ from the presynaptic cell for the refilling of the synaptic vesicles with newly synthesized catecholamines and their acidic contents. This hypothesis of TH activation also addresses the inconsistencies of the current catecholamine-dissociation/phosphorylation model of TH activation.

Abnormal catecholamine metabolism has been implicated in neuronal disorders. Since the biosynthesis of the catecholamines is primarily regulated through TH, modulating the TH activity could be the key in regulating the catecholamine levels for therapeutic purposes. For the first time, our findings provide a molecular connection between TH activity and $[H^+]_o$, Cl^-/HCO_3^- and Na^+/H^+ exchangers. Therefore, these exchangers could be targeted in the development of

therapeutic agents for the treatment of diseases associated with catecholaminergic dysfunctions or imbalance in central and peripheral nervous systems.

CHAPTER VI

CONCLUSION

The mechanism of TH activation has been extensively studied; however, there are areas of concern and questions left unanswered in the current model of *in vivo* TH activation. Our studies clearly show that the extracellular H^+ ions activate TH by using catecholaminergic MN9D and PC12 under normal physiological conditions. However, these findings were performed in transformed cell lines and must be confirmed with primary cultures and animal models. In addition, the increase of cytosolic Ca^{2+}, as a consequence of the intracellular acidification, is still not understood. Therefore, further studies are necessary to more fully address these issues.

MN9D is a well characterized dopaminergic cell line which was derived from the fusion of mouse embryonic ventral mesencephalic and neuroblasoma cells (67). Intracellular catecholamine profiles of both undifferentiated and differentiated MN9D cells are comparable to CNS dopaminergic neurons (62). These cells also express high levels of DAT but not NET, although they do not take up DA in the presence of extracellular Ca^{2+} (67). The poor uptake could be due to the high levels of intracellular catecholamine in these cells. Therefore, these cells have the major characteristics of CNS dopaminergic neurons. However, while undifferentiated MN9D cells are different from the brain specific dopaminergic neurons with respect to key electrophysiological properties, butyric acid-differentiated cells closely resemble that of dissociated matured CNS DA neurons (63).

Undifferentiated MN9D cells show that the $[H^+]_o$-dependent activation of TH requires extracellular Cl^-, but not Na^+ or Ca^{2+}. In addition, while Cl^-/HCO_3^- transporter inhibitor, DIDS,

inhibits, the Na^+/H^+ exchanger inhibitor, amiloride, promotes the TH activation. $[H^+]_o$ increases the intracellular H^+ ($[H^+]_i$), intracellular Ca^{2+} and phosphorylation of the Ser 40 of TH. Similar to undifferentiated MN9D cells, $[H^+]_o$-mediated TH activation is also observable in differentiated cells. In addition, undifferentiated PC12 cells also show similar TH activation in response to $[H^+]_o$. Thus, these findings show that the activation of TH in response to increase in $[H^+]_o$ is a general phenomenon of catecholaminergic cells. Based on these findings, we hypothesize that the acidity of the synaptic release may play a role in the *in vivo* activation of TH in catecholaminergic neurons.

Finally, there is a molecular connection between TH activity and $[H^+]_o$, Cl^-/HCO_3^-, and Na^+/H^+ exchangers. Therefore, development of therapeutic agents specifically for these exchangers could work against catecholaminergic dysfunctions or imbalance in central and peripheral nervous system that are implicated in neurological diseases. In addition, our findings provide the first *in vitro* cell model for future studies related to TH regulation and drug screening.

REFERENCES

REFERENCES

1. Brady, S. T., Siegel, G. J., Albers, R. W., Price, D. L., Benjamins, J., Fisher, S., Hall, A., Bazan, N., Coyle, J., and Sisodia, S. (2012) *Basic Neurochemistry: Principles of Molecular, Cellular, and Medical Neurobiology*, 8th ed., Elsevier Inc., Oxford

2. Eisenhofer, G., Kopin, I. J., and Goldstein, D. S. (2004) Catecholamine Metabolism: A Contemporary View with Implications for Physiology and Medicine. *Pharmacol Rev***56**, 331-349

3. Ramsey, A. J., Hillas, P. J., and Fitzpatrick, P. F. (1996) Characterization of the active site iron in tyrosine hydroxylase: Redox states of the iron. *J Biol Chem***271**, 24395-24400

4. Frantom, P. A., Servalli, J., Ragsdale, S. W., and Fitzpatrick, P. F. (2006) Reduction and oxidation of the active site iron in tyrosine hydroxylase: kinetics and specificity. *Biochemistry***45**, 2372-2379

5. Andersson, K. K., Cox, D. D., Que, L., Jr., Flatmark, T., and Haavik, J. (1988) Resonance Raman studies on the blue-green colored bovine adrenal tyrosine 3-monooxygenase (tyrosine hydroxylase). Evidence that the feedback inhibitors adrenaline and noradrenaline are coordinated to iron. *J Biol Chem***263**, 18621-18626

6. Ramsey, A. J., and Fitzpatrick, P. F. (1998) Effects of phosphorylation of serine 40 of tyrosine hydroxylase on binding of catecholamines: Evidence for novel regulatory mechanism. *Biochemistry* **37**, 8980-8986

7. Alterio, J., Ravassard, P., Haavik, J., Le Caer, J. P., Biguet, N. F., Waksman, G., and Mallet, J. (1998) Human tyrosine hydroxylase isoforms. Inhibition by excess tetrahydropterin and unusual behavior of isoform 3 after camp-dependent protein kinase phosphorylation. *J Biol Chem***273**, 10196-10201

8. Flatmark, T., and Steven, R. C. (1999) Structural Insight into the Aromatic Amino Acid Hydroxylases and Their Disease-Related Mutant Forms. *Chem Rev***99**, 2137-2160
9. Fitzpatrick, P. F. (1999) The tetrahydropterin-dependent amino acid hydroxylases. *Annu Rev Biochem***68**, 355-381

10. Okuno, S., and Fujisawa, H. (1982) Purification and some properties of tyrosine-3-monooxygenase from rat adrenal. *Eur J Biochem***122**, 49-55

11. Abate, C., and Joh, T. H. (1991) Limited proteolysis of rat brain tyrosine hydroxylase defines an N-terminal region required for regulation of cofactor binding and directing substrate specificity. *J Mol Neurosci***2**, 203-215

12. Daubner, S. C., Le, T., and Wang, S. (2011) Tyrosine hydroxylase and regulation of dopamine synthesis. *Arch Biochem Biophys***508**, 1-12

13. Goodwill, K. E., Sabtier, C., Marks, C., Raag, R., Fitzpatrick, P. F., and Stevens, R. C. (1997) Crystal structure of tyrosine hydroxylase at 2.3 A and its implications for inherited diseases. *Nat Struct Biol***4**, 578-585

14. Kaneda, N., Kobayashi, K., Ichinose, H., Kishi, F., Nakazawa, A., Kurosawa, Y., Fujita, K., and Nagatsu, T. (1987) Isolation of a novel cDNA clone for human tyrosine hydroxylase: alternative RNA splicing produces four kinds of mRNA from a single gene. *Biochem Biophys Res Commun***146**, 971-975

15. Grima, B., Lamouroux, A., Boni, C., Julien, J. F., Jovoy-Agid, F., and Mallet, J. A. (1987) single huan gene encoding multiple tyrosine hydroxylases with different predicted functional characteristics. *Nature***326**, 707-711

16. Kobayashi, K., Kandeda, N., Ichinose, H., Kishi, F., Nakazawa, A., Kurosawa, Y., Fujita, K., and Nagatsu, T. (1988) Structure of the human tyrosine hydroxylase gene: Alternative splicing from a single gene accounts for generation of four mRNA types. *J Biochem***103**, 907-912

17. Haycock, J. W. (1990) Phosphorylation of tyrosine hydroxylase in situ at serine 8, 19, 31, and 40. *J Biol Chem***265**, 11682-11691

18. Karasawa, N., Hayashi, M., Yamada, K., Nagatsu, I., Iwasa, M., Takeuchi, T., Uematsu, M., Watanabe, K., and Onozuka, M. (2007) Tyrosine Hydroxylase (TH)- and Aromatic L-Amino Acid Decarboxylase (AADC)- Immunoreactive Neurons of the Common Marmoset (Callithrix jacchus) Brain: An Immunohistochemical Analysis. *Acta Histochem Cytochem***40**, 83-923

19. Winkler, H., Apps, D. K., and Fischer-Colbrie, R. (1986) The molecular function of adrenal chromaffin granules: established facts and unresolved topics. *Neuroscience***18**, 261-290

20. Saxena, A., and Fleming, P. J. (1983) Isolation and reconstitution of the membrane-bound form of dopamine beta-hydroxylase. *J Biol Chem***258**, 4147-4152

21. Oyarce, A. M., and Fleming, P. J. (1991) Multiple forms of human dopamine-b-hydroxylase in SH-SY5Y neuroblastoma cells *Arch Biochem Biophys***290**, 503-510

22. Joh, T. H., and Hwang, O. (1987) Dopamine b-Hydroxylase: biochemistry and molecular biology. *Ann N Y Acad Sci***493**, 342-350

23. Stanley, W. C., Li, B., Bonhaus, D. W., Johnson, L. G., Lee, K., Porter, S., Walker, K., Martinez, G., Eglen, R. M., Whiting, R. L., and Hegde, S. S. (1997) Catecholamine modulatory effects of nepicastat (RS-25560-197), a novel, potent and selective inhibitor of dopamine-β-hydroxylase. *Br J Pharmacol***121**, 1803-1809

24. Goldstein, M., Anagnoste, B., Lauber, E., and McKeregham, M. R. (1964) INHIBITION OF DOPAMINE-BETA-HYDROXYLASE BY DISULFIRAM. *Life Sciences***3**, 763-767

25. Wurtman, R. J. (2002) Stress and the adrenocortical control of epinephrine synthesis. *Metabolism***51**, 11-14

26. Durcan, M. J., Lister, R. G., and Linnoila, M. (1990) Behavioral effects of the inhibitors of phenylethanolamine-N-methyltransferase, LY 78335 and LY 134046, and their interactions with ethanol. *Psychopharmacology (Berl)***101**, 196-202

27. Adams Jr., J. D., Chang, M. L., and Klaidman, L. (2001) Parkinson's disease--redox mechanisms. *Curr Med Chem***8**, 809-814

28. Batch, A. W., Lan, N. C., Johnson, D. L., Abell, C. W., Bembenek, M. E., Kwan, S. W., Seeburg, P. H., and Shih, J. C. (1988) cDNA cloning of human liver monoamine oxidase A and B: molecular basis of differences in enzymatic properties. *Proc Natl Acad Sci U S A***85**, 4934-4938

29. Yi, H., Akao, Y., Maruyama, W., Chen, K., Shih, J., and Naoi, M. (2006) Type A monoamine oxidase is the target of an endogenous dopaminergic neurotoxin, N-methyl(R)salsolinol, leading to apoptosis in SH-SY5Y cells *J Neurochem***96**, 541-549

30. Dennis, A. M., Rhee, W. J., Sotto, D., Dublin, S. N., and Bao, G. (2012) Quantum Dot-Fluorescent Protein FRET Probes for Sensing Intracellular pH. *ACS Nano***6**, 2917-2924

31. Nelson, D. L., and Cox, M. M. (2008) *Principles of Biochemistry*, 5th ed., W.H. Freeman and Company, New York

32. Slepkov, E. R., Rainey, J. K., Sykes, B. D., and Fliegel, L. (2007) Structural and functional analysis of the Na+/H+ exchanger. *Biochem J***401**, 623-633

33. Orlowski, J., and Grinstein, S. (1997) Na+/H+ exchangers of mammalian cells. *J Biol Chem***272**, 22373-22376

34. Orlowski, J., and Grinstein, S. (2004) Diversity of the mammalian sodium/proton exchanger SLC9 gene family. *Pflugers Arch***447**, 549-565

35. Nakamura, N., Tanaka, S., Teko, Y., Mitsui, K., and Kanazawa, H. (2005) Four Na+/H+ exchanger isoforms are distributed to Golgi and post-Golgi compartments and are involved in organelle pH regulation. *J Biol Chem***280**, 1561-1572

36. Khadilkar, A., Iannuzzi, P., and Orlowski, J. (2001) Identification of sites in the second exomembrane loop and ninth transmembrane helix of the mammalian Na+/H+ exchanger important for drug recognition and cation translocation. *J Biol Chem***276**, 43792-43800

37. Orlowski, J., Kandasamy, R.A., and Shull, G.E. (1992) Molecular cloning of putative members of the Na+/H+ exchanger gene family. *J Biol Chem***267**, 9331-9339

38. Noel, J., Roux, D., and Pouyssegur, J. (1996) Differential localziation of Na+/H+ exchanger isoforms (NHE1 and NHE3) in polarized epithetlial cell lines. *J Cell Sci***109**, 929-939

39. Baird, N. R., Orlowski, J., Szabo, E. Z., Zaun, H. C., Schultheis, P. J., Menon, A. G., and Shull, G. E. (1999) Molecular cloning, genomic organization, and functional expression of Na+/H+ exchanger isoform5 (NHE5) from human brain. *J Biol Chem***274**, 4377-4382

40. Attapitya, S., Park, K., and Melvin, J. E. (1999) Molecular cloning and functional expression of a rat Na+/H+ exchanger (NHE5) highly expressed in brain. *J Biol Chem***274**

41. Brett, C. L., Wei, Y., Donowitz, M., and Rao, R. (2002) Human Na+/H+ exchanger isoform 6 is found in recycling endosomes of cells, not in mitochondria. *Am J Physiol Cell Physiol***282**, C1031-C1041

42. Numata, M., and Orlowski, J. (2001) Molecular cloning and characterization of a novel (Na+, K+)/H+ exchanger localized to the trans-Golgi network. *J Biol Chem***276**, 17387-17394

43. Labelle, E. F., Woodard, P. L., and Cragoe, C. E., Jr. (1984) The interaction of amiloride analogues with the Na+/H+ exchanger in kidney medulla microsomes. *Biochim Biophys Acta***778**, 129-138

44. Romero, M. F. (2001) The Electrogenic Na+/HCO3- Cotransporter, NBC. *JOP***2**, 182-191

45. Chang-Zheng, W., Yano, H., Nagashima, K., and Seino, S. (2000) The Na+-driven Cl-/HCO3- Exchanger: CLONING, TISSUE DISTRIBUTION, AND FUNCTIONAL CHARACTERIZATION. *J Biol Chem***275**, 35486-35490

46. Hubner, C. A., and Holthoff, K. (2013) Anion transport and GABA signaling. *Front Cell Neurosci***7**, 1-12

47. Russell, J. M., and Boron, W. F. (1976) Role of Choloride transport in regulation of intracellular pH. *Nature***264**, 73-74

48. Bjerregaard-Andersen, K., Perdreau-Dahl, H., Guldsten, H., Praetorius, J., Jensen, J. K., and Morth, J. P. (2013) The N-terminal cytoplasmic region of NCBE displays features of an intrinsic disordered structure and represents a novel target for specific drug screening. *Front Physiol***4**, 1-9

49. Alper, S. L. (2009) Molecular physiology and genetics of Na+-independent SLC4 anion exchangers. *J Exp Biol***212**, 1672-1683

50. Alpher, S. L., Darman, R. B., Chernova, M. N., and Dahl, N. K. (2002) The AE gene family of Cl/HCO3- exchangers. *J Nephrol***15**, S41-S53

51. Romero, M. F. (2005) Molecular pathophysiology of SLC4 bicarbonate transporters. *Curr Opin Nephrol Hypertens***14**, 495-501

52. Jasti, J., Furukawa, H., Gonzales, E. B., and Gouaux, E. (2007) Structure of acid-sensing ion channel 1 at 1.9 A resolution and low pH. *Nature***449**, 316-323

53. Waldmann, R. (2001) Proton-gated cation channels-- neuronal acid sensors in the central and peripheral nervous system. *Adv Exp Med Biol***502**, 293-304

54. Lingueglia, E. (2007) Acid-sensing ion channels in sensory perception. *J Biol Chem***282**, 17325-17329

55. Chai, S., Li, M., Branigan, D., Xiong, Z. G., and Simon, R. P. (2010) Activation of Acid-sensing Ion Channel 1a (ASIC1a) by Surface Trafficking. *J Biol Chem***285**, 13002-13011

56. Holzer, P. (2009) Acid-Sensitive Ion Channels and Receptors. *Handbook of Experimental Pharmacology***194**, 283-332

57. Yermolaieva, O., Leonard, A. S., Schnizler, M. K., Abboud, F. M., and Weish, M. J. (2004) Extracellular acidosis increases neuronal cell calcium by activating acid-sensing ion channel 1a. *Proc Natl Acad Sci U S A***101**, 6752-6757

58. Qadri, Y. J., Song, Y., Fuller, C. M., and Benos, D. J. (2010) Amiloride Docking to Acid-sensing Ion Channel-1. *J Biol Chem***285**, 9627-9635

59. Daubner, S. C., Lohse, D. L., and Fitzpatrick, P. F. (1993) Expression and characterization of catalytic and regulatory domains of rat tyrosine hydroxylase. *Protein Sci***2**, 1452-1460

60. Phillips, J. H. (1982) Dynamic aspects of chromaffin granule structure. *Neuroscience***7**, 1595-1609

61. Choi, H. K., Won, L.A., Kontur, P.J., Hammond, D.N., Fox, A.P., Wainer, B.H., Hoffmann, P.C., and Heller, A. (1991) Immortalization of embryonic mesencephalic dopaminergic neurons by somatic cell fusion. *Brain research***552**, 67-76

62. Rick, C. E., Ebert, A., Virag, T., Bohn, M. C., and Surmeier, D. J. (2006) Differentiated dopaminergic MN9D cells only partially recapitulate the electrophysiological properties of midbrain dopaminergic neurons. *Dev Neurosci***28**, 528-537

63. Dong, Y., Heien, M. L., Maxson, M. M., and Ewing, A. G. (2008) Amperometric measurements of catecholamine release from single vesicles in MN9D cells. *J Neurochem***107**, 1589-1595

64. Greene, L. A., and Tischler, A.S. (1976) Establishment of a noradrenergic clonal line of rat adrenal pheochromocytoma cells which respond to nerve growth factor. *Proceedings of the National Academy of Sciences of the United States of America***73**, 2424-2428

65. Gunning, P. W., Landreth, G.E., Layer, P., Ignatius, M., and Shooter, E.M. (1981) Nerve growth factor-induced differentation of PC12 cells: evaluation of changes in RNA and DNA metabolism. *The Journal of Neuroscience***1**, 368-379

66. Schubert, D., and Klier, F.G. (1977) Storage and release of acetylcholine by a clonal cell line. *Proceedings of the National Academy of Sciences of the United States of America***74**, 5184-5188

67. Choi, H. K., Won, L. A., Kontur, P. J., Hammond, D. N., Fox, A. P., Wainer, B. H., Hoffman, P. X., and Heller, A. (1991) Immortalization of embryonic mesencephalic dopaminergic neurons by somatic cell fusion. *Brain Res***552**, 67-76

68. Bradford, M. M. (1976) A rapid and sensitive method for the quantitation of microgram quantities of protein utilizing the principle of protein-dye binding. *Anal Biochem***72**, 248-254

69. Wimalasena, D. S., and Wimalasena, K. (2004) Kinetic evidence for the channeling of dopamine between monoamine transporter and membrane dopamine b-monooxygenase in chromaffin granule ghosts *J Biol Chem***279**, 15298-15304

70. Wimalasena, K., and Wimalasena, D. S. (1995) The Reduction of Membrane-bound Dopamine b-Monooxygenase in Resealed Chromaffin Granule Ghosts: Is Intra-granular Ascorbic Acid a Mediator for the Extra-granular Reducing Equivalents? *J Biol Chem***270**, 27516-27524

71. Solovyova, N., Veselovsky, N., Toescu, E. C., and Verkhratsky, A. (2002) Ca(2+) dynamics in the lumen of the endoplasmic reticulum in sensory neurons: direct visualization of Ca(2+)-induced Ca(2+) release triggered by physiological Ca(2+) entry. *EMBO J***21**, 622-630

72. Takahashi, A., Camacho, P., Lechleiter, J. D., and Herman, B. (1999) Measurement of intracellular calcium. *Physiol Rev***79**, 1089-1125

73. Martinez-Zaguilan, R., Parnami, G., and Lynch, R. M. (1996) Selectrion of fluorescent ion indicators for simulaneous measurements of pH and Ca2+. *Cell Calcium***19**, 337-349

74. Church, J., Baxter, K. A., and McLarnon, J. G. (1998) pH modulation of Ca2+ responses and a Ca2+-dependent K+ channel in cultured rat hippocampal neurons. *Journal of Physiological***511**, 119-132

75. Sura, G., Daubner, S. C., and Fitzpatrick, P. F. (2004) Effects of phosphorylation by protein kinase A on binding of catecholamines to the human tyrosine hydroxylase isoforms. *J Neurochem***90**, 970-978

76. McCulloch, R. I., Daubner, S. C., and Fitzpatrick, P. F. (2001) Effects of substitution at serine 40 of tyrosine hydroxylase on catecholamine binding. *Biochemistry***40**, 7273-7278

77. Ramsey, A. J., and Fitzpatrick, P. F. (2000) Effects of phosphorylation on binding of catecholamines to tyrosine hydroxylase: specificity and thermodynamics. *Biochemistry***39**, 773-778

78. Briggs, G. D., Gordon, S. L., and Dickson, P. W. (2011) Mutational analysis of catecholamine binding in tyrosine hydroxylase. *Biochemistry***50**, 1545-1555

79. Krishtal, O. A., Osipchuk, Y. V., Shelest, T. N., and Smirnoff, S. V. (1987) Rapid extracellular pH transients related to synaptic transmission in rat hippocampal slices. *Brain Res***436**, 352-356

80. Shuba, Y. M., Dietrich, C. J., Oermann, E., Cleeman, L., and Moad, M. (2008) Local extracellular acidification caused by Ca^{2+}-dependent exocytosis in PC12 cells. *Cell Calcium***44**, 220-229

81. DeVries, S. H. (2001) Exocytosed protons feedback to suppress the Ca^{2+} current in mammalian cone photoreceptors. *Neuron***32**, 1107-1117

82. Palmer, M. J., Hull, C., Vigh, J., and von Gersdorff, H. (2003) Synaptic cleft acificication and modulation of short-term depression by exocytosed protons in retinal bipolar cells. *J Neurosci***23**, 11332-11341

83. Dietrich, C. J., and Moad, M. (2010) Synaptic acification enhances GABAA signaling. *J Neurosci***30**, 16044-16052

84. Chen, J. C., and Chesler, M. (1992) pH transients evoked by excitatory synaptic transmission are increased by inhibition of extracellular carbonic anhydrase. *Proc Natl Acad Sci U S A***89**, 7786-7790

85. Teti, A., Blair, H. C., Teitelbaum, S. L., Kahn, A. J., Koziol, C., Konsek, J., Zambonin-Zallone, A., and Schlesinger, P. H. (1989) Cytoplasmic pH regulation and chloride/bicarbonate exchange in avian osteoclasts. *J Clin Invest***83**, 227-233

86. Fitzpatrick, P. F., Chlumsky, L. J., Daubner, S. C., and O'Malley, K. L. (1990) Expression of rat tyrosine hydroxylase in insect tissue culture cells and purification and characaterization of the cloned enzyme. *J Biol Chem***265**, 2042-2047

87. Haavik, J., Martinez, A., and Flatmark, T. (1990) pH-dependent release of catecholamines from tyrosine hydroxylase and the effect of phosphorylation of Ser-40. *FEBS Lett***262**, 363-365

PART II: IDENTIFICATION OF NOVEL MECHANISM(S) OF PARKINSON'S DISEASE CAUSING 1-METHYL-4-PHENYLPYRIDINIUM NEUROTOXICITY

CHAPTER I

INTRODUCTION

Neurodegenerative diseases, including Parkinson's, Alzheimer's, ALS, and Huntington's cause progressive degeneration of the neurons in specific areas of the central or peripheral nervous systems. Although the symptoms of these diseases can be treated by various drugs, no drugs are available to cure these debilitating diseases. Therefore, the understanding of the molecular causes of, and preventive strategies for these diseases is an immediate and urgent challenge for research in the field.

Parkinson's disease (PD) is the second most common neurodegenerative disease after Alzheimer's disease (AD) and 50-60,000 new cases of PD are diagnosed each year in the United States, adding to the one million people who currently have PD (1). According to the Parkinson's disease Foundation (PDF), there are approximately 7-10 million people worldwide living with PD. In 2010, there were approximately 630,000 people diagnosed with PD in the United States and it is projected to increase to 819,000 by 2020, 1.06 million by 2030, 1.24 million by 2040, and 1.34 million by 2050 (2). The medical cost for the treatment of the population with PD exceeded $14 billion in 2010 (approximately $22,800 per patients) and is expected to increase significantly over the next few decades. Those projections have led to the need to develop effective preventive and therapeutic strategies in order to decrease the financial cost and burden to society.

PD is characterized by the loss of dopaminergic neurons in the substantia nigra, a specific region in the midbrain causing symptoms of tremors, muscular rigidity, and bradykinesia (3-5). The loss of dopaminergic neurons in this area of the brain leads to reduction of dopamine (DA) in the midbrain augmenting the symptoms of PD. L-DOPA which is a precursor of DA is currently used as a clinical drug to improve symptoms of PD patients. Since DA itself does not cross the blood brain barrier, it cannot be used to treat PD. On the other hand, DOPA crosses the blood brain barrier through the aromatic amino acid transporter and, once inside the brain, it is efficiently converted to DA by brain DOPA decarboxylase supplementing the depleted DA levels in the midbrain. However, DOPA treatment becomes increasingly ineffective after extended periods of treatment. The causes of PD remain unknown and death of DA neurons in PD cannot be reversed. Therefore, preventive strategies of dopaminergic cell death are essential to protect the aging population from PD.

There has been increasing evidence indicating that environmental factors and toxins together with defects in cellular protective mechanisms against oxidative stress may play roles in the etiology of PD (5,6). The finding that the neurotoxin 1-methyl-4-phenylpyridine (MPP^+) selectively kills dopaminergic neurons and causes PD-like symptoms in humans and other primates has led to its wide usage as a model for the investigation of the causes of PD. The specific dopaminergic toxicity of MPP^+ is thought to be due to the specific entry into dopaminergic cells through plasma membrane dopamine transporter (DAT) followed by the inhibition of mitochondrial complex I of the electron transport chain, leading to a decrease in cellular energy production (7). However, recent studies suggest that MPP^+ is taken up not only into dopaminergic cells, but also into other cells including non-neuronal cells through various transporters i.e. organic cation transporters (OCT) and non-specific plasma membrane

monoamine transporters (PMAT). Thus, the mechanism of the specific *in vivo* toxicity of MPP^+ towards dopaminergic neurons remains inconclusive. Since MPP^+ has been the most widely utilized model for non-familial PD research and pharmacological therapeutics development, understanding its mechanism(s) of uptake and specific toxicity to dopamine cells is of prime importance.

Neurodegenerative diseases can be modeled in animals so as to replicate the hallmarks of the diseases and are useful for testing therapeutic strategies. Most studies on specific toxicity of MPP^+ have been performed using animal models as well as midbrain slices since these models closely mimic the characteristics of CNS. However, since multiple MPP^+ uptake pathways are present in various cell types; these heterogeneous systems may not provide specific details on the mechanism of MPP^+ uptake and toxicity. On the other hand, cell lines exhibit a relatively high degree of homogeneity which would provide better molecular details to identify various proteins and factors responsible for the specific cellular uptake and toxicity of MPP^+. Although the findings from these transformed cell models may not be directly correlated with those of CNS, they may still provide important clues on the mechanisms of the specific toxicity of MPP^+ that are inaccessible with those complex heterogeneous systems. Without a doubt, findings from these transformed cell models can always be confirmed using neuronal primary cultures or animal models.

Human SH-SY5Y and mouse MN9D cell lines with distinct neurobiological characteristics are gaining popularity as models of dopaminergic neurons. Human SH-SY5Y cell- line is originated from a metastic neuroblastoma. SH-SY5Y cells express DAT, NET, and VMAT and synthesize, store, and release DA and NE. SH-SY5Y cells have been extensively used in the studies of various neurotoxins. Mouse MN9D cell line was derived from the fusion of

mouse embryonic venral mesencephalic and neuroblastoma cells which express high levels of TH and DAT. MN9D cells possess the major characteristics of CNS dopaminergic neurons and are a good model for CNS dopaminergic neurons. The adrenergic PC12 cell line is derived from pheochromocytoma of the rat adrenal medulla and is one of the most widely used cell models for the studies of catecholamine biosynthesis and metabolism. PC12 cells express high levels of TH and synthesize and store catecholamine neurotransmitters, DA and NE but do not convert NE to E. The non-neuronal human HepG2 cell line is a liver carcinoma cell line derived from the liver hepatocellular carcinoma. The HepG2 cell line has been widely used in the mitochondrial functions and dysfunction and the metabolism of various toxins since they are rich in mitochondria. Therefore, they are a good non-neuronal cell model for the comparative neurotoxicological studies. The overall goal of this research was to identify the protein(s) and factors that are responsible for the specific uptake and dopaminergic toxicity of MPP^+ using these model cell lines.

The specific aims of this research were (I) to characterize the uptake of MPP^+ into dopaminergic and non-dopaminergic cell lines, (II) to determine whether the MPP^+ toxicity is specific to dopaminergic cells and (III) to determine the mechanism of dopaminergic toxicity of MPP^+

CHAPTER II

BACKGROUND AND SIGNIFICANCE

2.1 Neurological Disorders

Neurological Disorder is any disorder that disrupts the normal function of the central nervous system. According to the American Academy of Neurology, there are more than 600 neurological disorders and one in every five Americans suffers from some form of neurological disorder. Some of the major types of neurological disorders are listed in table below (8):

Table 1: Major Types of Neurological Disorders

Type	Example
Neurogenetic Diseases	Huntington's Disease
Developmental Disorders	Cerebral palsy
Degenerative Diseases	Alzheimer's Disease and Parkinson's Disease
Metabolic Diseases	Gaucher's Disease
Cerebrovascular Disease	Stroke
Trauma	Spinal Cord and Head Injury
Convulsive Disorders	Epilepsy
Infectious Disease	AIDS

2.2 Parkinson's Disease

PD was first characterized by James Parkinson, the British physician, most famous in his most prominent article "An Essay on the Shaking Palsy" in 1817 (9,10). The key pathophysiologies of PD are the degradation of dopaminergic neurons and accumulation of cytoplasmic Lewy bodies (LB) in the substania nigra pars compacta. Numerous studies have shown that patients diagnosed with PD have a loss of 50-70% dopaminergic cells in the substantia nigra pars compacta (3-5). Dopamine (DA) is an important neurotransmitter that is responsible for voluntary (11) and involuntary (12) movements and cognition (13). PD

symptoms can generally be described as tremor, bradykinesia, rigid muscles, and change in speech. As mentioned above, one of the key pathophysiological hallmarks of PD is the accumulation of cytoplasmic Lewy bodies (LB) in the substania nigra pars compacta. LB are insoluble aggregates that mainly consist of insoluble fibrils made of α-synuclein, a small 14 kDa protein predominately expressed in neurons of the central nervous system, (14) and small amounts of ubiquitin and β-crystallin (5,15). Despite extensive research, the exact cause of PD is not known and there is no cure, and thus most treatments are developed to control the symptoms.

AD and PD are progressive neurodegenerative diseases that share some similarities, but are not related (5,16,17). Both diseases are distinct in mechanisms, symptoms, and treatments. PD is primarily a movement disorder resulting from the loss of DA-producing neurons in substantia nigra that is responsible for motor coordination (1). AD is a memory disorder in which areas that are responsible for learning and memory such as hippocampus and entorhinal cortex are being affected (18,19). In PD, the cholinergic system in the brain is primarily affected and with the progression of the diseases acetylcholine levels in the affected areas are gradually diminished (20).

Since most neurological diseases share similar pathological symptoms, the ability to make an accurate diagnosis of PD is difficult (21). The physician can perform the diagnosis based on the patient's neurological history and physical examination (5). Physicians may also treat the patients with L-DOPA to support the diagnosis since it alleviates the symptoms of PD temporarily (22). However, there is no standard diagnosis that can make an accurate diagnosis of PD (21,23). Biological markers such as blood tests or brain imaging could be used to confirm the diagnosis of PD (24).

There is increasing evidence that PD is caused by genetic and environmental factors, or a combination of both (5,6). While 5% of the PD population is known to be associated with genetic factors, the rest could be associated with environmental factors including toxic pesticides and environmental toxins (6). However, many animal studies have failed to completely reproduce the pathological and clinical features of PD using suspected pesticides and toxins. However, these studies have not been able to completely reproduce some selective pathological features of PD (25).

2.2.1 Oxidative Stress and PD

Oxidative stress refers to the physiological state in which the production of the intracellular reactive free radical species exceed their deactivation through intracellular natural antioxidants defense mechanisms (26). Free radicals are highly reactive and unstable chemical species which usually contain one or more unpaired electrons. Free radicals associated with oxygen, is referred to as reactive oxygen species (ROS), and the species that are associated with nitrogen referred to as reactive nitrogen species (RNS) are the two most common biological forms of free radicals (27,28). ROS such as superoxide ($O_2^{\bullet-}$), hydrogen peroxide (H_2O_2) and hydroxyl radical ($OH^{\bullet}$) and RNS such as nitric oxide ($NO^{\bullet}$), peroxinitrite ($ONOO^-$), nitrogen dioxide ($^{\bullet}NO_2$), dinitrogen trioxide (N_2O_3), and dinitrogen tetroxide (N_2O_4) can cause chemical modification to DNA, proteins, lipids and other biological molecules, and damage to membranes (29-31) leading to apoptotic and/or even necrotic cell death. Oxidative stress has been implicated in many cardiovascular disorders (32,33), cancers (34-36), and neurodegenerative diseases (37-39), and aging.

Although there are many pathways for the increased production of ROS, the mitochondria is responsible for the production of a large fraction of intracellular ROS. The uncoupling or inhibition of the electron transport chain could result in the partial reduction of O_2 to produce reactive oxygen species such as superoxide ($O_2^{\bullet-}$) and hydrogen peroxide (H_2O_2). Under physiological conditions, these species could be further broken down to highly reactive $OH^{\bullet}$ (40). In addition, activities of enzymes such as NADH oxidases and cytochrome P_{450} as well as conditions such as inflammation, smoking, UV radiation, toxins, and aging can lead to the excessive ROS production (41). In addition, redox active metals like iron and copper and organic compounds like quinones can also induce the excessive production of ROS (Scheme 1). For example, $Fe^{2+}$and Cu^{2+} ions induce the production of OH radicals from H_2O_2 through the Fenton reactions (equation 1). OH radicals can also form in the cells by Haber-Weiss reaction (equation 2).

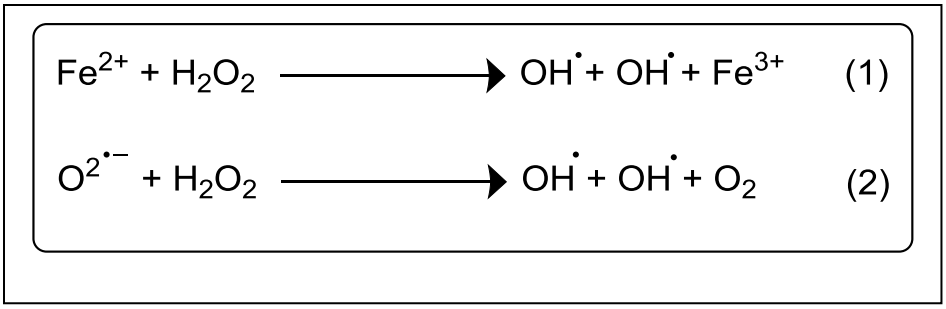

Scheme 1- The Fenton reaction (equation 1) and Haber-Weiss reaction (equation 2)

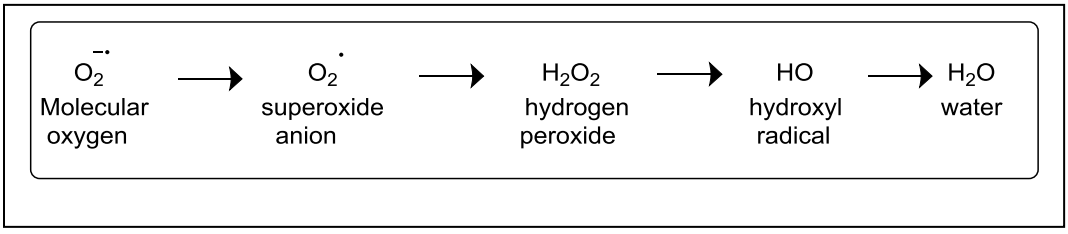

Scheme 2: Oxidants Formation by Electron Transfer Reactions

Under normal physiological conditions, anti-oxidant enzymes such as superoxide dismutase (SOD) and catalase, and glutathione peroxidase and small molecular antioxidants such as ascorbic acid, glutathione, and tocopherol can scavenge free radicals and protect cells from oxidative damage. For example, SOD catalyzes the conversion of superoxide into oxygen and hydrogen peroxide (equation 3) (Scheme 3) and catalase reacts with hydrogen peroxide to produce water and oxygen (equation 4). While high concentration of catalase is present in peroisomes, SOD is present in extracellular space, cytoplasm, and mitochondria.

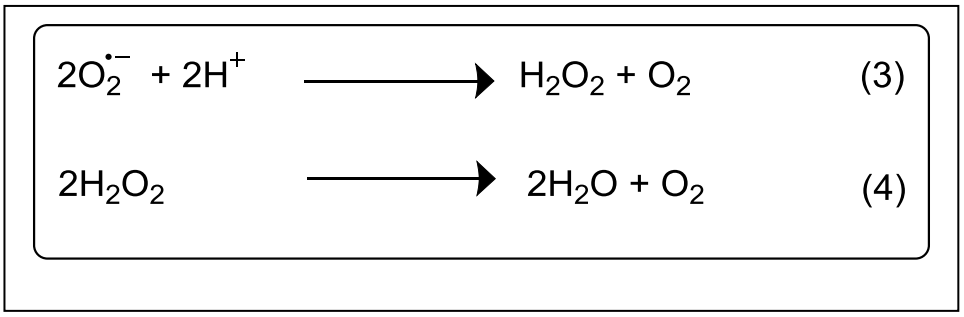

Scheme 3: Reactions catalyzed by superoxide dismutase (equation 3) and catalase (equation 4)

Increased oxidative stress is believed to be responsible for the toxicity of many toxins and pesticides that are implicated in neurodegenerative diseases (42). Increased oxidative stress is also implicated in several other diseases such as heart failure, atherosclerosis ischemia-reperfusion, endothelial dysfunction, hypertension (43), rheumatoid arthritis (44), and diabetes (45,46). However, Zhou, *et al.*, (47) and others have suggested that oxidative stress may not be the only contributor to the dopaminergic degeneration in PD.

2.2.2 Apoptosis and Necrosis Cell Death

The life span of a cell depends on the type of cell and older and damaged cells are being continually replaced with the new ones (48,49). When a cell is damaged or infected, it is removed through apoptosis or necrosis processes. There are three types of cell death; apoptosis,

necrosis, and autophagy (50). Apoptosis and necrosis are irreversible and programmed processes while autophagy is a reversible and programmed process. Necrosis and apoptosis differ in many observable morphological and biochemical changes, but the key difference is cell shrinkage occurs in apoptosis while cell swelling is a main characteristic of necrosis. Autophagy, on the other hand, involves vesicular sequestration of cytoplasmic proteins and organelles. The breakdown of cellular components may occur through nutrient starvation and infection. Formation of a membrane around a targeted region of the cell that separates the contents from the rest of the cytoplasm is the common mechanism of autophagy. This process is known as double-membrane vesicles or autophagosome formation (51).

Apoptosis is often implicated in neurodegenerative diseases (50,52) and is associated with specific cysteine proteases called caspases. There are many caspases that work together in the cell that can activate themselves and one another. Among the family of caspases, caspase-3 is a frequent mediator of apoptosis (53) and known to be implicated in PD (54,55). Especially, dopaminergic toxicity of neurotoxins like MPP^+ and 6-OHDA have been shown to involve the caspase-3 mediated apoptosis.

DNA fragmentation into multiples of ~200 bp oligonucleosomal fragments is one of the hallmarks of apoptosis (56). In human chromosome, histone and a DNA strand including ~180-200 bp are tightly joint to form one nucleosomal unit which is believed to drive DNA functions. In apoptosis, activation of nuclear endonucleases selectively cleave DNA at a site located between nucleosomal units (57). Therefore, under apoptotic conditions a DNA ladder containing multiples of 180-200 bp units is produced and can be easily detected in nuclear DNA cell extract by gel electrophoresis. Therefore, observation of the DNA ladder during cell death is widely used as a diagnosis for apoptosis.

2.3 Dopaminergic toxin 6-OHDA

The neurotoxin 6-hydroxydopamine (6-OHDA), first isolated by Senoh and Witkop (1959), is a structural analog of DA which can be taken up through monoamine transporters such as DAT and NET (58,59). 6-OHDA does not readily cross the blood-brain barrier, thus it has to be injected directly into the brain to observe the toxicity effect. The specific dopaminergic toxicity of 6-OHDA is proposed to be due to the uptake through DAT or NET into catecholaminergic cells followed by rapid oxidation in the cytosol leading to the excessive ROS production. Although 6-OHDA is structurally similar to DA, the presence of an additional hydroxyl group makes it highly susceptible to oxidation and toxic ROS production in catecholaminergic neurons (7). 6-OHDA is oxidized rapidly by molecular oxygen to form the superoxide anion, hydrogen peroxide, and ρ-quinone (scheme 4) (60). It has been shown that 6-OHDA is readily oxidized within matter of minutes to produce H_2O_2 and ρ-quinone in the extracellular fluid before it reaches the intracellular fluid (60-62). Therefore, a combination of production of ROS and ρ-quinone in the extracellular space is proposed to be responsible for the 6-OHDA induced cell death (61). Although, studies of 6-OHDA as a model have contributed to an understanding of the etiology of PD. 6-OHDA induces aphagia, adipsia, and seizures in animals limiting its usefulness as a PD model (59,63).

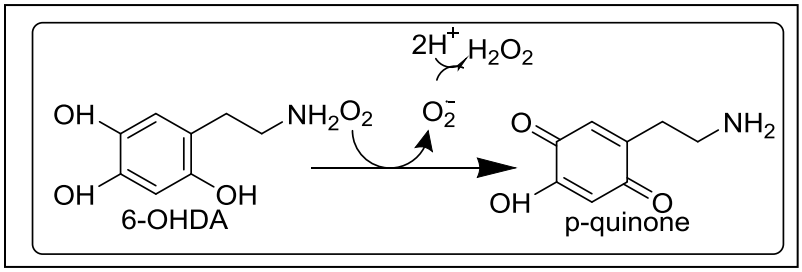

Scheme 4: 6-OHDA and ρ-quinone

2.2.4 MPTP and MPP^+

Barry Kidston was a chemistry graduate student at the University of Maryland who synthesized MPPP (Fig 1) as a street drug and injected it into himself and sold it to others (64). MPPP is a pethidine (Demerol) or meperidine analog. Pethidine or meperidine is generally used to treat moderate to severe pain. The synthetic analog MPPP is slightly less potent than morphine and has a shorter duration of the effect. Relative to pethidine, the ester group in MPPP is inverted (Fig 1). Within a week after taking a batch of the MPPP, Kidson and all the other users began to exhibit Parkinsonian like symptoms. Dr. J. William Langston treated the symptoms with a combination of L-DOPA and carbidopa, standard treatment for PD, and all patients responded to the treatment positively (64,65). It was later found that the particular batch of MPPP was contaminated with MPTP (Fig 1).

In the synthesis of MPPP, 1-methyl-4-piperidone (MP), the starting material, was mixed with phenyl lithium to convert to the intermediate product 4-hydroxyl-4-phenyl-N-methylpiperidine (HPMP) (Fig 2). The intermediate product was then reacted with propionic anhydride and acidified with sulfuric acid to produce the ester and desired product, MPPP. However, this synthesis is sensitive to temperature and acidity. If the conditions are not kept under tight control, then the ester group in eliminated product, MPTP, may be produced. It was believed that Barry Kidston may have performed this synthesis with increased temperatures and shorter reaction times, thereby inadvertently producing MPTP contaminated batches of MPPP. In 1982, Dr. J. William Langston first published the accidental discovery of the Parkinson-causing toxin MPTP and suggested that it may be a good model to study the mechanism of PD at the molecular level (66). However; despite all the studies, it was not clear at the time whether it was MPTP or a possible metabolite that elicited the Parkinsonian effects.

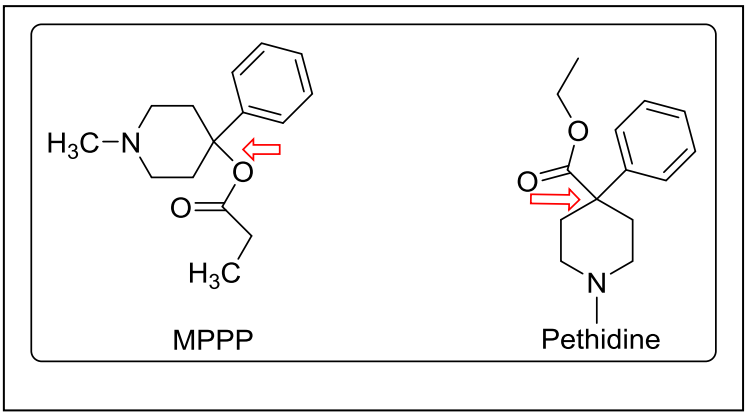

Figure 1: Structure of MPPP and Pethidine

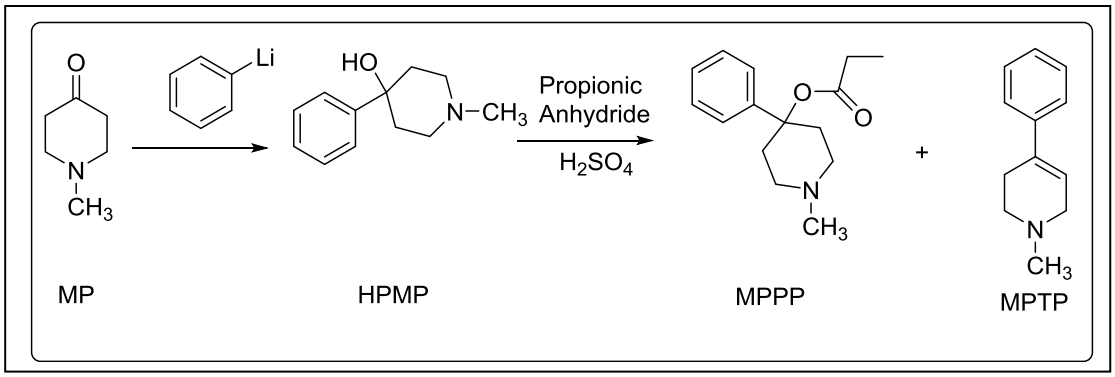

Figure 2: Synthesis of MPPP and MPTP

MPTP is a lipophilic compound that is known to cross the blood brain barrier (67), enters into the cerebrospinal fluid of the CNS (65,66,68), and become sequestered in the lysosomes of astrocytes and other cells. MPTP is then oxidized to the metabolite MPP^+ in a two-step biotransformation process. First, MPTP is oxidized by MAO-B which is highly abundant in astrocytes and serotonergic neurons to 1-methyl-4-phenyl-1, 2-dihydropyridinium ($MPDP^+$). $MPDP^+$ is then disproportionated to produce MPP^+ (69). Subsequent studies have shown that MPP^+, not MPTP, exerts its toxic effect to dopaminergic neurons. As mentioned above, the specific dopaminergic toxicity of MPP^+ is proposed to be due to the uptake through DAT

followed by the inhibition of complex I of the electron transport chain leading to the production of ROS and inhibition of the cellular energy production (22). In addition, MPP^+ may compete with cytosolic DA for synaptic vesicle VMAT-2 (70) leading to the increase of cytosolic DA and production of ROS (71).

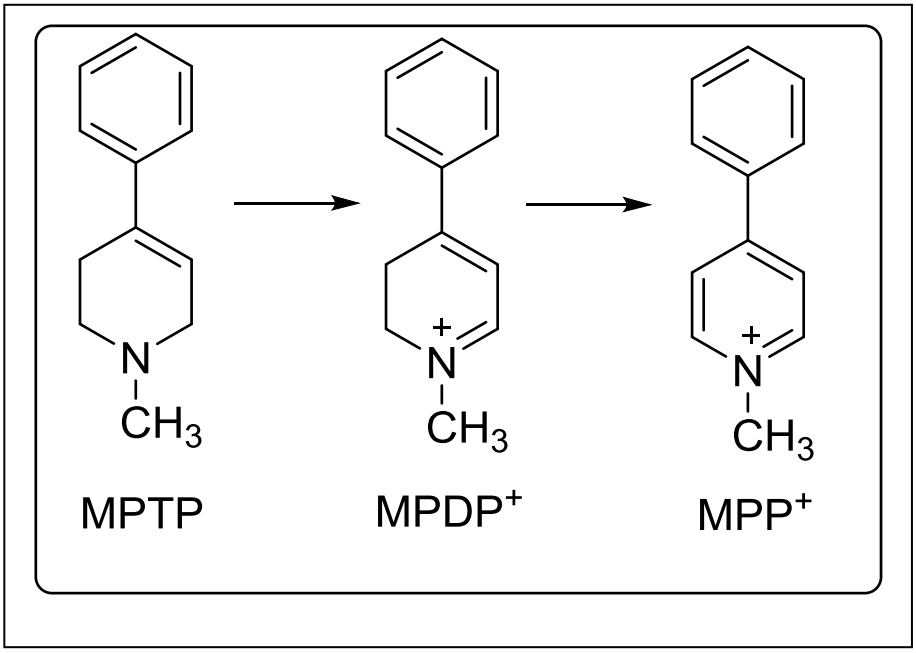

Figure 3: Conversion of MPTP to MPP^+

Despite extensive studies, MPTP/MPP^+ failed to develop LB (72), a key pathology in PD, but selectively destroyed dopaminergic cells in compacta of the substantia nigra as seen in PD.

2.2.5 Rotenone

Rotenone (Fig 4) is a naturally occurring substance derived from the roots of tropical plants (7). Rotenone is an effective herbicide as well as an insecticide. Similar to MPTP, rotenone is a lipophilic compound that can cross the blood brain barrier, accumulate in the cell,

and then effectively inhibits mitochondrial complex I of the electron transport chain with an IC_{50} at nanomolar range (73,74).

Takeshige and Minakami (75) demonstrate the production of superoxide ions in the bovine sub-mitochondrial particles by using rotenone. In addition, Li *et al.* (76) also demonstrate cell apoptosis induced by superoxide that was produced by rotenone in HL-60 cells. Hasegawa (77) demonstrated the superoxide production caused by MPP^+ as a complex I inhibitor.

Rotenone replicates almost all the hallmarks of PD including the LB formation (7).

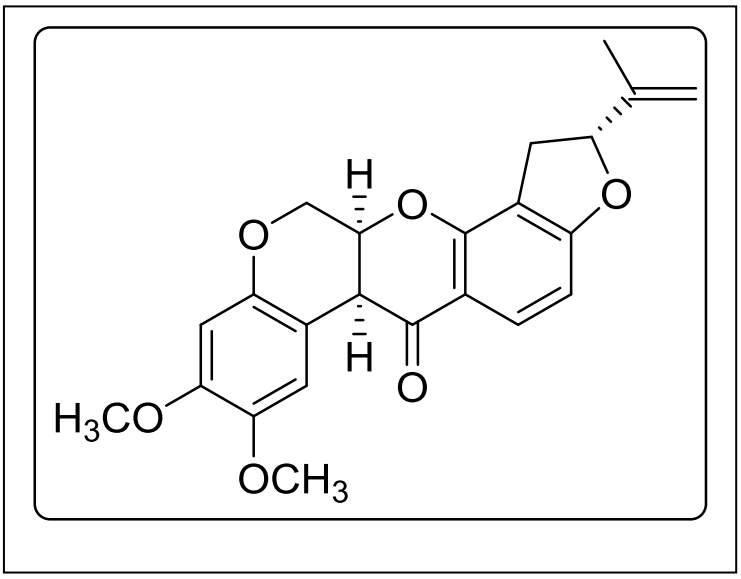

Figure 4: Structure of rotenone

2.2.6 Paraquat

Paraquat (1,1'-Dimethyl-4,4'-bipyridinium) (PQ) is a herbicide widely used in agriculture and structurally resembles to MPP^+ (7). PQ is synthesized by coupling pyridine using sodium and anhydrous ammonia to give 4,4'-bipyridine, which is then methylated with

chloromethane to give the desired product (Fig 5) (78). Although it was first synthesized in 1882, PQ's herbicidal properties were not recognized until 1955 (79). Despite its high hydrophilicity and positive charge, it has been shown to cross the blood brain barrier in mice (80). McCormack, *et al.*, (81) have demonstrated the neuroprotection against PQ by co-treatment of L-valine which is not observed with co-treatment of L-DOPA. Hence, it is believed that PQ cross the blood brain barrier through L-neutral amino acid transporter. Several *in vivo* studies using cell lines demonstrated the uptake of PQ is independent of DAT and does not interfere with DA uptake (82,83). Although PQ inhibits mitochondrial complex I of the electron transport chain, the IC_{50} of PQ is 7 mM compared to MPP^+ which has an IC_{50} of 30 μM making it highly unlikely that PQ effectively inhibits mitochondrial complex I under normal *in vivo* conditions (80). Nevertheless, it was able to replicate almost all the hallmarks of PD including the production of LBs (7).

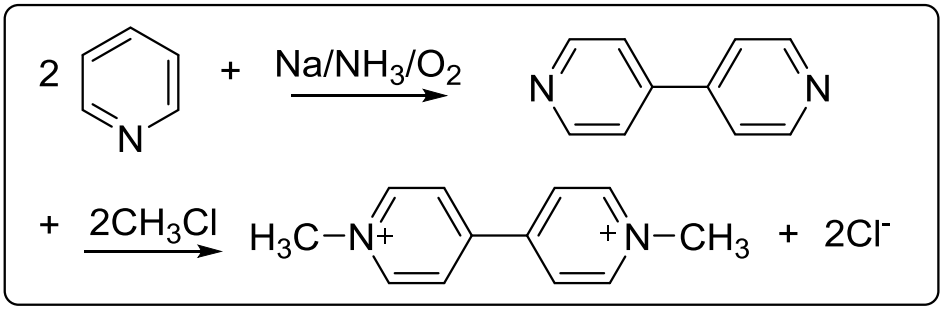

Figure 5: Synthesis of paraquat

2.3 DA and MPP^+ Uptake Mechanism(s)

MPP^+ has been known to deplete DA content and it is known to interfere with the uptake and storage of the DA (71,84,85). As stated above, selective dopaminergic toxicity of MPP^+ was proposed to be due to selective entry through DAT. Transfection gene knockout and other

studies have clearly demonstrated that DAT is the site of cellular entry of MPP^+ (86). Therefore, it is believed that DA and MPP^+ may have similar uptake mechanisms and properties.

2.3.1 Dopamine Transporter (DAT)

Dopamine transporter (DAT) is a Na^+/Cl^- dependent symporter that co-transports two Na^+ ions and one Cl^- ion into the cell for every one molecule of DA transported into the cell. It is constituted of 620 AA with the calculated molecular weight of 68,517 Da and 12 transmembrane segments. Both N- and C- termini are on the cytoplasmic face of the protein while three putative glycosylation sites are on the extracellular face (87,88). DAT may function in the reverse mode if the ionic gradients are altered, decreased $[Na^+]$ or $[Cl^-]$ (89). Therefore, it is critical to set the conditions and the composition of the extracellular medium closely to the physiological conditions in the laboratory testing of DAT activity. Giros, *et al.*, (90) determined K_m of dopamine and MPP^+ for DAT are approximately 1.2 μM ± 0.2 and 3.7 μM ± 0.3 in human neuroblastoma, respectively. However, recent studies show that in addition to DAT there are other transporters that may play a role in DA and MPP^+ uptake into dopaminergic cells (91-95).

2.3.2 Norepinephrine Transporter (NET)

Norepinephrine transporter (NET), similar to DAT, is a Na^+/Cl^- dependent symporter that is responsible for the reuptake of NE. NET can also take up DA as well as MPP^+. It contains 617 AA and 12 transmembrane segments with both N- and C- termini on the cytoplasmic face. There is also a large intracellular loop between the 3^{rd} and 4^{th} transmemebrane segments (96).

2.3.3 Organic Cation Transporter (OCT)

Wu, *et al.*, (97) reported MPP^+ uptake may alternatively occur through the organic cation transporter (OCT), a Na^+-independent bi-directional cation transporter which is expressed throughout the brain. Many drugs, toxins and compounds that carry a net positive charge at physiological pH are considered as "organic cations" and are substrates for OCTs (95,98). Three isoforms of OCT, OCT-1, OCT-2, and OCT-3, have been identified and characterized (99). These proteins also constitute 12 transmembrane segments, with both N- and C- terminus on the cytoplasmic face similar to DAT and NET with large intracellular and extracellular loops. OCT-1 and OCT-2 are mostly express in kidney, liver, and intestine (95,100) whereas OCT-3 is extensively expressed throughout the body including heart, placenta, and brain (95,97,101). All three OCT isoforms have been known to transport both MPP^+ and DA.

2.3.4 Plasma Monoamine Transporter (PMAT)

Plasma Monoamine Transporter (PMAT) is a protein of 530 AA residues containing 11 transmembrane segments, C-terminus in the extracellular face, N-terminus in the cytoplasmic face with a large intracellular loop (95,98). Similar to OCT, PMAT also can mediate the transport of various drugs, toxins, and others that carry a net positive charge at physiological pH. It is also a Na^+-independent reversible cation transporter. Engel, *et al.*, (98) determined the K_m of DA and MPP^+ are 329±8 μM and 33±7 μM, respectively. Therefore, it is a low-affinity, high-capacity plasma membrane transporter for catecholamines and MPP^+.

2.3.5 Vesicular Monoamine Transporter (VMAT)

Vesicular monoamine transporter (VMAT) is an integral membrane protein with an apparent molecular weight of 65-85 kDa and it is composed of 12 transmembrane segments with

both N- and C- terminus facing the cytosolic side of the membrane (102,103). VMAT is also proposed to have a large hydrophilic loop containing multiple putative N-glycosylation sites facing the vesicular side of the membrane (104). It is a non-specific antiporter that mediates an exchange of DA or other monoamines from the cytosol into the granule for H^+ ion. There are two isoforms of VMAT; VMAT-1 and VMAT-2. VMAT-1 is expressed in neuroendocrine cells (105) whereas VMAT-2 is expressed in the CNS and within the chromaffin granules of the adrenal medulla (102,106). VMAT utilizes the electrochemical and protein gradient to transport catecholamine into vesicles against a concentration gradient.

VMAT requires less structural specificity for transport than DAT and studies have shown that MPP^+ is a good substrate for VMAT (71,103). Accumulation of MPP^+ into the acidic granule causes rapid efflux of H^+ resulting in loss of the electrochemical gradient. This progress prevents an influx of DA and shuttles DA into the cytosol leading to the production of oxidative stress.

2.4 Regulation and Perturbation of Ca^{2+} Homeostasis

Neurons are excitable cells that transmit information through electrical and chemical signals (107). Ca^{2+}, one of the most widely used intracellular messengers, is responsible for many physiological functions in neurons. A large Ca^{2+} gradient exists across the plasma membrane. These gradients are actively maintained by various plasma membrane transporters and specific endoplasmic reticulum (ER) and mitochondria Ca^{2+} store pumps (108). Under resting conditions, free cytosolic Ca^{2+} levels are maintained in the range of 200-500 nM (109). Increasing Ca^{2+} influx, decreasing Ca^{2+} efflux, and release of Ca^{2+} from intracellular stores can elevate the cytosolic Ca^{2+} level to low micromolar level. This occurs transiently under normal

physiological activity and is usually harmless to the neurons. However, perturbation of Ca^{2+} homeostasis for an extended period of time may disrupt cellular functions and induce apoptosis in neurons (52,110). Although the exact mechanism of cell death under these conditions is not clearly understood, the increasing evidence suggests that there is strong correlation between perturbation of Ca^{2+} homeostasis and apoptotic cell death. Interestingly, Chen, *et al.* (111), have demonstrated an elevation of intracellular Ca^{2+} in response to 24 h MPP^+ treatment in mesencephalic neurons in the absence and presence of extracellular Ca^{2+} suggesting that MPP^+ perturbs Ca^{2+} homeostasis in these neurons. There are several other mechanisms that are implicated in the perturbation of Ca^{2+} homeostasis including alteration of cellular Ca^{2+} buffering capacity, deregulation of Ca^{2+} regulating proteins, and perturbation of energy metabolism (110).

2.4.1 Ca^{2+} buffering proteins

To date, more than 200 cellular proteins that bind and buffer Ca^{2+} have been identified (112-117). Although the function of some of these proteins such as calbindin-D28k and parvalbumin have not been fully understood, many studies have reported the alterations in the expression of these proteins perturb Ca^{2+} homeostasis and may have serious implication in neurodegenerative diseases (118). Nevertheless, decrease in Ca^{2+} binding protein expression, reduces neuron's ability to buffer cytosolic free Ca^{2+}, resulting in an initiation of irreversible apoptosis (119). Thus, the Ca^{2+} buffer proteins may have a neuroprotective role.

2.4.2 Ca^{2+} Influx and Efflux

There are several pathways that may allow Ca^{2+} entry into cytoplasm including the activation of the voltage-gated Ca^{2+}channels and ligand-gated receptors. These will cause the

increase of cytosolic Ca^{2+} by opening the plasma membrane Ca^{2+} channels or the release of stored Ca^{2+} from ER and mitochondria.

2.4.2.1 Voltage-gated Ca^{2+}channels (VGCC)

Voltage-gated Ca^{2+}channels (VGCC) are expressed on the membrane of excitable cell and regulate cellular processes, such as cell contraction, gene transcription, synaptic plasticity, and also modulate neuronal firing, memory, vision, and hormone secretion (120). Under resting conditions, membrane potential is in the range of -50 mV to -70 mV (121). This potential is maintained by electrogenic Na^+/K^+ ATPase in which 3 Na^+ ions are being pumped out for every two ions of K^+ pumped in, resulting in a negatively charge inside relative to the outside. Under these conditions, the membrane is said to be polarized. The opening of VGCC occurs by the influx of positively charged ions such as Na^+ or efflux of negatively charged ions such as Cl^- which increases the membrane potentials and depolarizes the cell membrane. While the Ca^{2+} ion concentration in the extracellular space is ~1.5 mM, the cytosolic Ca^{2+}ion concentration inside, is very low (~100 nM) (122). Thus, the opening of VGCC will allow spontaneous Ca^{2+}ion influx (123). The sudden and sharp increases in the intracellular Ca^{2+} concentration lead to the initiation of a number of Ca^{2+} sensitive pathways including exocytotic release of neurotransmitters.

VGCC are broadly classified as high voltage-active (HVA) and low voltage-active (LVA) and further sub-grouped into L, P/Q, N, R and T-types based on their pharmacological properties and AA sequences. High voltage-active are long-lasting when the membrane potential rises to -30 mV; low voltage-active are short-lasting and activate when the membrane potential rises to -70 mV (120,124,125). L-type Ca^{2+} channels are expressed in heart, smooth muscles,

retina, and neurons. P, Q, and N-type Ca^{2+} channels are expressed in neurons. T-type Ca^{2+} channels are exclusively found in cardiac tissues and neurons.

2.4.2.2 Na^{+}/Ca^{2+} Exchanger Channels (NCX)

In addition to VGCC, there are other channels and transporters that are associated with the regulation of Ca^{2+} levels. Na^{+}/Ca^{2+} Exchangers (NCX) use Na^{+} concentration gradients to mainly extrude excess Ca^{2+} from the cytosol (forward mode) (126). There are main 3 isoforms of NCX transporters (NCX1, NCX2, and NCX3) that have been detected in most brain areas (127). These transporters may operate in the forward and reverse direction depending on the physiological conditions of the cell. It transports three Na^{+} ions out against the electrochemical gradient across the membrane in exchange for the counter-transport of one Ca^{2+} ion into the cytosol (reverse mode). It also transports three Na^{+} ions into the cell along the concentration gradient in exchange for one Ca^{2+} ion out of the cells (forward mode).

2.4.2.3 Transient Receptor Potential Channels (TRP)

Transient Receptor Potential (TRP) Channels are non-selective cation channels that are permeable to monovalent and divalent cations and expressed widely in neuronal tissues (128,129). Several studies have confirmed that several TRP channels are tetrameric. The transmembrane domain of each TRP channel subunit contains 6 putative transmembrane segments (129,130) with both N- and C- termini on the cytoplasmic face of the protein. Between the 5^{th} and 6^{th} transmembrane segment, there is a pore-forming loop. There are 28 TRP channels which have been identified in mammalian cells and they can be classified into 6 broad subfamilies based on their amino acid sequence locations and functions. They are TRPC (canonical; 1-7), TRPV (vanilloid; 1-6), TRPM (melastatin; 1-8), TRPP (polycystin; 1-3),

TRPML (mucolipin; 1-3), and TRPA (ankyrin; 1). All TRP channels except TRPM4 and TRPM5 have been found to mediate the transmembrane transport of Ca^{2+} ions. However, many of these TRP channels have low affinity for Ca^{2+} in comparison to Na^{+}. TRPV5 and TRPV6 channels have about 100 times more affinity for Ca^{2+} than Na^{+}. The mechanisms of the activation of TRP channels widely differ from each other with respect to the stimuli and their specific function. For example, TRPC channels can be activated by the activation of phospholipase C causing the increase of the level of diacylglycerols or decreasing the level of phosphatidylinositol 4, 5-bisphosphate through the depletion of intracellular Ca^{2+} stores. On the other hand, TRPM channels are activated by temperature. TPRC1 and TRPC6 channels have been implicated in neurodegenerative diseases; for example reduced expression of TRPC1 is observed in brain lysate of patients with PD (131) and down-regulation of TRPC6 is shown to lead to neuronal cell death (132).

2.4.2.4 Intracellular Ca^{2+} Stores

There are several intracellular organelles that store and release Ca^{2+}. As mentioned above, Ca^{2+} release from the endoplasmic reticulum (ER) and the mitochondria may elevate the cytosolic Ca^{2+} levels. Therefore, intracellular and extracellular Ca^{2+} transport is strictly regulated by specific receptors and transporters present on both intracellular organelles (121,122) and the plasma membrane. ER, one of the largest intracellular organelles, mainly store and release Ca^{2+} upon the activation of the receptors. There are two main pathways that are associated with the Ca^{2+} released from the ER into the cytoplasm, namely "storage-operated Ca^{2+}entry" (SOCE) (133) and "Ca^{2+}-induced Ca^{2+}release" (CICR) (134). First, Ca^{2+} and inositol 1, 4, 5-triphosphate (IP_3) together activate the IP_3-receptor on the ER causing the release of Ca^{2+} from ER to the cytoplasm (SOCE). Secondly, Ca^{2+} binds to the ryanodine receptor on the membrane of the ER,

resulting in release of Ca^{2+} from the ER to the cytoplasm (Ca^{2+}-induced Ca^{2+}). The concentration of Ca^{2+} in the ER is in the millimolar range. Mitochondria is the powerhouse of the cell and takes up excess Ca^{2+} through the uniporter or mitochondrial NCX and reduces the cytosolic Ca^{2+}concentration. The main mitochondrial Ca^{2+}transporter is the uniporter which is an ATP-dependent transporter (135).

2.4.2.5 Store Operated Ca^{2+} Entry (SOCE)

Store Operated Ca^{2+} Entry (SOCE) is the plasma membrane Ca^{2+}-influx channel that is widely expressed in almost every tissue (136). There are two families of proteins that regulate SOCE; STIM and Orai molecules. STIM acts as a Ca^{2+}sensor on the ER while Orai acts as the pore-forming subunits of SOCE channels (137). When Ca^{2+}ions are depleted in ER, STIM molecules from ER relocate themselves near the plasma membrane leading to the activation of ORA1 Ca^{2+}-influx channels.

2.4.2.6 Plasma Membrane Ca^{2+} ATPase (PMCA)

Plasma membrane Ca^{2+} ATPase is responsible in maintaining a very large concentration of gradient about 10,000 between the cytoplasm and the extracellular matrix (138). When cytosolic Ca^{2+} levels are elevated due to the release of Ca^{2+} from intracellular stores or influx of Ca^{2+} from extracellular matrix, it is necessary to remove the excess cytosolic Ca^{2+} to low cytosolic Ca^{2+} levels. Under these conditions, Ca^{2+}-ATPase pump excess Ca^{2+} from the cell against a concentration gradient at the expense of ATP hydrolysis. Ca^{2+} ATPase consists of 10 transmembrane segments with N- and C- termini on the cytoplasmic face (139) and expresses on the plasma membrane (140) and ER (139) of all these cells. In the case of ER or mitochondria,

Ca^{2+}-ATPase transfers Ca^{2+} from the cytosol of the cell to the lumen of the ER or to the mitochondria matrix against the gradient concentration at the expensive of ATP hydrolysis.

2.5. Inhibitors

The underlying mechanisms of MPP^{+}-induced neurotoxicity remain elusive and many studies suggest that multiple pathways including perturbation of Ca^{2+} metabolism may be involved. In order to test some of these possibilities, we have used a number of well characterized pharmacological agents that are known to interfere with the Ca^{2+} metabolism in the cells. The known pharmacological properties of these agents are listed in Table 2.

Table 2: Pharmacological agents known to perturb the Ca^{2+} metabolism in the cell

Inhibitor	Function	Reference
2-Aminoethoxydiphenylborane (2-APB)	IP_3 antagonist At low concentration: stimulate SOCE At high concentration: inhibits SOCE, TRPC1, TRPC3, TRPC5, TRPC6, TRPV6, TRPVM3, TRPM7, TRPM8, and TRPP2 inhibitor At high concentration: stimulate TRPV1, TRPV2, and TRPV3	Maruyama (1997)(141) Xu (2005)(142) Bai (2006)(143) Togashi (2008)(144) Varnai (2009)(145)
BAPTA-AM	Membrane permeable Ca^{2+}chelator	Tang (2007)(146)
Benzamil	T-type VGCC inhibitor NCX inhibitor TRPP3 inhibitor	Fischer (2002)(147) Dai (2007)(148) Page (2007)(149)
CGP 37157	Mitochondrial NCX inhibitor	Cox (1993)(150)
Desipramine	NET Inhibitor	Torres (2003)(151)
EGTA	Ca^{2+} Chelator	Boullerne (2001)(152)

Table 2 (continued)

Flufenamic Acid	Activate TRPC6 TRPC3 and TRPC7 inhibitor	White and Aylwin (1990)(153) Foster (2009)(154) Tu (2009)(155) Chi (2011)(156)
Gadolinium	T-type VGCC inhibitor	Mlinar (1993)(157)
GBR 12909	DAT Inhibitor	Rothman (2008)(158)
Mefenamic Acid	Derivative of Flufenamic Acid	Keinanen (1978)(159)
Mibefradil	T-type VGCC inhibitor L-type VGCC inhibitor	Mehrke (1994)(160)
Nickel	T-type VGCC inhibitor	Mlinar (1993)(157)
Nitrendipine	L-type VGCC inhibitor	Watanabe (1995)(161)
SKF 96365	TRPC Channels inhibitor SOCE (STIMI) inhibitor	Varnai (2009)(145)
Tetradotoxin	Voltage-gated Na^{+} channel Inhibitor	Lee (2008)(162)
Thapsigargin	Inhibits Ca^{2+} ATPase of ER	Yu (1998)(163)
Tolfenamic Acid	Derivative of Flufenamic Acid	Keinanen (1978)(159)
Verapamil	PMAT inhibitor L-type VGCC inhibitor	Engel and Wang (2005)(95) David and Bauer (2012)(164)

2.6 Catecholaminergic Neuronal as Cell Models

2.6.1 Cell Culture

The cell Culture model serves numerous purposes such as studying passive and active transport of drugs, cell physiology, protein expression, and *in vitro* toxicity tests (165). Cell culture refers to one derived from dispersed cells derived from an original tissue, from a primary tissue, from a cell line, or from a cell strain by enzymatic, mechanical, or chemical disaggregation (166). Primary culture refers to cells that are obtained from a tissue or tumor.

Unlike tumor cells, most of the primary cell cultures have limited life. When a primary culture is sub-cultured or passaged, it becomes a cell line.

Mammalian cells are grown in suspensions or adherent cultures and maintained typically at 37˚C and 5% CO_2. Culture conditions vary widely for each cell type. Growth media, one of the culture conditions, can vary in pH, glucose concentration, growth factors, and other nutrients. Once cells are grown to their confluence layer, that is when all the available growth area is utilized and cells make close contact with one another, they need to be sub-cultured. The cell culture growth media is changed every 2-3 days until the cells grown confluently.

2.6.2 PC12 Cells

PC12 cells are derived from pheochromocytoma of the rat adrenal medulla (167) which was established by Green and Tischler in 1976. PC12 cells express DAT (168,169); therefore this cell is widely used to investigate MPP^+ toxicity mechanisms. K. Chiasson, *et al.* (168), demonstrated that GBR12909, an inhibitor of DAT, was not able to completely reverse PC12 cell death induced by MPP^+. Bromocriptine, a DA agonist, significantly raised DAT protein expression in PC12 when treated for 24 h and intensified MPP^+-induced cell death. GBR12909 completely abolished the enhanced cell death induced by bromocriptine on MPP^+ toxicity. These findings may suggest that MPP^+ toxicity may be both dependent and independent of DAT.

PQ and rotenone are potent inhibitors of mitochondrial complex I of the electron transport chain and PQ is structurally similar to MPP^+. Under similar conditions, Klintworth, *et al.* (170), show that PC12 is more sensitive to PQ than to rotenone; although there are reports that rotenone causes cell death in PC12 (171,172). The reason for cell death caused by rotenone from other studies may be due to higher concentrations or longer periods of incubation time of

rotenone. Richardson, *et al.* (83), demonstrate that unlike MPP^+, toxicity of PQ is DAT-dependent. However, Rappoid, *et al.* (173), demonstrate toxicity of PQ is DAT-independent. Therefore, the role of DAT in PQ toxicity remains inconclusive.

2.6.3 SH-SY5Y Cells

The human neuroblastoma cell line, SH-SY5Y, is the thrice cloned subline of SK-N-SK cells. SK-N-SK cells are the parent cell line that was first subcloned as SH-SY, which was subcloned again as SH-SY5, then subcloned a third time to produce the SH-SY5Y cell line (174).

When SH-SY5Y cells are treated with a high concentration of MPP^+ for 72 h, they undergo cell death with clear morphological evidence of apoptosis. However, neurotoxicity of SH-SY5Y cells requires higher concentrations of MPP^+ than those needed for mesencephalic cultures; e.g. 5 mM MPP^+ for 12 h (175) or prolonged treatment of low concentration of MPP^+ (5 μM for 4 days) (176) or 1 mM for 3 days (177). Perhaps the requirement of cell death is due to the low expression of DAT in SH-SY5Y cells rather than the speculation of MPP^+ toxicity being independent of DAT.

Sorensen, *et al.* (178), demonstrated an elevation of intracellular Ca^{2+} caused by MPP^+ at concentrations lower than the lethal concentration in SH-SY5Y cells and the elevation of intracellular Ca^{2+} is effectively blocked by Nifedipine, a L-type Ca^{2+} channel blocker. This finding may suggest that intracelluar Ca^{2+} may play an important role in MPP^+ neurotoxicity of Ca^{2+} and the prevention of perturbating the concentration of intracellular Ca^{2+} may be critical in cellular protection.

2.6.4 MN9D Cells

MN9D cell is an immortalized cell-line that is derived from the fusion of mouse embryonic ventral mesencephalic cells (rostral mesencephalictegmentum –RMT) and neuroblastoma cell line (N18TG2) (179). This cell line is widely used as a cell model to investigate the toxicity mechanism of MPP^+ because it expresses monoamine transporters; e.g. DAT, NET, and VMAT-2 (180) that are known to be a better substrate for MPP^+.

2.7 HepG2 Cells as Non-neuronal Cells

HepG2 cell is a human liver carcinoma cell line derived from the liver tissue of a fifteen year old Caucasian American male with a well differentiated hepatocellular carcinoma. Since this cell line does not synthesize catecholamines, it can generally be used as a non-neuronal model. Qi, *et al.* (181), demonstrated the cytotoxicity of DA in PC12, SH-SY5Y, and HepG2 and found that treatment of 500 μM DA for 24 h is toxic to both PC12 and SH-SY5Y cells while the toxicity of DA is not observed in HepG2 cells. HepG2 cells predominately express OCT1 that is known to be a better substrate for MPP^+ (182).

CHAPTER III

EXPERIMENTAL METHODS

3.1 Materials

All reagents and supplies were purchased from Fisher Scientific (Pittsburg, PA, USA), Sigma-Aldrich (Milwaukee, WI, USA), or Torcis (Bristol, United Kingdom) unless otherwise noted. Fetal bovine serum (FBS) was purchased from Valley biomedical (Winchester, VA, USA). F-12K medium and horse serum (HS) were purchased from American Type Culture Collection, ATCC (Manassas, VA, USA). All the solutions were prepared in Milli Q-deionized water (Millipore, Billerica, MA, USA). When DMSO was used as co-solvent, final DMSO concentration was kept to a minimum usually < 0.5% volume. KRB-HEPES contained 109.5 mM NaCl, 5.34 mM KCl, 0.77 mM NaH_2PO_4, 1.3 mM $CaCl_2$, 0.81 mM $MgSO_4$, 5.55 mM Dextrose, 25 mM HEPES, pH 7.4. KRB-HCO_3^- contained 109.5 mM NaCl, 5.34 mM KCl, 0.77 mM NaH_2PO_4, 1.3 mM $CaCl_2$, 0.81 mM $MgSO_4$, 5.5 mM Dextrose, 44 mM $NaHCO_3$. In experiments where Na^+ free incubations were necessary, Na^+ salt in the incubation media was replaced with equimolar concentrations of Lithium, N-methyl-D-glucamine, or Choline. Ca^{2+} in the incubation media was replaced with equimolar concentrations of EGTA (for further details see individual Figure legends).

3.2 Instrumentation

UV-visible spectra were recorded on a Cary Bio 300 UV-visible spectrophotometer (Varian, Inc). Fluorescence emission spectra were recorded on a JobinYvon-Spex Tau-3 spectrophotometer (ISA Instruments, Inc). Analysis of catecholamines was analyzed using reversed-phase HPLC with electrochemical detection (HPLC-EC) on a C_{18} reversed-phase

column. HPLC-EC analyses were performed using ESA Model 582 solvent delivery module and Coulochem-II electrochemical detector with ESA 501 chromatographic software (ESA, Chelmsford, MA, USA). Reversed-phase HPLC with ultraviolet detection (HPLC-UV) analyses were performed on a Spectra System P4000 gradient pump equipped with a SCM 1000 vacuum degasser coupled to an LDC Analytical SM 4000 UV detector using a C_{18} reversed-phase column (Supelco). Elution buffer consisted of a 48:52 ratio of 20mM CH_3COOH, 20mM H_3PO_4, 30mM TEA, pH 7.0: CH_3CN. Flow rate was 0.8 mL/min. Intracellular Ca^{2+}levels are measured using a Nikon ECLIPS-Ti microscope equipped with a Nikon S FLURO 40X lens.

3.3 Methods

3.3.1 Cell Culture

Rat pheochromocytoma PC12 and human neuroblastoma SH-SY5Y cell lines were purchased from ATCC (Manassas, VA). The mouse hybridoma MN9D cell line was a generous gift from Dr. Alfred Heller's Lab at University of Chicago. Human hepatocellular liver carcinoma HepG2 cells were obtained from Dr. Tom Wiese (Fort Hays University, Hays KS). All cell lines except PC12 were grown in high-glucose Dulbecco's Modified Eagle's Medium (DMEM) and 50 μg/mL streptomycin and 50 (4500 mg/L) supplemented with 10% FBS at 37˚C and 5% CO_2 in humidified air. PC12 cells were grown in F-12K medium supplemented with 2.5% FBS and 15% HS at 37˚C and 5% CO_2 in humidified air. All cell lines except PC12 were cultured in 100 mm^2 Falcon tissue culture plates until they reach to approximately 80% confluence. PC12 were cultured in 100 mm^2 Biocoat tissue culture plates coated with rat tail collagen type I until they reach to approximately 80% confluence. Cells were fed three times

weekly, passaged by incubation in Trypsin-versene, and then seeded into approximately-sized multi-well plates.

3.3.2 Differentiation of MN9D cells

Differentiation of MN9D cells were carried out using *n*-butyrate according to the published procedure of Choi *et al.* (179). Briefly, MN9D cells were seeded at a density of 0.1 x 10^6 cells/well in 6-well culture plates and were treated with 1 mM *n*-butyrate for 3 days in DMEM media, at which time the media was replaced with fresh 1 mM *n*-butyrate containing media and incubated for an additional 3 days. All differentiated cells were used in appropriate experiments after the 6^{th} day of differentiation. All experiments with differentiated MN9D cells were carried out using the same protocol outlined above for undifferentiated cells.

3.3.3 Measurement of Cellular Uptake of MPP^+, 3'OH-MPP^+, and 4'I-MPP^+

Cells were seeded into 12 well plates and grown to 70-80% confluence. The media was removed, cells were washed with KRB, and a solution containing the desired concentration of MPP^+ (or 4'I-MPP^+ or 3'OH-MPP^+) in warm KRB-HEPES (or KRB-$H_2CO_3^-$ depending on the experiment) was added and incubated for the desired period of time at 37°C. After the incubation, the media was removed and cells were washed three times with ice-cold KRB-HEPES, gently scraped, and collected in 1.0 mL of ice-cold KRB-HEPES. Aliquots were removed for protein assay and the remainder was centrifuged for 3 min at 6,000 rpm at 4 °C. The cell pellet was suspended in 75 µL of 0.1 M $HClO_4$ and centrifuged at 13,200 g for 8 min at 4 °C. The MPP^+ (or 3'OH-MPP^+) in acidic extracts were separated by reversed-phase HPLC-UV with UV detection at 295 nm (288 nm for 3'OH-MPP^+ and 310 nm for 4'I-MPP^+) using a solvent system containing 46 % buffer [20 mM Na_3PO_4, 20 mM CH_3CO_2Na, 30 mM triethylamine, pH

7.0 (adjusted with NaOH)] and 54% CH_3CN at a flow rate of 0.8 mL/min and quantified using a standard curve constructed based on the peak areas of MPP^+ (or 4'I-MPP+ or 3'OH-MPP^+) under identical separation conditions. All MPP^+ (or 4'I-MPP^+ or 3'OH-MPP^+) levels were normalized to the respective protein concentrations and all the readings were corrected for non-specific membrane binding by subtracting the corresponding zero time point readings for each MPP^+ (or 4'I-MPP^+ or 3'OH-MPP^+) concentration (normally < 1-2% of the intra-cellular concentration). Protein contents of the samples were determined by the Bradford method (183). MPP^+ uptake experiments with differentiated MN9D cells were carried out using the same protocol.

3.3.4 Quantification of the inhibition of MPP^+ Uptake by various inhibitors

Cells were grown in 12-well plates as described above and were incubated with the desired concentration of the inhibitor in KRB-HEPES or KRB-$H_2CO_3^-$, pH 7.4 (depending on the experiment) for 10 min. Then, the desired concentration of MPP^+ or derivatives of MPP^+ was added, incubated for the desired period of time, and the intracellular MPP^+ content was determined by the HPLC-UV as described above. All MPP^+ levels were normalized to the respective protein concentration of each sample.

3.3.5 Quantification of the reverse transport of MPP^+ from MPP^+ loaded cells

Cells grown in 12-well plates were treated with 100 μM MPP^+ in Ca^{2+}-free KRB-HCO_3^- at pH 7.4 for 1 h. Then the incubation media was remove and cells were washed with KRB-HCO_3^-, incubated under the desired conditions for 1.5 h at 37 °C (*see* figure legends for further details), and the remaining intracellular MPP^+ content was quantified by the HPLC-UV as described above. All MPP^+ levels were normalized to the respective protein concentrations.

3.3.6 Measurement of the inhibition of reverse transport of MPP^+ by uptake inhibitors

All cells were grown in 12-well plates as describe above and were incubated with 100μM MPP^+ in Ca^{2+} free KRB-HCO_3^-, pH 7.5 for 1 h. Then the incubation media was removed and cells were washed with MPP^+-free media and incubated for 90 min under the desired conditions in the presence of the inhibitor and the content of intracellular MPP^+ was quantified by HPLC-UV as described above (*see* the corresponding figure legends for further details). All MPP^+ levels were normalized to the respective protein concentrations.

3.3.7 Measurements of Intracellular $[Ca^{2+}]_i$

Cells were grown in 35 mm glass bottomed culture plates, washed with Ca^{2+} free KRB-HEPES, pH 7.4, and incubated with 15 μM Fura-2AM and 0.3% *v/v* pluronic acid for 20 min at 37°C in the same buffer, in the dark. Cells were washed and incubated in 1.0 mL of Ca^{2+}-free KRB-HEPES for an additional 20 min at room temperature in the dark and were placed on the stage of a Nikon ECLIPS-Ti microscope equipped with a Nikon S FLURO 40X lens. The regions of interests (ROI) were selected (20-30) based on the uniformity of fluorescence emission at 540 nm for 340 and 380 nm excitations and the baseline 540 nm emission intensity ratio at 340 and 380 nm excitations (F_{340}/F_{380}) were recorded for 3 min. Then the $[Ca^{2+}]$ of the incubation media was rapidly changed to the desired concentration by carefully and quickly adding a 2.0 mL of Ca^{2+}containing buffer and continued to record the F_{340}/F_{380}ratio for a desired period of time. Raw intensity data were corrected for background and the corrected F_{340}/F_{380} ratios were used to estimate $[Ca^{2+}]_i$.

3.3.8 Protein Determination

Protein contents of various cell preparations were determined by the method of Bradford (183) using bovine serum albumin as the standard. Samples of cell suspensions (50 μL) in KRB-HEPES were incubated with 950 μL of Bradford protein reagents for 10 min and absorbance a 595 nm was measured. The protein concentrations were determined using a standard curve constructed using bovine serum albumin.

3.3.9 Data Analysis

All quantitative uptakes were normalized to protein content of individual incubations to correct the results for the variations of cell densities between individual experiments. All the experiments were carried out in triplicates for 3-5 times and average of all the data or a set of representative data are shown. The error bars represent the standard derivations of the data.In the experiments where uptake or inhibition kinetic parameters were determined, the means of the experimental data were directly fitted to the hyperbolic form of Michaels-Menten equation.

3.3.10 Cell Viability Measurements

Cellular toxicity of MPP^+ was determined by using the MTT [(3-(4,5-dimethylthiazol-2-yl)-2,5-diphenyl tetrazolium bromide)] cell viability assay. Cells were seeded into 96-well plate and grown 2-3 days to achieve about 70-80% confluence. Cells were treated with the desired concentration of MPP^+ in a total volume of 50 μL in KRB-HCO_3^- buffer and incubated for desired timeat 37˚C. After the incubation period, 10 μL of 5 mg/mL MTT solution was added to each well and plates were incubated for 2 h at 37˚C. The resulting intracellular formazan was solublized by incubating overnight at 37˚C with 210 μL of detergent solution containing 50% DMF and 20% SDS. Cell viabilities were measured by quantifying reduced MTT by measuring

the difference in the absorbance at 570 nm and 650 nm. Results are expressed as % viability of untreated controls.

3.3.11 Toxicity Studies of MPP^+ by various inhibitors

Cells were grown in 96-well plates as describe above and were incubated with the desired concentration of the inhibitor in KRB-HEPES or KRB-$H_2CO_3^-$, pH 7.4 (depending on the experiment) for desired time. Then, the desired concentration of MPP^+ or derivatives of MPP^+ was added, incubated for the desired period of time, and cell viability was determined by the MTT assay as described above. Results are expressed as percentage of MPP^+-untreated control subjects.

3.3.12 Toxicity Studies of Reverse-Transport of MPP^+ from MPP^+-loaded cells

Cells were grown in 48-well plates as described above and were incubated with 0-500 μM MPP^+ in the absence of both $[Ca^{2+}]_o$ and $[EGTA]_o$ KRB-HCO_3^-, pH 7.4 for 1 h. Then, the incubation media was removed and cells were washed with MPP^+ free media and incubated for 15 h under the desired conditions. Cell viability was determined by the MTT assay as described above. Results are expressed as percentage of MPP^+- untreated control subjects.

3.3.13 Toxicity Studies of Reverse-Transport of MPP^+ from MPP^+-loaded cells with various inhibitors

Cells were grown in 48-well plates as described above and were incubated with 0-500 μM MPP^+ in the absence of both $[Ca^{2+}]_o$ and $[EGTA]_o$ KRB-HCO_3^-, pH 7.4 for 1 h. Then the incubation media was removed and cells were washed with MPP^+ free media and incubated for 15 h under the desired conditions in the presence of the inhibitor. Cell viability was determined by the MTT assay as described above. Results are expressed as percentage of MPP^+-untreated and control subjects.

3.4 Western Blot

Cells were grown in 100 mm^2 plate to 70-80% confluence. Cells were washed with PBS, harvested and centrifuged at low speed. The pellets containing OCT, NCX, or PMAT were solubilized with 50 mM Tris, 150 mM NaCl, 1% Triton X-100, and 2.5% protein inhibitor cocktail (Sigma), pH 7.5, for 1 h at 4 ^oC. After the incubation, the samples were centrifuged for 10 min at 1200 g and the supernatants were used for the Western blotting experiments.

Samples of solubilized proteins (100 μg) were boiled in Laemmli buffer for 5 min and subjected to 8.5% SDS gel electrophoresis under standard conditions. Protein bands were transferred onto 0.2 μm PVDF membranes (Bio-Rad, Hercules, CA) using standard protocols. After blocking the protein binding sites of PVDF membranes with 5% nonfat dried milk in TBS (Invitrogen, CA) containing 1% Tween 20, they were incubated with rabbit polyclonal anti-rat OCT3 (Alpha Diagnostic International), rabbit polyclonal anti-rat NCX1 (Alpha Diagnostic International), or goat polyclonal anti-PMAT (Santa Cruz, TX) in an antibody buffer (TTBS, 0.05% Tween-20, 10% nonfat dried milk). Hybridized membranes were washed with TBS, 0.05% Tween 20 (TTBS; Invitrogen, CA), and incubated with the appropriate HRP-conjugated secondary antibodies (Bio-Rad, Hercules, CA, USA and Santa Cruz, TX, USA) hybridizing buffer (TBS, 1% Tween-20, 1% nonfat dried milk). After washing the membranes, the protein bands were visualized using the HRP color development reagent kit (Bio-Rad, Hercules, CA, USA). The intensities of bands were quantified by using a Gel Logic 100 imaging system. Protein contents of the cell preparations were determined by the method of Bradford using the Bio-Rad protein assay with bovine serum albumin as the standard.

3.5 Technical Statement

Due to high toxicity and obvious health hazard of MPP^+, extreme caution was used in its handling in accordance with published procedures (184).

CHAPTER IV

RESULTS

4.1 Characteristics of MPP^+ Uptake into Dopaminergic and Non-Dopaminergic Cells

MPP^+ is taken up into all cell types. Cellular uptake of MPP^+ was measured at a concentration range of 25-100 µM MPP^+ in KRB-HEPES pH 7.4 buffer for a fixed incubation time of 45 min and intracellular MPP^+ levels were quantified by HPLC-UV as detailed in "*Experimental Methods*". As shown in Fig. 6, while PC12 take up MPP^+ most efficiently, both SH-SY5Y and MN9D cells take up MPP^+ less efficiently than HepG2 cells under similar incubation conditions.

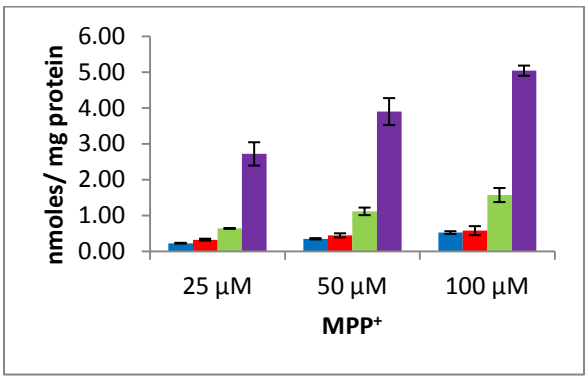

Figure 6- MPP^+ Uptake into HepG2, PC12, SH-SY5Y, and MN9D Cells. HepG2, SH-SY5Y, and MN9D cells were grown in DMEM and PC12 cells in an F-12K medium supplemented with 2.5% FBS and 15% horse serum to 70-80% confluence in 12 well plates as detailed in Experimental Methods. Cells were incubated with 25-100µM MPP^+ in KRB-HEPES buffer (1.0 mL, pH 7.4) for 45 min at 37˚C. Cells were washed, collected, and intracellular MPP^+ levels were quantified by reversed phase HPLC-UV. All the intracellular MPP^+ concentrations were normalized to respective protein concentrations as detailed in Experimental Methods. Data are represent as mean ± S.D (n = 3). HepG2 (Green), PC12 (Purple), SH-SY5Y (Red), MN9D (Blue)

4.2 The Effect of Extracellular Na^+ and Ca^{2+}on MPP^+ Uptake

As mentioned above, DA uptake through DAT is dependent on the extracellular Na^+. The effect of extracellular Na^+ on MPP^+ uptake into MN9D cells was investigated. In these experiments, Na^+ in the incubation buffer was replaced with equimolar concentrations of Li^+, N-methyl-D-glucamine, and choline. During these experiments, it was observed that the extracellular Ca^{2+} also affects the MPP^+ uptake into MN9D cells. Therefore, the effect of Ca^{2+} on the uptake of MPP^+ into all the cells was also investigated in detail. In these experiments where complete removal of Ca^{2+} from the incubation medium was necessary, Ca^{2+} was omitted and 1.3 mM EGTA was included in the incubation medium. In all experiments, cells were incubated with a constant 50 μM MPP^+ concentration for 45 min and cellular MPP^+ concentrations were measured by HPLC-UV as detailed in *"Experimental Methods"*.

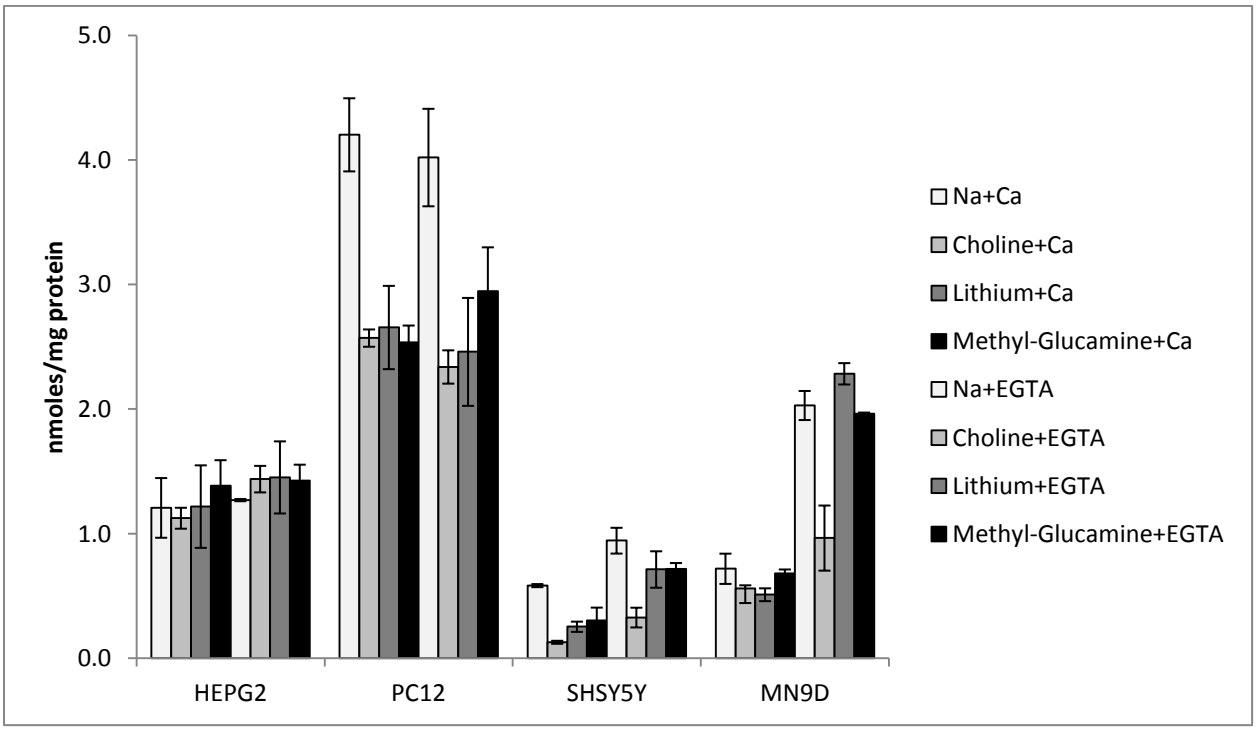

Figure 7- MPP^+ Uptake in HepG2, PC12, SH-SY5Y, and MN9D Cells with the Effect of Extracellular Na^+ and Ca^{2+}. HepG2, SH-SY5Y, and MN9D cells were grown in DMEM and

PC12 cells in an F-12K medium supplemented with 2.5% FBS and 15% horse serum to 70-80% confluence in 12 well plates as detailed in Experimental Methods. In experiments where Na^+-free conditions were necessary Na^+ in the incubation media were replaced with equimolar concentrations of Li^+ or N-methyl-D-Glucamine. Similarly, when Ca^{2+}-free conditions were necessary Ca^{2+} is omitted from the incubation media and in some cases, 1.3 mM EGTA was included. In all experiments cells were incubated with 50 μM MPP^+ in KRB-HEPES buffer (1.0 mL, pH 7.4) for 45 min at 37˚C. Cells were washed, collected, and intracellular MPP^+ levels were quantified by reversed phase HPLC-UV. All the intracellular MPP^+ concentrations were normalized to respective protein concentrations as detailed in Experimental Methods. Data are represent as mean ± S.D (n = 3).

As shown from the data in Fig. 7, MPP^+ is taken up into all cell types i.e. catecholaminergic (MN9D, SH-SY5Y, and PC12) and liver (HepG2) cells with varying efficiencies. For example, while PC12 take up MPP^+ most efficiently, both SH-SY5Y and MN9D cells take up MPP^+ less efficiently than HepG2 cells under similar incubation conditions (Fig. 7). More intriguingly, MPP^+ uptake into MN9D cells increased by about 3 to 4 fold in the absence of $Ca^{2+}{}_o$ and presence of EGTA in the incubation medium (Fig. 7). The substitution of equimolar concentration of Li^+ or N-methyl-D-glucamine in place of extracellular Na^+ ($Na^+{}_o$) or gluconate in place of Cl^- (data not shown) in the incubation medium had no significant effect on the MPP^+ uptake in the absence of $Ca^{2+}{}_o$ under similar experimental conditions. The effect of $Ca^{2+}{}_o$ on the MPP^+ uptake into SH-SY5Y cells was similar to that of MN9D cells but was less pronounced (Fig. 7). On the other hand, $Ca^{2+}{}_o$ had no measurable effect on the uptake of MPP^+ into PC12 or HepG2 cells under similar experimental conditions (Fig. 7). In addition, while MPP^+ uptake into PC12 cells is partially dependent on the $Na^+{}_o$, uptake into HepG2 cells is completely independent of $Na^+{}_o$.

Analysis of the uptake data as shown in Table 3 revealed that the MPP^+ uptake into MN9D cells consists of at least three distinct components and the major component of ~65% is $Na^+{}_o$ independent and sensitive to $Ca^{2+}{}_o$. The $Na^+{}_o$ dependent component is minor comprising

only about 3% of the total uptake and the remaining 32% is Ca^{2+}_o insensitive and also Na^+_o independent. Parallel to MN9D cells, MPP^+ uptake into SH-SY5Y also has three similar components consisting 38% Ca^{2+}_o sensitive, 25% Na^+ dependent and 37% Na^+ independent. In contrast, MPP^+ uptake into PC12 has only two components both of which are Ca^{2+}_o insensitive and ~28% is Na^+_o dependent and ~72% is Na^+_o independent. On the other hand, MPP^+ uptake into HepG2 cells occurs primarily through a Ca^{2+}_o and Na^+_o independent pathway.

Table 3: Approximation Contributions of Different Pathways to MPP^+ uptake into HepG2, PC12, SH-SY5Y, and MN9D Cells.

MPP^+ uptake	**HepG2**	**PC12**	**SH-SY5Y**	**MN9D**	**Likely Transporter**
Na^+-dependent,Ca^{2+}-independent irreversible	0	28%	25%	3%	DAT
Na^+ & Ca^{2+} independent irreversible	0	72%	37%	32%	PMAT
Na^+ & Ca^{2+} independent reversible	100%	0	0	0	PMAT/OCT?
Na^+ independent Ca^{2+} dependent reversible	0	0	38%	65%	Unknown

In addition, the uptake characteristics of 3'OH-MPP^+ and 4'I-MPP^+into HepG2 (Fig. 8A), PC12 (Fig. 8B), SH-SY5Y (Fig. 8C), and MN9D (Fig. 8D)are also similar to MPP^+. Furthermore, differentiated MN9D cells show similar uptake characteristics as undifferentiated MN9D cells (Fig. 8E).

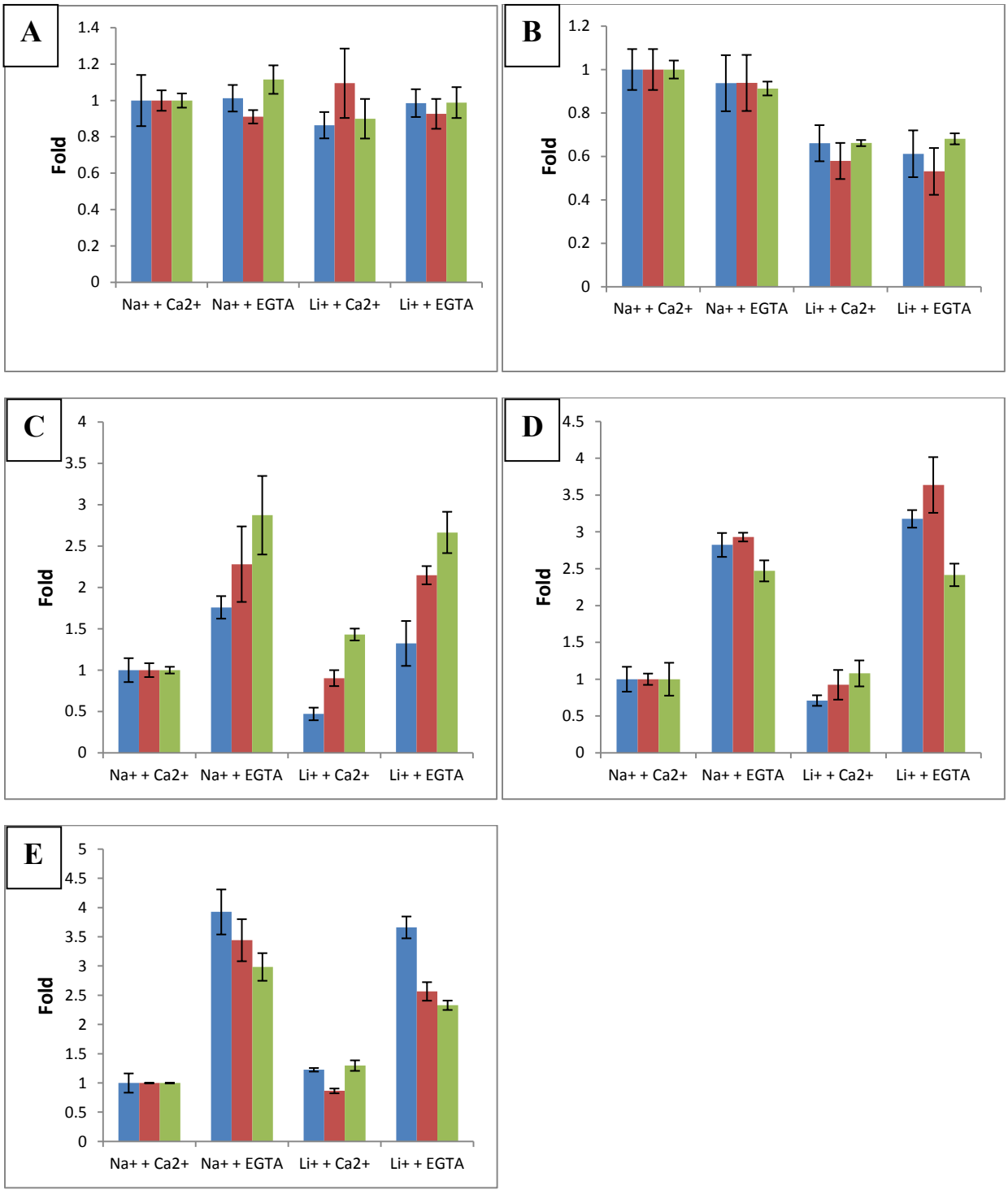

Figure 8- MPP^+ and its Derivatives Uptake with the Effect of Extracellular Na^+ and Ca^{2+} in HEPG2, PC12, SH-SY5Y, and Undifferentiated and Differentiated MN9D Cells. MN9D cells were differentiated with 1.0 mM butyrate. The uptake of MPP^+, 3'OH-MPP^+, and 4'I-MPP^+ were measured under similar conditions as detailed above. The data are presented as mean ± S.D. (n =

3). MPP^+ (Blue), 3'OH-MPP^+ (Red), 4'I-MPP^+ (Green) . HepG2 (A), PC12 (B), SH-SY5Y (C), MN9D (D), Differentiated MN9D (E).

4.3 The Na^+_o independent MPP^+ uptake into dopaminergic cells is competitively inhibited by Ca^{2+}_o

The MPP^+ (50 μM in KRB-HEPES) uptake time course data presented in Fig. 9A shows the MPP^+ uptake into MN9D cells in the absence of Ca^{2+}_o is saturable and sigmoidal. A similar behavior was also observed with butyric acid differentiated MN9D cells (Fig. 9B). However, Ca^{2+}_o has no effect on the MPP^+ uptake into PC12 in contrast to MN9D cells (Fig. 9C).The uptake kinetic data indicated in Fig. 9A the increase of MPP^+ uptake into MN9D cells in the absence of Ca^{2+}_o is primarily due to the inhibition of MPP^+ uptake by Ca^{2+}_o under the standard incubation conditions. Analysis of the kinetic data of the MPP^+ uptake inhibition demonstrate that Ca^{2+}_o inhibits MPP^+ uptake into MN9D in an apparent competitive manner with a K_i of 13.2 ± 1.5 μM (Fig. 10B). In addition, in the absence of Ca^{2+}_o, the MPP^+ uptake was saturable with apparent V_{max} and K_m parameters of 91.7 ± 4.5 pmoles/mg.min and 39.9 ± 5.4μM, respectively in the MPP^+ concentration range of 0-150 μM (Fig. 10B).

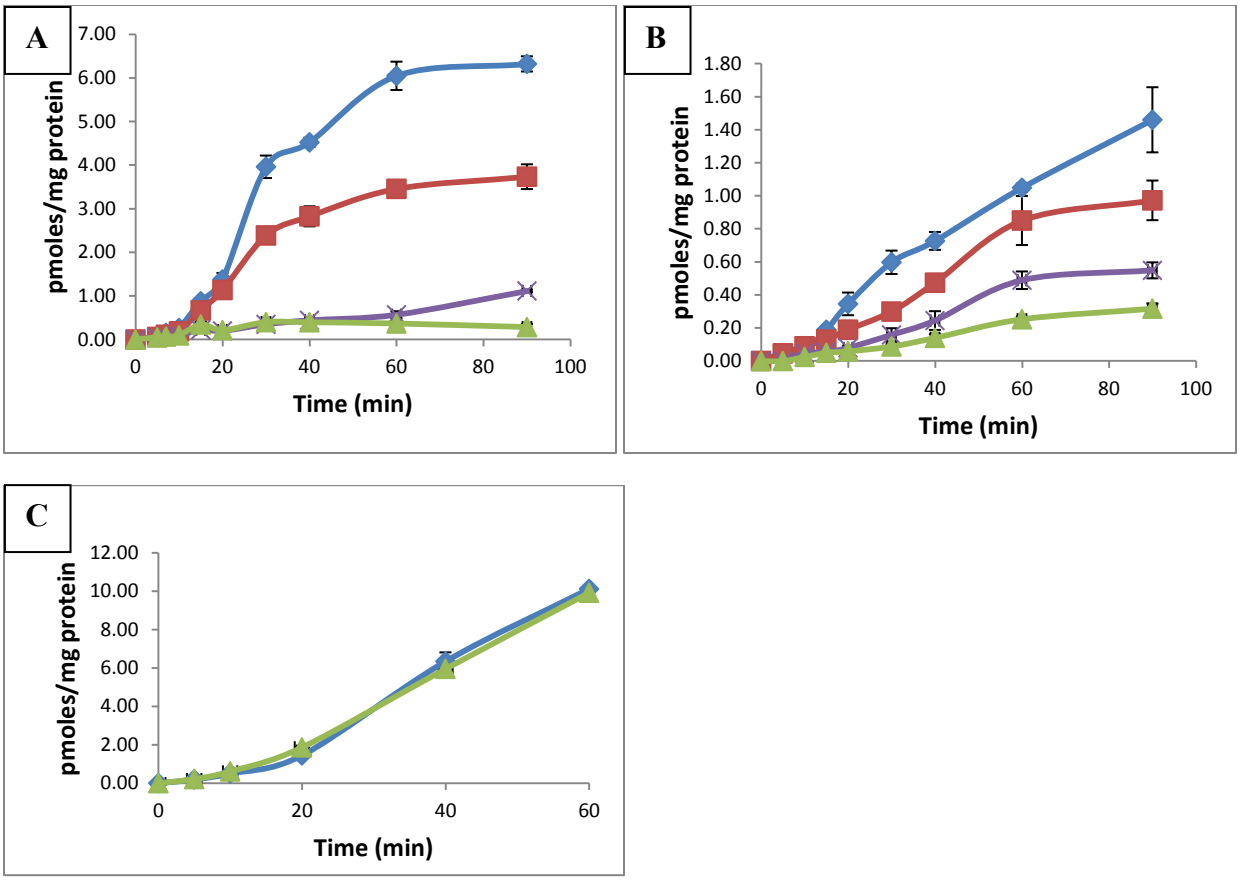

Figure 9- Time Course of MPP^+ Uptake in Undifferentiated and Differentiated MN9D cells and PC12 cells: Cells were incubated with 1 mL of 50 µM MPP^+ in the presence or absence of Ca^{2+} and in KRB-HEPES, pH 7.4, or HCO_3 for 0-90 min. A. Undifferentiated MN9D cells. B. Differentiated MN9D cells. C. PC12. 1.3 mM EGTA-HCO3 (Blue), 1.3 mM EGTA HEPES (Red), 1.3 mM Ca^{2+}-HEPES (Purple) , 1.3 mM Ca^{2+}-HCO3 (Green). Intracellular MPP^+ levels were determined by reversed phase HPLC-UV as detailed in *"Experimental Methods"*. Data represent mean ± S.D. of triplicate samples.

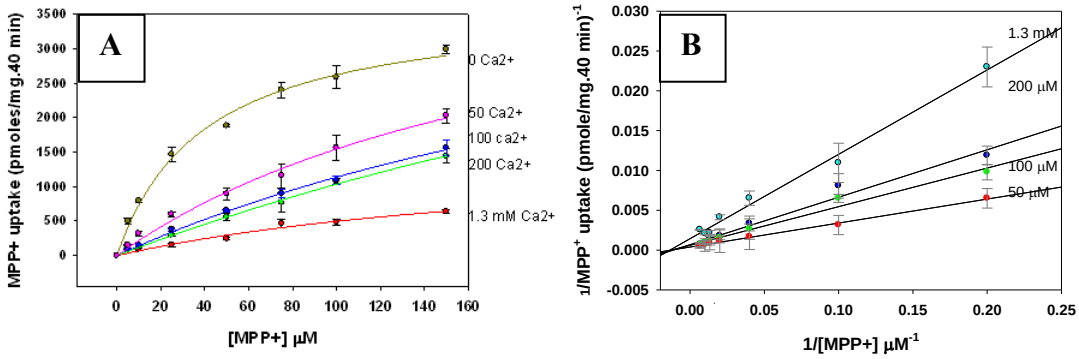

Figure 10- Kinetic Uptake of MPP^+ in Ca^{2+}-Dependent Course in MN9D Cells. Cells were grown in 12-well plates and incubated with 0-250 µM MPP^+ in the presence of 0-1.3 mM Ca^{2+}_o in 1.0 mL of KRB-HCO_3 buffer for 45 min. *B. The double reciprocal plots of data in Figure 15A.* In all experiments cells were washed several times after the incubations and intracellular MPP^+ concentrations were determined by reversed phase HPLC-UV as detailed in Experimental methods. All intracellular MPP^+ concentrations were normalized to respective cellular protein concentrations. Data are presented as mean ± S.D. (n=3).

4.3.1 The effect of other Ca^{2+} channel blockers and cation channel inhibitors on the MPP^+ uptake into MN9D cells.

To test whether the Ca^{2+}_o sensitivity of MPP^+ uptake into dopaminergic cells was associated with voltage gated or other types of calcium and/or cation channels, the effect of various Ca^{2+} channel blockers and cation channel inhibitors on the MPP^+ uptake into MN9D cells were investigated. These studies have revealed that verapamil, nitrendipine and irasadipine, mibefradil, benzamil, CGP37517, SKF96365, and GBR12909 were strong inhibitors for MPP^+ uptake into MN9D cells especially in the absence of extracellular Ca^{2+} (Fig. 11). Under similar conditions, nitrendipine has no effect on MPP^+ uptake in the presence of but observe a moderate inhibition in the absence of extracellular Ca^{2+} (Fig. 11E). However, flufenamic acid, CGP37157, and 2-APB have no significant effect on MPP^+ uptake in the presence or absence of extracellular Ca^{2+} and therefore, they are not effective inhibitors of MPP^+ uptake into MN9D (Fig 11). Similarly, metal ions such as nickel and galladium which are known to inhibit several types of

calcium channels including VGCC and NCX also have no effect on MPP^+ uptake in MN9D cells in the absence or presence of extracellular Ca^{2+} (Fig. 12A and 12B). In addition, voltage-gated Na^+ channel inhibitor tetradotoxin also has no effect on MPP^+ uptake in MN9D cells (Fig. 12). Thapsigargin is a SERCA pump inhibitor that raises cytosolic Ca^{2+} concentration by preventing the Ca^{2+} pump into the ER causing this Ca^{2+} store to become depleted. To investigate whether the cytosolic Ca^{2+} plays a role in MPP^+ uptake the effect of 0-25 μM Thapsigargin on the MPP^+ (50 μM) uptake into MN9D cells was determined. As shown in Fig. 13, Thapsigargin has no effect on the uptake of MPP^+ into MN9D cells. Similarly, BAPTA-AM is the intracellular Ca^{2+}-chelator which depletes the cytosolic Ca^{2+}. As shown in Fig. 14, BAPTA did not increase or decrease MPP^+ uptake significantly in both the presence and absence of extracellular Ca^{2+}.

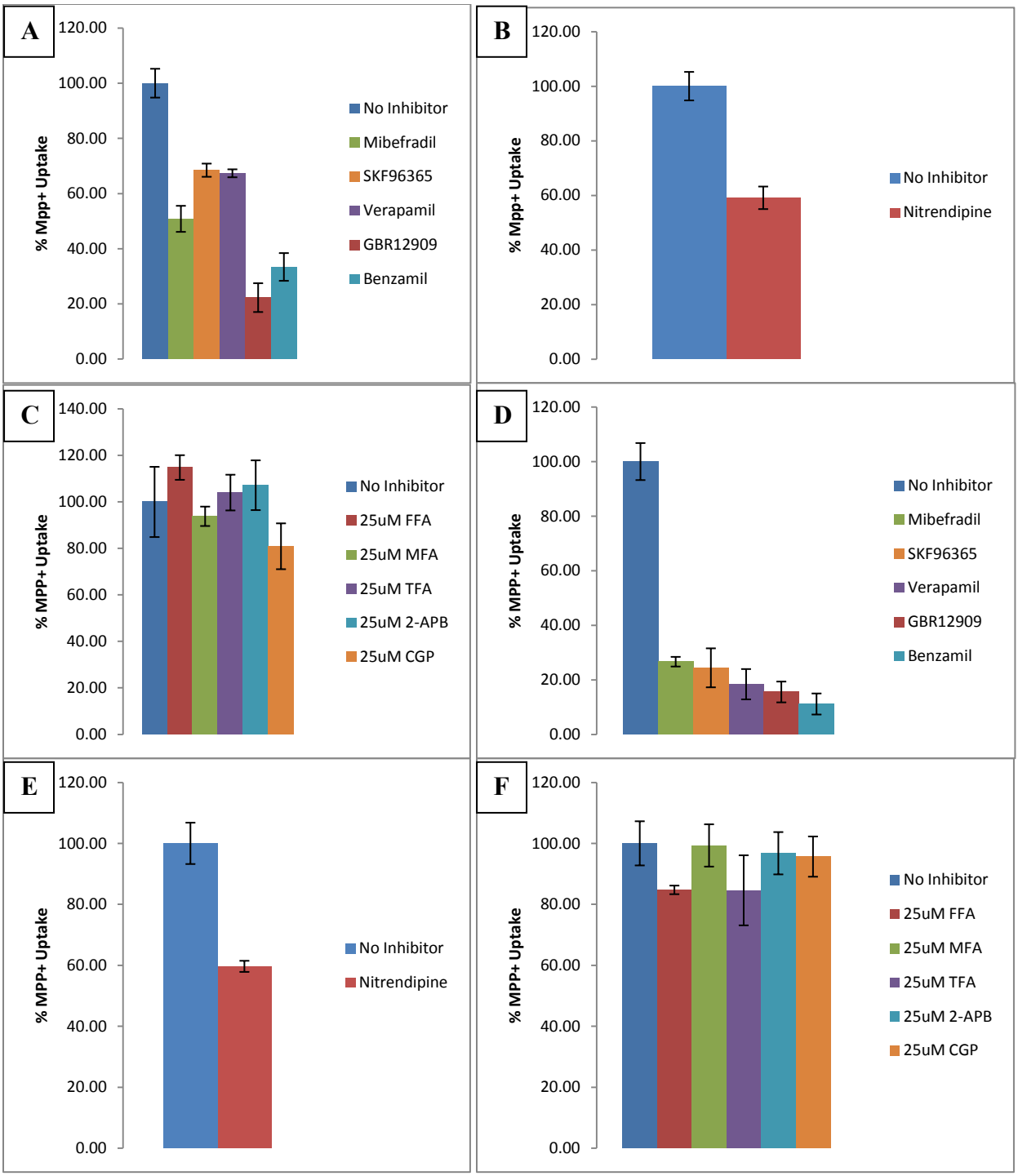

Figure 11- Inhibitory Effect on MPP^+ Uptake in MN9D Cells. Cells were grown in 12-well plates under standard conditions in as detailed in Experimental Methods. The growth media was removed and cells were washed with warm KRB-HEPES, pH 7.4 and incubated in 990 µL of KRB-HEPES, pH 7.4 containing a constant concentration of the desired inhibitor in KRB-HEPES, pH 7.4 for 10 min at 37˚C. Then, 10 µL MPP^+ was added and incubated for additional 45 min at 37˚C. In all experiments the final inhibitor concentrations of the inhibitor and MPP^+

were fixed at 25 µM and 50 µM, respectively. Cells were washed several times, harvested, and intracellular MPP^+ concentrations were determined by reversed phase HPLC-UV as detailed in Experimental Methods and all intracellular MPP^+ concentrations were normalized to respective cellular protein concentrations. Data are presented as mean ± S.D. (n=3).Strong Inhibitors in $Ca^{2+}{}_o$ medium (A), Moderate Inhibitors in $Ca^{2+}{}_o$ medium (B), Weak Inhibitors in $Ca^{2+}{}_o$ medium (C), Strong Inhibitors in EGTA medium (D), Moderate Inhibitors in EGTA medium (E), Weak Inhibitors in EGTA medium (F).

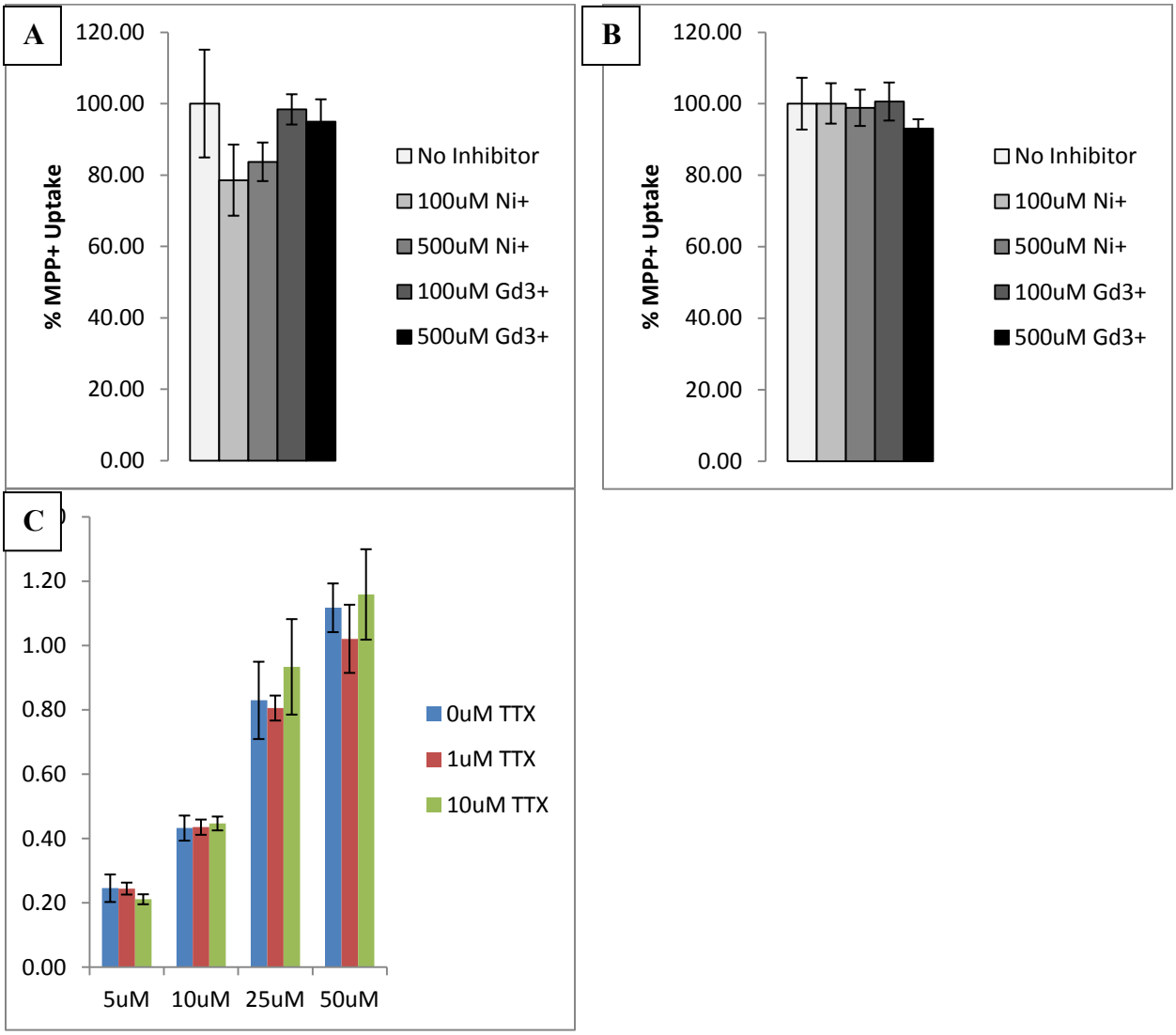

Figure 12: The Effect of VGCC and VGNC Inhibitor on MPP^+ Uptake in MN9D Cells. Cells were grown in 12-well plates under standard conditions in as detailed in Experimental Methods. The growth media was removed and cells were washed with warm KRB-HEPES, pH 7.4and incubated in 990 µL of KRB-HEPES, pH 7.4 containing a constant concentration of the desired inhibitor in KRB-HEPES, pH 7.4 for 10 min at 37˚C. Then, 10 µL MPP^+ was added and incubated for additional 45 min at 37˚C.Nickel (A), Galladium (B), and Tetradotoxin (C). Cells

were washed several times, harvested, and intracellular MPP^+ concentrations were determined by reversed phase HPLC-UV as detailed in Experimental Methods and all intracellular MPP^+ concentrations were normalized to respective cellular protein concentrations. Data are presented as mean ± S.D. (n=3).

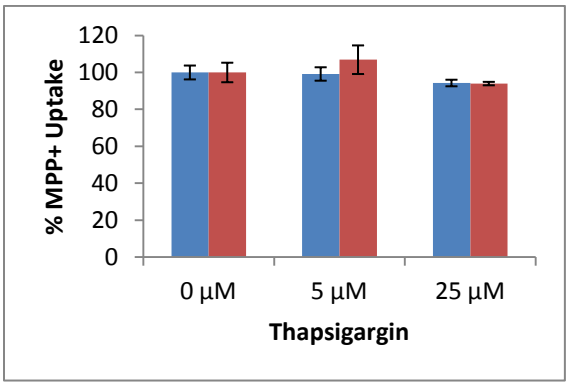

Figure 13: The Effect of SERC Pump Inhibitor on MPP^+ Uptake in MN9D Cells. Cells were treated initially with 990 µL of various concentrations of Thapsigargin for 10 min followed by 10 µL of MPP^+ in KRB-HEPES pH 7.4 for 45 min. Cells were washed several times, harvested, and intracellular MPP^+ concentrations were determined by reversed phase HPLC-UV as detailed in Experimental Methods and all intracellular MPP^+ concentrations were normalized to respective cellular protein concentrations. Data are presented as mean ± S.D. (n=3)
Ca^{2+} (Blue), EGTA (Red).

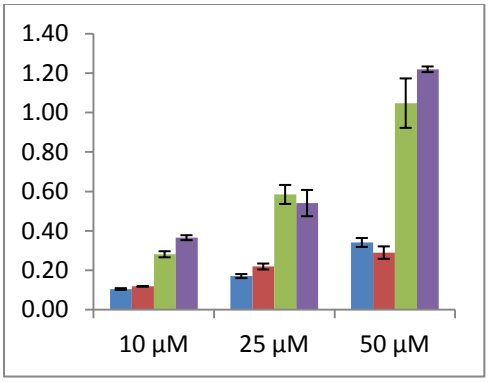

Figure 14: The Effect of BAPTA on MPP^+ Uptake in MN9D Cells. Cells were incubated with 990 µL of 50 µL BAPTA-AM in KRB-HEPES (pH 7.5) for 30 minutes followed by 10 µL of MPP^+ for 45 additional min at 37˚C. Cells were washed several times, harvested, and intracellular MPP^+ concentrations were determined by reversed phase HPLC-UV as detailed in Experimental Methods and all intracellular MPP^+ concentrations were normalized to respective cellular protein concentrations. Data are presented as mean ± S.D. (n=3). 500 µM Ca^{2+} and 0 µM BAPTA (Blue), 500 µM Ca^{2+} and 50 µM BAPTA (Red), 0 µM Ca^{2+} and 0 µM BAPTA (Green) , 0 µM Ca^{2+} and 50 µM BAPTA (Purple).

4.3.2 Characteristics of the inhibition of MPP^+ uptake into dopaminergic cells by benzamil, SKF96365, verapamil, mibefradil, and GBR12909

The above results show that mibefradil, verapamil, benzamil, SKF96365, and GBR12909 are strong MPP^+ uptake inhibitors and thus, they were characterized in detail. These studies show that these were relatively moderate inhibitors at 25 μM inhibitor and 50 μM MPP^+ concentrations in the presence of 1.3 mM Ca^{2+}_o in the incubation medium (Fig. 15). However, in the absence of Ca^{2+}_o more pronounced inhibitions were observed with these inhibitors in the order benzamil ~GBR12909> verapamil ~SKF96365 ~mibefradil (Fig. 15). As expected, benzamil, GBR12909, verapamil, are also modest inhibitors for the MPP^+ uptake into SH-SY5Y in the presence, and better inhibitors in the absence of Ca^{2+}_o (Fig. 15). Unexpectedly, the same inhibitors inhibit the MPP^+ uptake into PC12 as well (Fig. 15). However, in contrast to MN9D and SH-SY5Y cells the inhibition of MPP^+ uptake into PC12 cells was not significantly affected by Ca^{2+}_o (Fig. 15). On the other hand MPP^+ uptake into HepG2 cells was somewhat weakly inhibited by SKF96365 and benzamil, but not by verapamil or GBR12909 and again the inhibition was not dependent on Ca^{2+}_o (Fig. 15).

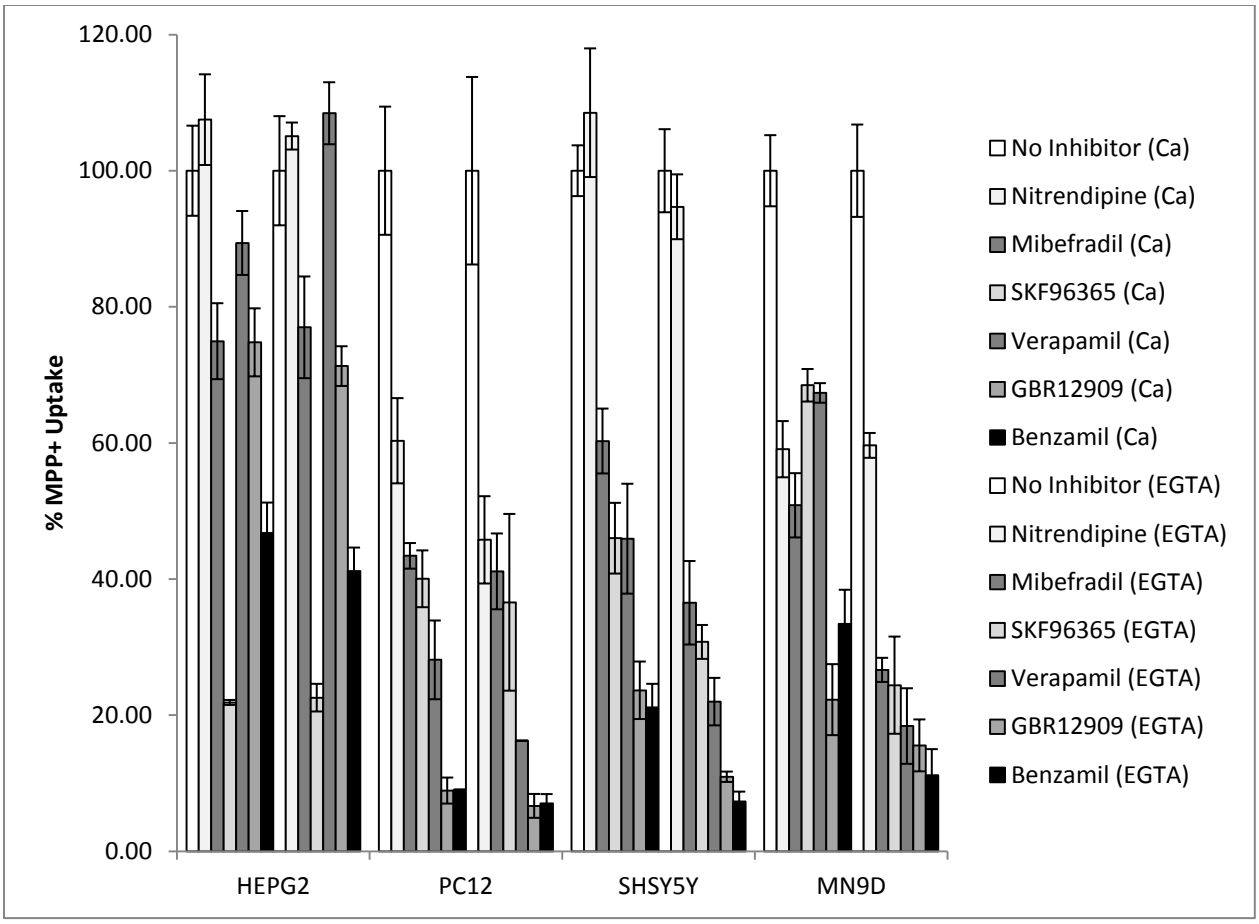

Figure 15- The Inhibition of MPP^+ uptake by various pharmacological agentsin the presence and absence of Ca^{2+}_o. Cells were grown in 12-well plates under standard conditions in as detailed in Experimental Methods. The growth media was removed and cells were washed with warm KRB-HEPES, pH 7.4 and incubated in 990 µL of KRB-HEPES, pH 7.4 containing a constant concentration of the desired inhibitor in KRB-HEPES, pH 7.4 for 10 min at 37˚C. Then, 10 µL MPP^+ was added and incubated for additional 45 min at 37˚C. In all experiments the final inhibitor concentrations of the inhibitor and MPP^+ were fixed at 25 µM and 50 µM, respectively. Cells were washed several times, harvested, and intracellular MPP^+ concentrations were determined by reversed phase HPLC-UV as detailed in Experimental Methods and all intracellular MPP^+ concentrations were normalized to respective cellular protein concentrations. Data are presented as mean ± S.D. (n=3).

Table 4: Percentage of MPP^+ Uptake in the Presence and Absence of Extracellular Ca^{2+} in HepG2, PC12, SH-SY5Y, and MN9D Cells.

	HepG2		**PC12**		**SHSY5Y**		**MN9D**	
	Percent	STDEV	Percent	STDEV	Percent	STDEV	Percent	STDEV
$Na^+ + Ca^{2+}$	100.00	6.62	100.00	9.42	100.00	3.73	100.00	5.23
Nitrendipine	107.51	6.66	60.33	6.26	108.52	9.45	59.08	4.13
GBR12909	74.78	5.00	8.92	1.91	23.66	4.22	22.28	5.22
Mibefradil	74.95	5.58	43.41	1.88	60.29	4.77	50.84	4.72
Verapamil	89.38	4.70	28.13	5.79	45.93	8.08	67.35	1.44
Benzamil	46.76	4.48	8.97	0.13	21.12	3.49	33.41	5.02
SKF96365	21.87	0.37	40.04	4.18	46.01	5.20	68.47	2.39
Na^+ + EGTA	100.00	8.02	100.00	13.78	100.00	6.10	100.00	6.78
Nitrendipine	105.10	1.98	45.76	6.41	94.70	4.77	59.64	1.82
GBR12909	71.29	2.92	6.68	1.76	10.95	0.76	15.56	3.81
Mibefradil	76.99	7.47	41.13	5.57	36.52	6.14	26.66	1.77
Verapamil	108.44	4.55	16.25	0.01	21.99	3.49	18.40	5.55
Benzamil	41.18	3.45	7.06	1.34	7.34	1.43	11.16	3.86
SKF96365	22.58	2.03	36.59	12.98	30.77	2.49	24.41	7.14

4.3.3 Kinetic Analysis of MPP^+ Inhibitors

Inhibition kinetic parameters of the above MPP^+ uptake inhibitors were determined by using HPLC-RP quantification of intracellular MPP^+ in the absence of $Ca^{2+}{}_o$. The standard inhibition kinetic analysis show that benzamil, SKF 96365, GRB12909, verapamil, and mibefradil are apparent competitive inhibitors with K_i parameters of 0.64 ± 0.17, 1.5 ± 0.5, 2.2 ± 0.3, 4.5 ± 0.5, and 9.2 ± 1.0 μM, respectively for MPP^+ uptake into MN9D cells in the absence of $Ca^{2+}{}_o$ (Fig. 16; SKF96365 data is not shown).

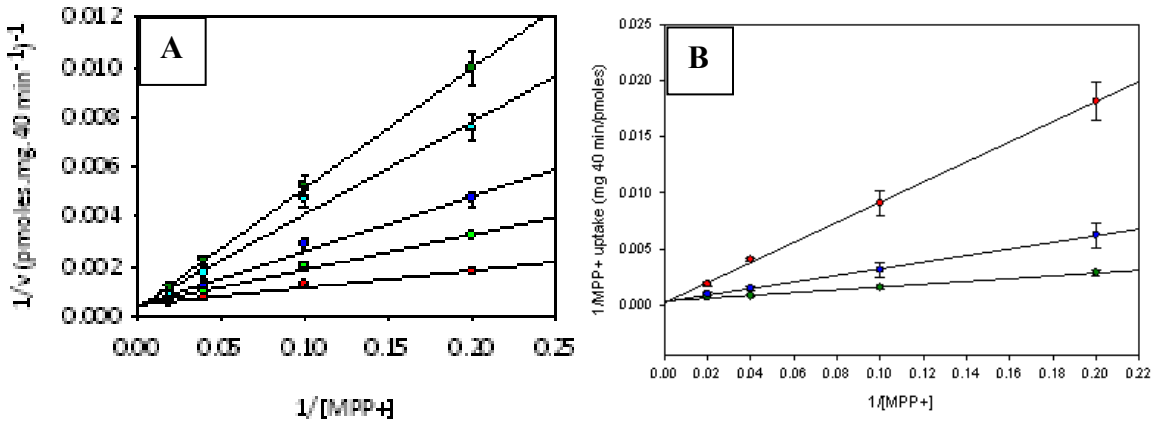

Benzamil (K_i = 0.64± 0.17µM) GBR12909 (K_i = 2.2 ± 0.5 µM)

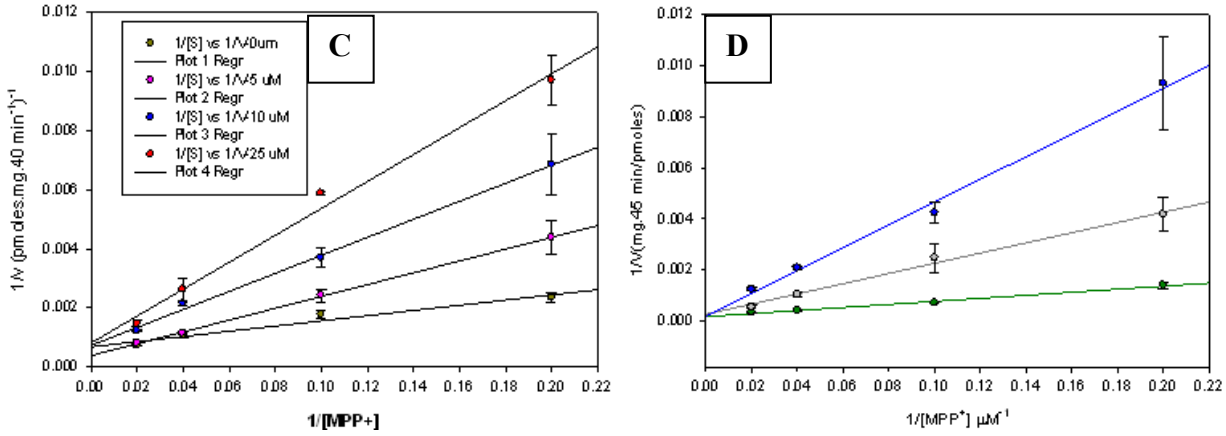

Verapamil (K_i = 4.5 ± 0.5 µM) Mibefradil (K_i = 9.2± 2.07 µM)

Figure 16: Kinetics of MPP^+ uptake inhibition into MN9D cells by benzamil, GBR12909, and verapamil. MN9D cells were grown in 12-well plates in DMEM as detailed in Experimental Methods. Cells were washed and incubated with 990 µL of KRB-HEPES pH 7.4 containing the desired concentrations of (A), benzamil, (B), GBR1209, (C), verapamil, or (D) mibefradil for 10 min. Then, 10 µL of MPP^+ containing the desired concentrations of MPP^+ was added and further incubated for 45 min in the absence of Ca^{2+} and presence of 1.3 mM EGTA. Cells were washed, harvested, and intracellular MPP^+ concentrations were determined by reversed phase HPLC-UV. The intracellular MPP^+ concentrations were normalized to respective cellular protein concentrations. The corresponding K_i values were determined by fitting the experimental data to the double reciprocal form of Michaelis-Menten equation. Data are presented as mean ± S.D. (n=3).

4.4 Intracellular MPP^+ is reverse transported from MN9D cells in a Ca^{2+}_o dependent manner

To determine the reversibility of MPP^+ uptake, a series of experiments was carried out with MPP^+ loaded MN9D cells under various incubation conditions. In these experiments, cells were initially incubated with 100 μM MPP^+ in a medium without Ca^{2+}_o for 60 min and then were washed and incubated for an additional 90 min in the absence of external MPP^+ under desired incubation conditions (*see* figure legends for more details). These experiments show that MN9D cells lose about 80% of intracellular MPP^+ during the 90 min post incubation in a standard medium containing Ca^{2+}_o (Fig. 17). However, in the absence of Ca^{2+}_o in the incubation medium, the MPP^+ loss was reduced to about 20% (Fig. 17). A similar, but less pronounced behavior was observed with MPP^+ loaded SH-SY5Y cells with respect to Ca^{2+}_o (Fig. 17). For example, while SH-SY5Y cells lost about 40% intracellular MPP^+ in the presence of Ca^{2+}_o, no significant loss of MPP^+ was observed in the absence of Ca^{2+}_o. In sharp contrast, PC12 cells do not lose intracellular MPP^+ significantly regardless of whether Ca^{2+}_o are present or not in the post incubation medium (Fig. 17). Intriguingly, HepG2 cells lost almost all intracellular MPP^+ during 90 min incubation regardless of whether Ca^{2+}_o was present or not in the post incubation medium (Fig. 17). Experiments with Na^+_o free post incubations (Na^+ was replaced with equimolar concentrations of choline) have confirmed that Na^+_o has no significant effect on the reverse transport of MPP^+ from any cell type [note that a weak but consistent inhibition of both MPP^+ uptake and reverse transport was observed at high concentration of choline (IC_{50} ~ 37.0 mM)].

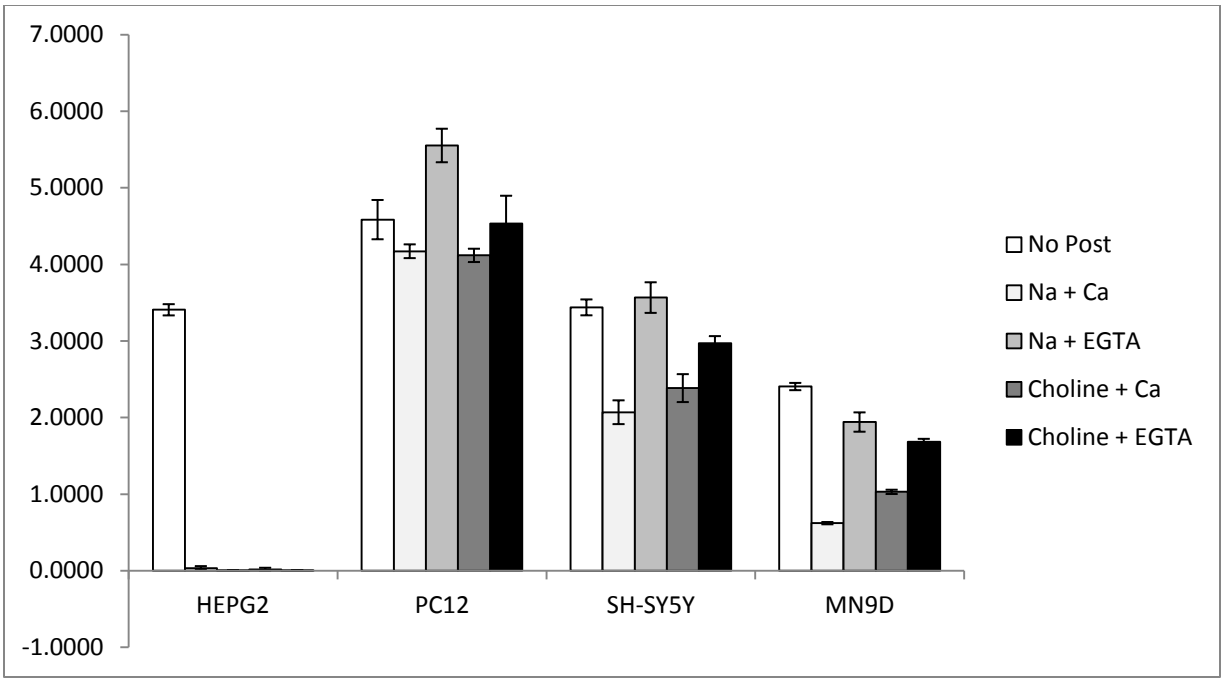

Figure 17– Back-Transport of Uptake of MPP^+ with the Effect of Extracellular Na^+ and Ca^{2+} in HepG2, PC12, SH-SY5Y, and MN9D Cells. HepG2, SH-SY5Y, and MN9D cells were grown in 12-well plates in DMEM as detailed in Methods. PC12 cells were grown to 70-80% confluence in 12 well plates in an F-12K medium supplemented with 2.5% FBS and 15% horse serum. Cells were incubated with 1 mL of 100 μM MPP^+ in the absence of both $[Ca^{2+}]_o$ and $[EGTA]_o$ in KRB-HCO_3 buffer for 1 h at 37˚C. Cells were washed several times with appropriate buffer and incubated with 1mL of KRB-HCO_3 buffer without MPP^+ for 90 min. Cells were washed several times, collected, and intracellular MPP^+ concentrations were determined by reversed phase HPLC-UV. The intracellular MPP^+ concentrations were normalized to respective cellular protein concentrations. Data represent mean ± S.D. of triplicate samples.

Table 5: Approximation Contribution of Different Pathways to MPP^+ back-transport of MPP^+-loaded HepG2, PC12, SH-SY5Y, and MN9D Cells.

	HepG2	**PC12**	**SH-SY5Y**	**MN9D**
Na^+-dependent	-	-	-	-
Ca^{2+}-dependent	-	10.00	35.00	65.00
Na^+/Ca^{2+}-Independent	100	-	5.00	25.00

The approximate contributions of different back transport pathways which were calculated from the Fig. 17 data is shown in Table 5. Clearly, there are three distinct pathways of

back transport of MPP^+ present in HepG2, PC12, SH-SY5Y, and MN9D cells. As shown in Fig. 17, MPP^+ uptake into HepG2 cells is independent of both extracellular Na^+ and Ca^{2+} which may suggest that only one Na^+ or Ca^{2+} independent pathway is involved in the back-transport of MPP^+ loaded HepG2 cells. In PC12 cells, ~10% of MPP^+ was back-transported through a Na^+-independent/Ca^{2+}-dependent transporter. In SH-SY5Y cells, MPP^+ is back-transported by at least two pathways: 35% Na^+ independent and Ca^{2+} dependent channel, 5% Na^+ and Ca^{2+} independent channel. Lastly in MN9D cells, 65% of MPP^+ is back-transported by a Na^+ independent and Ca^{2+} dependent pathway and 25% by a Na^+ and Ca^{2+} independent pathway.

4.4.1 The Effect of Inhibitors on Back-Transport of Uptake of MPP^+

The effects of uptake inhibitors on the reverse transport of MPP^+ in the presence of Ca^{2+}_o were also tested. In contrast to the efficient inhibition of uptake, DAT inhibitor, GBR12909 does not inhibit the intracellular MPP^+ loss in MN9D cells during 90 min post incubation in the presence of Ca^{2+}_o (Fig 18). However, benzamil, and verapamil inhibit the loss effectively. Parallel to that is observed with MN9D cells, MPP^+ loss from SH-SY5Y cells is also inhibited by the above inhibitors in the presence of Ca^{2+}_o. Similar to MN9D cells, GBR12909 does not inhibit the loss of MPP^+ from SH-SY5Y cells either. On the other hand, benzamil partially inhibits the MPP^+ loss from HepG2 cells while verapamil and GBR12909 were not effective under similar experimental conditions (Fig. 18). Interestingly, MPP^+ loss from PC12 cells is slightly increased by the above inhibitors in contrast to the behavior of the other cell types (Fig. 18).

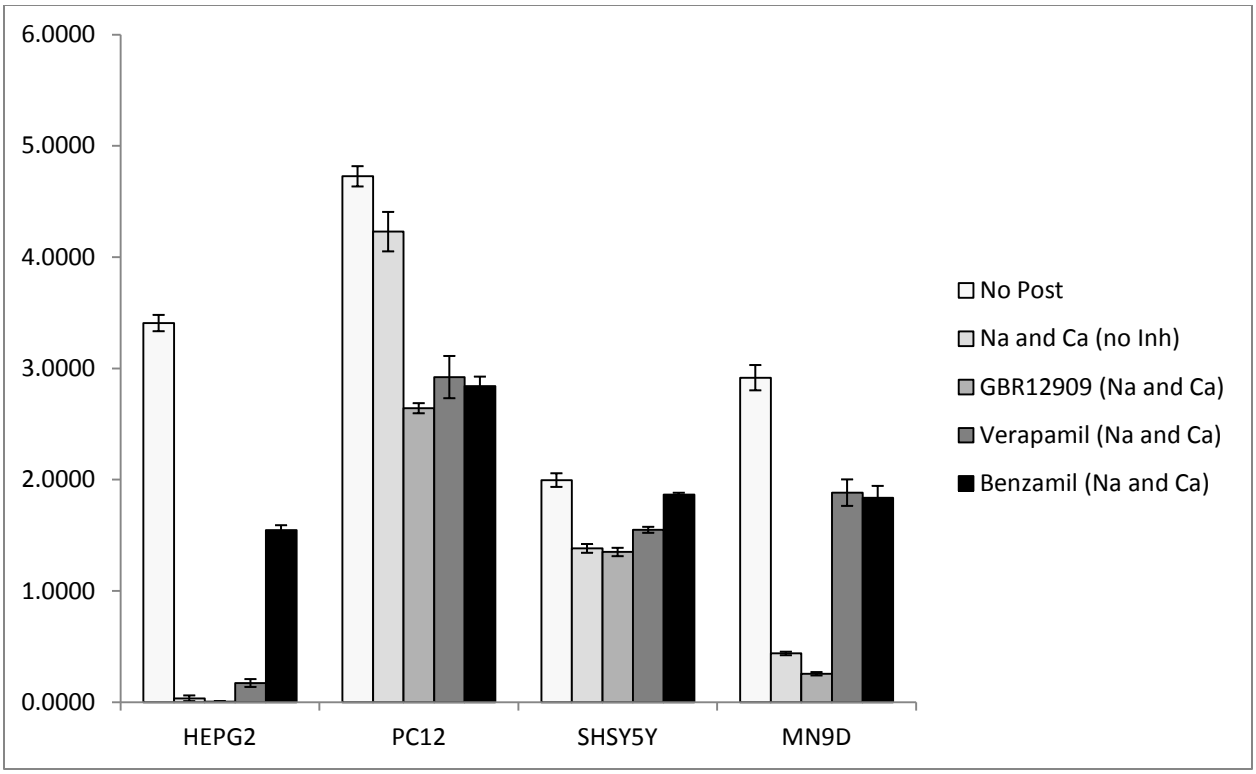

Figure 18- The Effect of Inhibitors on Back-Transport of MPP^+ in the Presence and Absence of Extracellular Na^+ and Ca^{2+} in HepG2, PC12, SH-SY5Y, and MN9D Cells. Cells were grown in 12-well plates in DMEM as detailed in Methods. Cells were incubated with 1 mL of 100 μM MPP^+ in the absence of both $[Ca^{2+}]_o$ and $[EGTA]_o$ in KRB-HCO_3 buffer for 1 h at 37˚C. Cells were washed several times with appropriate buffer and incubated with 1mL of 50 μM Inhibitor in KRB-HCO_3 buffer without MPP^+ for 90 minutes. Cells were washed several times, collected, and intracellular MPP^+ concentrations were determined by reversed phase HPLC-UV. The intracellular MPP^+ concentrations were normalized to respective cellular protein concentrations. Data represent mean ± S.D. of triplicate samples.

Table 6: Percent Inhibition of back-transport of MPP^+ in the presence and absence of extracellular Na^+ or Ca^{2+} or both in HepG2, PC12, SH-SY5Y, and MN9D cells.

	HepG2	PC12	SHSY5Y	MN9D
No Post				
Na^+ and Ca^{2+} (No Inhibitor)	98.97	10.52	30.76	84.99
GBR12909 (Na^+)	99.82	44.10	32.38	91.24
Verapamil (Na^+)	94.94	38.18	22.39	35.43
Benzamil (Na^+)	54.60	39.89	6.57	36.98
Choline and Ca^{2+} (No Inhibitor)	99.82	11.85	35.22	59.30
GBR12909 (choline)	99.82	45.98	28.05	49.30
Verapamil (choline)	93.67	45.63	17.61	10.16
Benzamil (choline)	34.55	43.57	-14.50	27.03

4.5 MPP^+ Toxicity Experiments

The relative sensitivity of M9ND, SH-SY5Y, PC12, and HepG2 cells toward MPP^+ toxicity were determined using standard MTT assays. As shown in Fig. 19, MN9D cells are the most and HepG2 cell are the least sensitive and both PC12 and SH-SY5Y are moderately sensitive to MPP^+ toxicity.

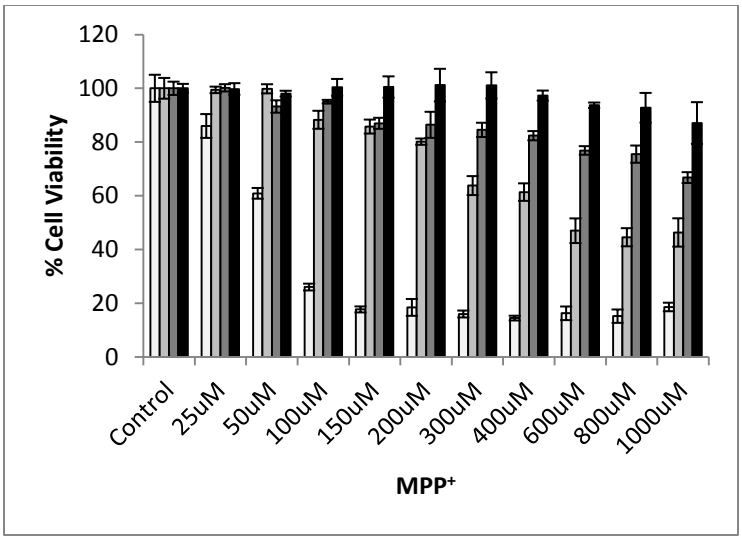

Figure 19- MPP^+ Toxicity in HepG2, PC12, SH-SY5Y, and MN9D cells. Cells were grown in 96-well plates and allowed to grow to 70-80% confluence under standard growing conditions. The media was removed and cells were incubated with 0-1000 μM of MPP^+ in KRB-HCO_3 buffer for 24 h and the cell viabilities were determined by the MTT assay as detailed in *"Experimental Methods"*. Results are expressed as % viability with respect to parallel untreated controls. Data are presented as mean ± SD (n=5). MN9D PC12 SH-SY5Y HepG2

4.5.1 Cellular Toxicities of novel 4'-Halogenated MPP^+ Derivatives

Initial screening experiments revealed that 4'-halogenated derivatives of MPP^+ were significantly more toxic to MN9D cells than the parent compound, MPP^+, suggesting 4'-halogenated MPP^+ derivatives could be better models for toxicological and structure-activity studies. As seen in Fig. 20A, these derivatives induced marked concentration-dependent cellular death of MN9D while their effects on SH-SY5Y cells is less pronounced (Fig. 20B) over a 24 h incubation period under similar experimental conditions. The estimated LC_{50} values for MN9D cells toxicity of the halogenated derivations range from 142 μM for 4'F-MPP^+ to 81 μM for 4'I-MPP^+. These results show that increasing the hydrophobicity of the halogen substituent of MPP^+ increases the toxic effect on both catecholaminergic cells MN9D and SH-SY5Y cells.

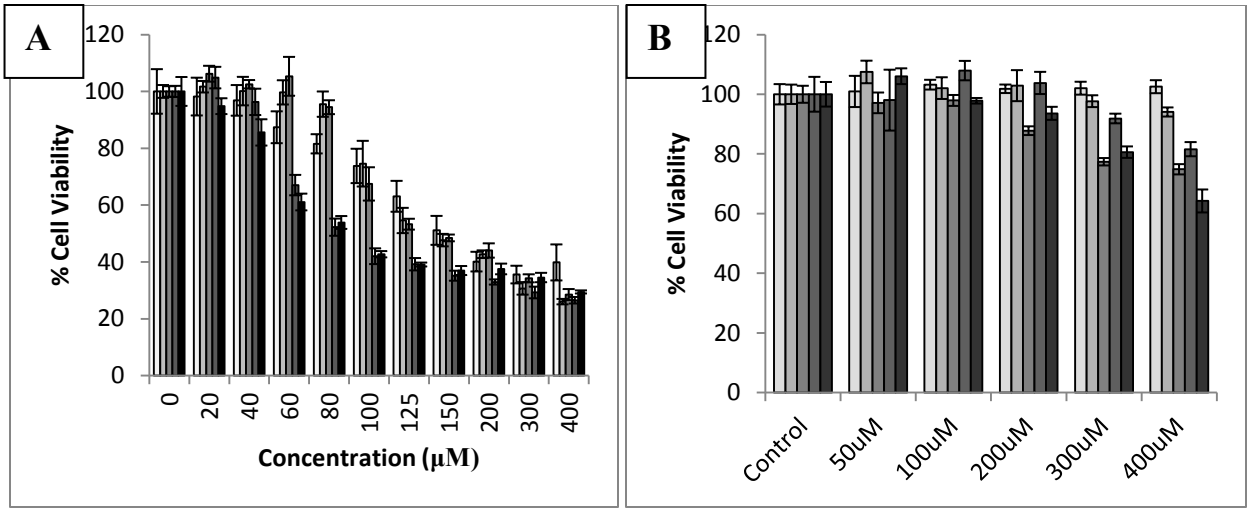

Figure 20- Toxicity of 4'-Halogenated MPP^+ in MN9D and SH-SY5Y Cells. MPP^+ was dissolved in water and 4'-halogenated MPP^+ was dissolved in DMSO where the final DMSO concentration was kept to a minimum <0.5% v/v. Cells were grown in 96-well plates and allowed to grow to 70-80% confluence under standard growing conditions. The media was removed and cells were incubated with 0-400 μM of MPP^+ derivatives in KRB-HCO_3 buffer for 24 h and the cell viabilities were determined by the MTT assay as detailed in *"Experimental Methods"*. Results are expressed as % viability with respect to parallel untreated controls. Data are presented as mean ± SD (n=5).MN9D (A).SH-SY5Y (B). MPP^+ 4'F-MPP^+ 4'Cl-MPP^+ 4'Br-MPP^+ 4'I-MPP^+

4.6. The Effect of GBR12909 on MPP^+ and its derivatives Uptake in MN9D cells

DAT has been shown to expressed in MN9D cells (unpublished; Hewawitharana 2007). Since the commonly accepted proposal that the MPP^+ toxicity is due to its specific accumulation through DAT, GBR12909, a potent DAT inhibitor, is used to investigate the role of DAT on MPP^+ uptake into MN9D cells. As shown from the data in Fig. 21, GBR12909 inhibits ~50% of MPP^+ uptake into MN9D cells. In addition, the more polar novel MPP^+ derivative, 3'OH-MPP^+ as well as the less polar derivative, 4'I-MPP^+ also taken up into all four cell types are also significantly inhibited by (~40-60%) GBR12909 (Figure 21).

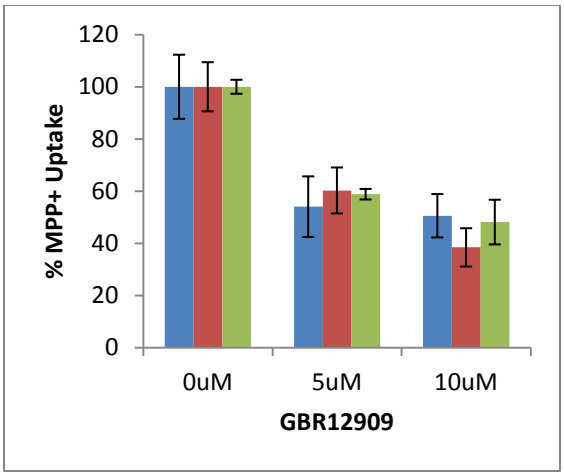

Figure 21- MPP^+ and its Derivatives Uptake with the Effect of GBR12909 in MN9D Cells. MN9D cells were grown in 12-well plates in DMEM as detailed in Methods. Cells were incubated with 0-10 µM GBR12909 in KRB-HEPES (pH 7.4) for 10 minutes followed by 50 µM MPP^+ for 45 additional min at 37˚C.Cells were washed, collected, and intracellular MPP^+ levels were quantified by reversed phase HPLC-UV. All the intracellular MPP^+ concentrations were normalized to respective protein concentrations as detailed in Experimental Methods. Data are represent as mean ± S.D (n = 3). MPP^+ (Blue), 3'OH-MPP^+ (Red), 4'I-MPP^+ (Green).

4.6.1 The Effect of GBR12909 on MPP^+ and its derivatives Toxicity in MN9D cells

Since GBR12909 significantly inhibits the uptake of MPP^+ into MN9D cells, its effect on the toxicity was investigated. In these experiments, MN9D cells were treated with 1 and 10 µM GBR12909 and various concentrations of MPP^+ or its derivatives for 24 h in KRB-HCO_3 and the cell viabilities were determined by the MTT assay. As shown in Fig. 22, GBR12909 has no significant effect on the toxicities of MPP^+ or its derivatives despite the significant inhibition of MPP^+ uptake. Further studies with fixed concentrations (close to LD_{50}) of MPP^+ (150 µM), more polar 3'OH-MPP^+ (300 µM), and less polar 4'I-MPP^+ (80 µM) with increasing concentrations of GBR12909 suggest that the specific toxicity of MPP^+ may not depends on DAT (Fig. 23).

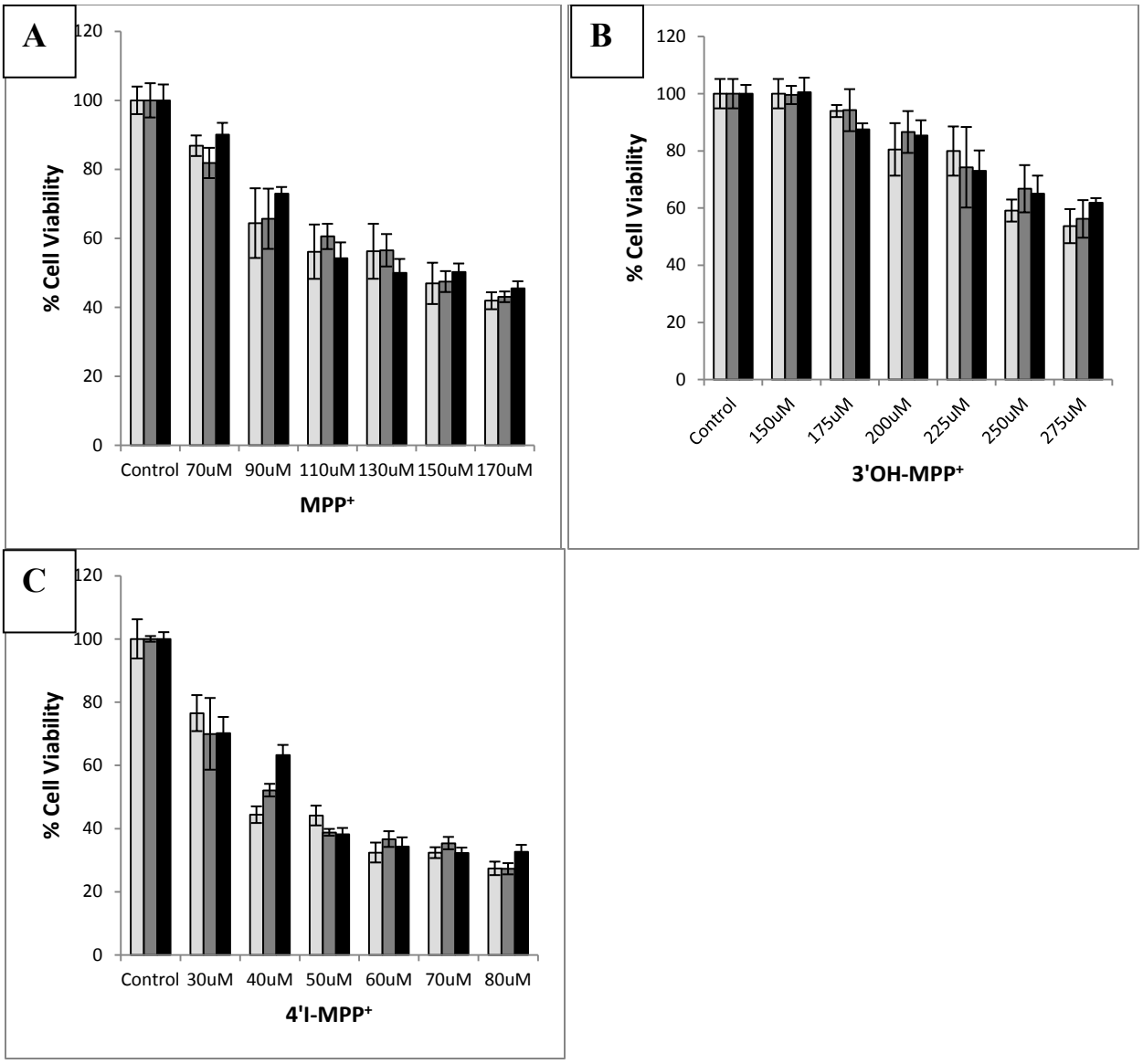

Figure 22: The Effect of GBR12909 on MPP^+ and its Derivatives Toxicity in MN9D Cells. MN9D cells were grown in 96-well plates to about 70-80% confluence and were incubated with 0-10 µM GBR12909 in KRB-HCO_3 for 10 min followed by desired various concentration of MPP^+ derivatives in KRB-HCO_3 for 24 h. Cell viabilities were determined by the MTT assay as detailed in *"Experimental Methods"*. Results are expressed as % viability with respect to parallel untreated controls. Data are presented as mean ± SD (n=5). MPP^+ (A), 3'OH-MPP^+ (B), 4'I-MPP^+ (C). 0 µM GBR 12909 (White), 1 µM GBR12909 (Gray), 10 µM GBR120909 (Black).

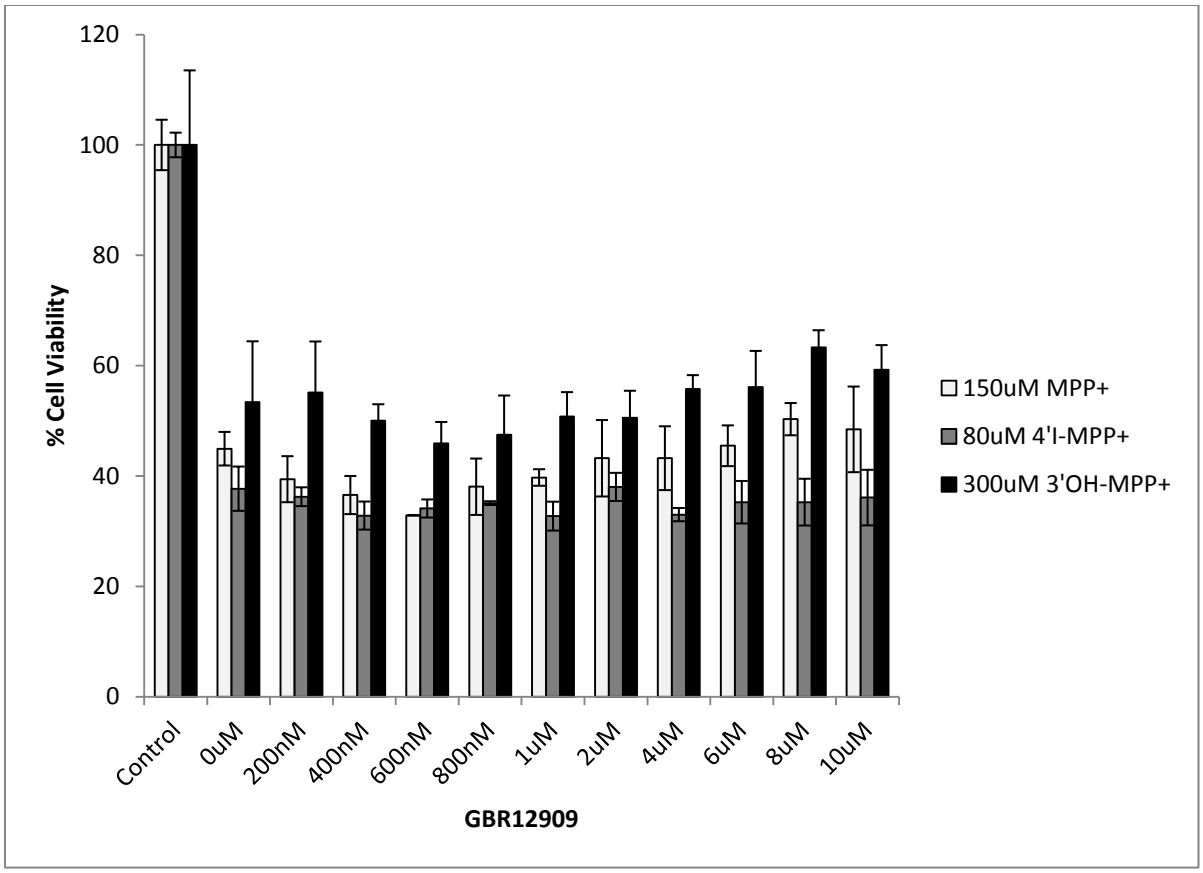

Figure 23: The Effect of GBR12909 on MPP^+ and its Derivatives Toxicity in MN9D cells. Cells were grown in 96-well plates and were incubated 0-10 μM GBR12909 followed by desired fixed concentration of MPP^+ derivatives in KRB-HCO_3 for 24 h. Cell viabilities were determined by the MTT assay as detailed in *"Experimental Methods"*. Results are expressed as % viability with respect to parallel untreated controls. Data are presented as mean ± SD (n=5).

4.7 The Effect of Extracellular Ca^{2+} on MPP^+ Toxicity

Since the uptake of MPP^+ into dopaminergic cells is dependent on the extracellular Ca^{2+}, the effect of extracellular Ca^{2+} on MPP^+ toxicity was studied. These experiments show the exclusion of extracellular Ca^{2+} from the incubation medium increased MPP^+ toxicity dramatically in MN9D and significantly in SH-SY5Y cells in KRB-HCO_3 during 12 h incubation period (Fig. 24A and B). On the other hand, extracellular Ca^{2+} had no significant effect on the MPP^+ toxicity towards both PC12 and HepG2 cells under similar experimental condition. Therefore, MN9D cell is chosen as the best model for toxicological and uptake studies with

respect to the effect of extracellular Ca^{2+}. Unfortunately the effect of extracellular Na^{+} on the MPP^{+} toxicity could not be determined since cells are highly sensitive to the Na^{+} free incubation conditions.

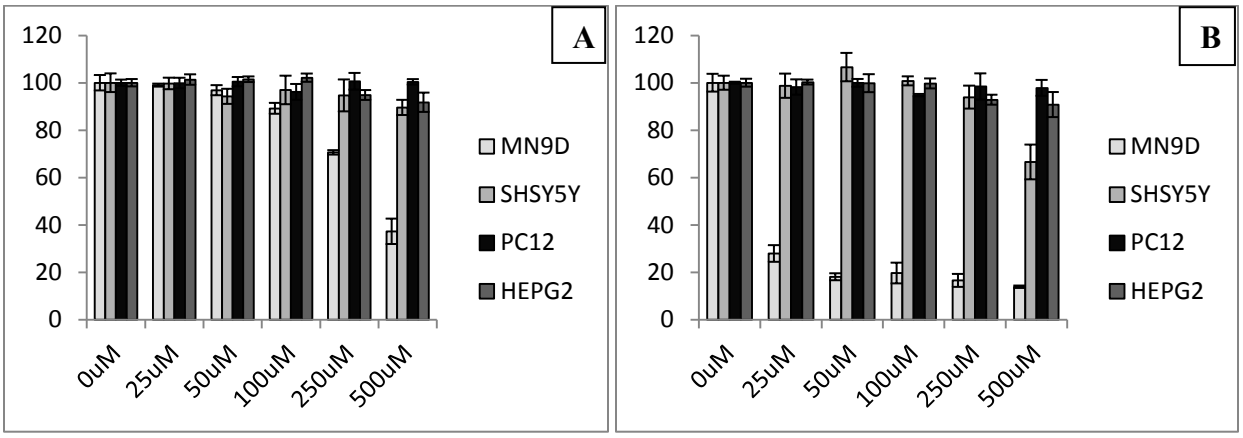

Figure 24- The Effect of Ca^{2+} on MPP^{+} Toxicity in HepG2, PC12, SH-SY5Y, and MN9D Cells.HepG2, SH-SY5Y, MN9D, and PC12 cells were grown in 96-well plates to about 70-80% confluence and were incubated with 50 µL of 0-500 µM MPP^{+} in KRB-HCO_3 for 12 h at 37˚C. The cell viabilities were determined by MTT assay and results are expressed as % viability of untreated MPP^{+} controls. Data are represented as mean ± SD (n=5). Ca^{2+} (A) and EGTA (B).

4.7.1 The Effect of Uptake Inhibitors on the MPP^{+} Toxicity of MN9D cells in the Presence and Absence of Extracellular Ca^{2+}

We used the above identified MPP^{+} uptake inhibitors to test whether the toxicity of MPP^{+} is proportional to the uptake of MPP^{+}. In the first set of experiments, MN9D cells were initially incubated with 0-50 µM concentration of one of the inhibitors for 10 min followed by a fixed 80 µM concentration of MPP^{+} in the presence of extracellular Ca^{2+} or 50 µM MPP^{+} in the absence of extracellular Ca^{2+} in KRB-HCO_3 for 12 h (Fig. 25A and B). In the second set of experiments, MN9D cells were incubated with the fixed 25 µM concentration of the inhibitors for 10 min followed by 0-250 µM varying concentrations of MPP^{+} with extracellular Ca^{2+} or 0-100 µM

MPP^+ in the absence of extracellular Ca^{2+} (Fig. 25C and D). The cell viabilities were measured by the MTT assay.

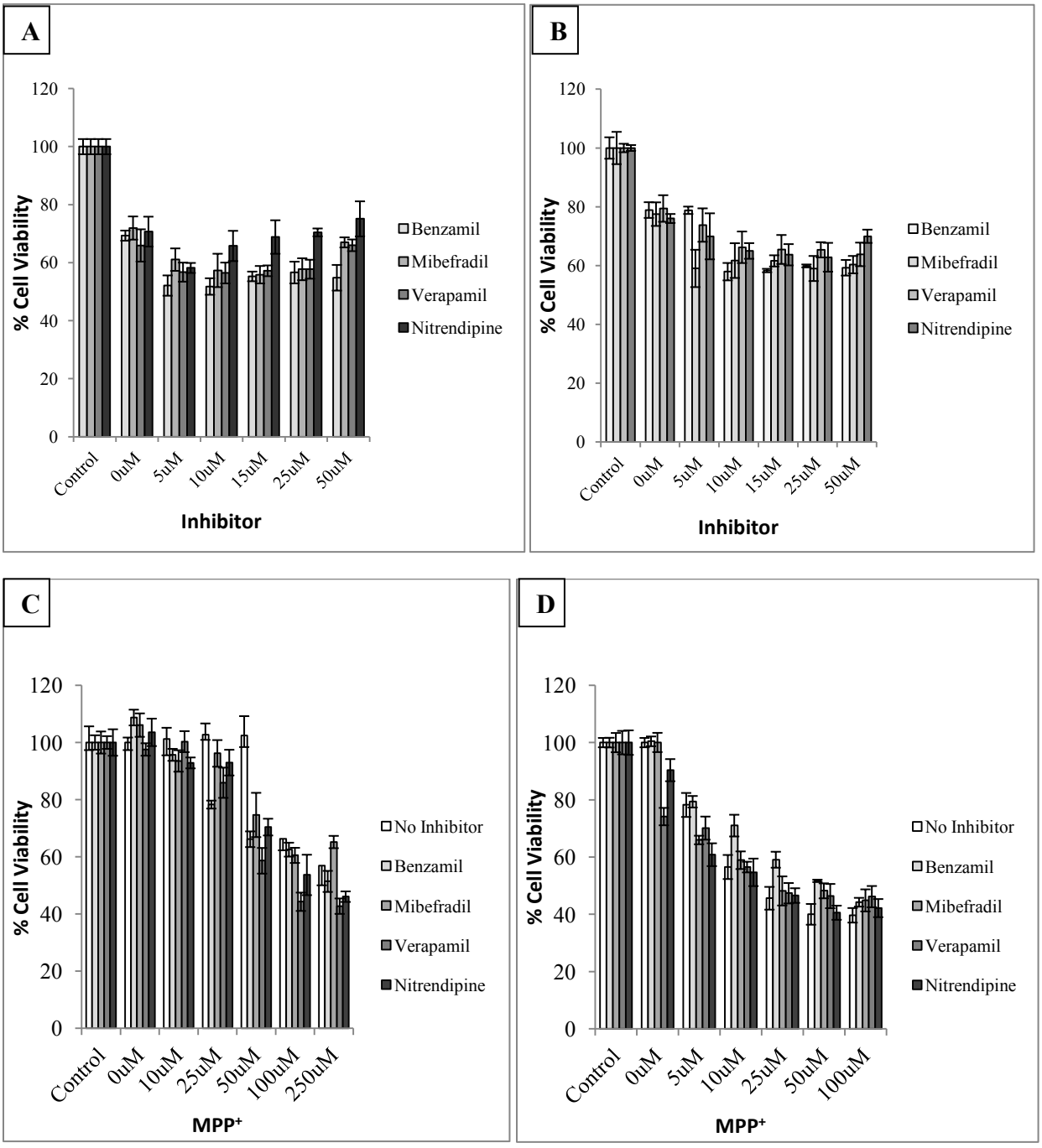

Figure 25- The Effect of Inhibitors on MPP^+ Toxicity in MN9D Cells. Panel A and B- MN9D cells in near confluence were initially treated with 40 µL of 0-50 µM inhibitor ($[Inhibitor]_{final}$ is pre-determined) for 10 min followed by the addition 10 µL of MPP^+ where $[MPP^+]_{final}$ is 80 µM MPP^+ in the presence of Ca^{2+}(A) or 50 µM MPP^+ in the absence of Ca^{2+}(B) in KRB-HCO_3 for

12 h. Panel C and D- MN9D cells were initially incubated with 25 µM inhibitor for 10 min followed by the addition of 0-250 µM MPP^+ in the presence of Ca^{2+} (C) and 0-100 µM MPP^+ in the absence of Ca^{2+} (D) in KRB-HCO_3 for 12 h. Cell viability was measured determined by the MTT assay as detailed in *"Experimental Methods"*. Data represent mean ± S.D. of five samples.

4.7.2 Effect of Intracellular Ca^{2+} on the MPP^+ toxicity on MN9D cells

To determine whether intracellular Ca^{2+} plays a role in MPP^+ toxicity, the effect of BAPTA on the MPP^+ toxicity was investigated. As found in Fig. 26, 50 µM BAPTA shows significant protection against MPP^+ toxicity in MN9D cells in the presence and absence of extracellular Ca^{2+} suggesting that the intracellular Ca^{2+} may play a role in MPP^+ toxicity of MN9D cells.

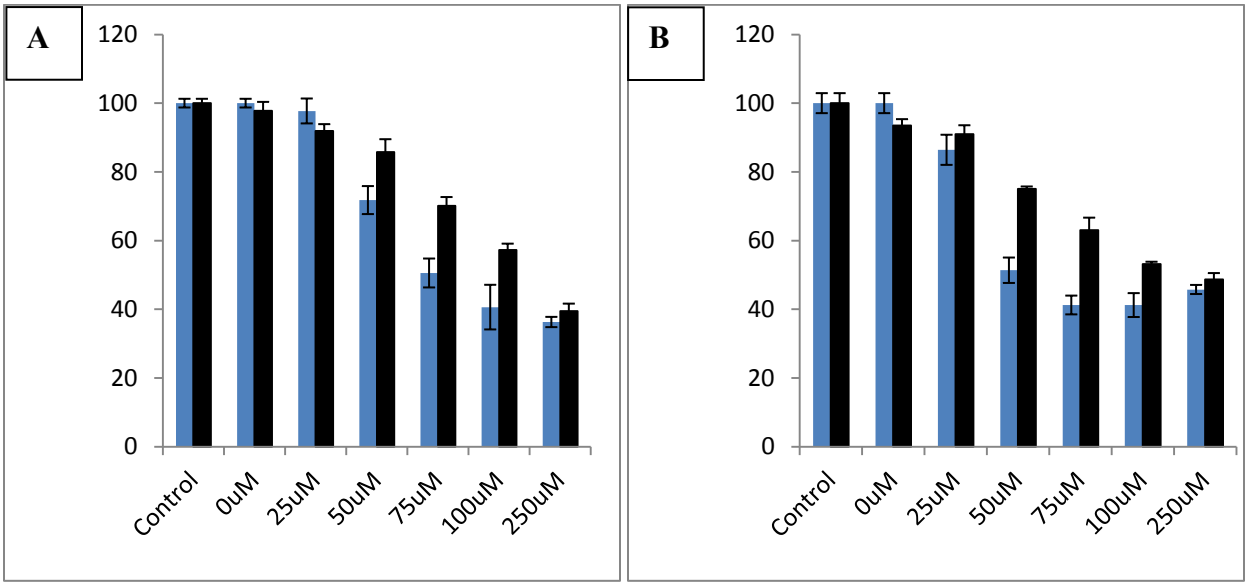

Figure 26- The Effect of BAPTA on MPP^+ Toxicity in MN9D Cells. Cell were grown in 96-well plates and were pre-incubated with 40 µL of 50 µM BAPTA-AM($[BAPTA\text{-}AM]_{final}$ is pre-determined) for 30 minfollowed by the addition 10 µL of MPP^+ where $[MPP^+]_{final}$ is 0-250 µM MPP^+ in the presence of Ca^{2+} (A) or 0-50 µM MPP^+ in the absence of Ca^{2+} (B) in KRB-HCO_3 for 12 h. Data represent mean ± S.D. of five samples. 0 µM BAPTA (Blue), 50 µM BAPTA (Black).

4.7.3 Flufenamic acid protects MN9D cells from MPP^+ toxicity

We found that the non-specific cation channel blocker flufenamic acid and its derivatives provide excellent neuroprotection activity against MPP^+ toxicity of MN9D cells (Fig. 27). However, the data in Fig. 28, flufenamic acids and its analogs show very weak MPP^+ uptake inhibition in the presence of Ca^{2+} or absence of Ca^{2+}. These findings suggest the protection of MN9D cells from MPP^+ toxicity by flufenamic acid and its derivatives could not be due to the inhibition of MPP^+ uptake.

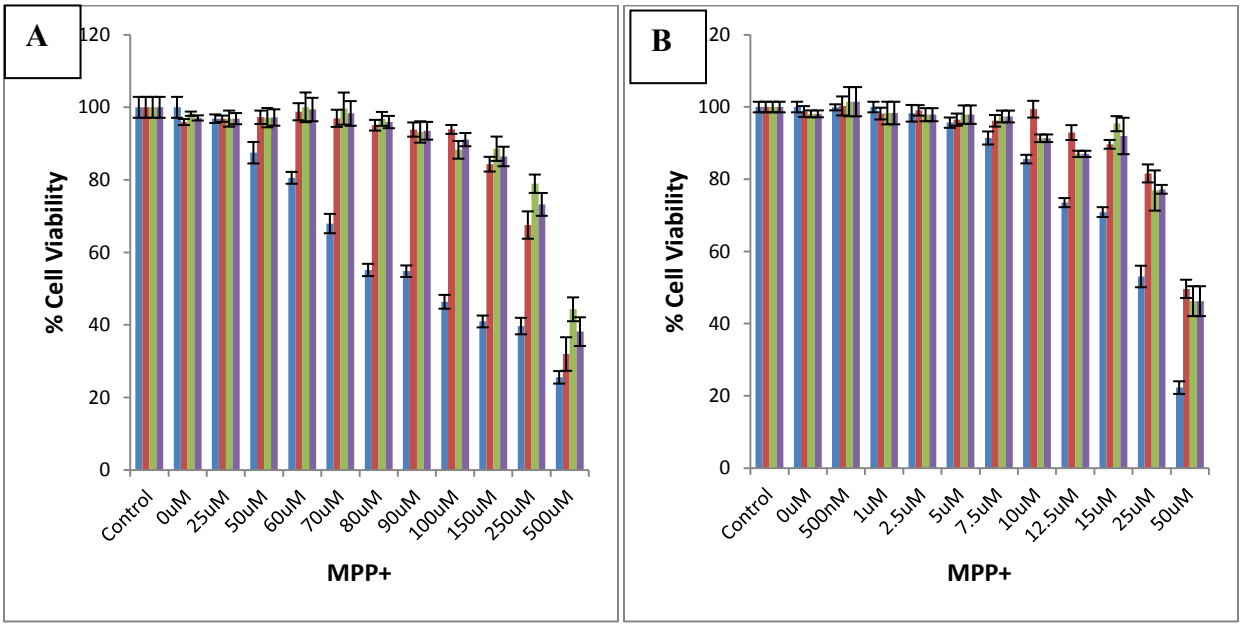

Figure 27- The Effect of Flufenamic Acid and its Analogs on MPP^+ Toxicity in MN9D Cells. Cell were grown in 96-well plates and were pre-incubated with 40 µL of 50 µM FFA and its analogs ($[FFA]_{final}$ is pre-determined) for 20 min followed by the addition 10 µL MPP^+ where $[MPP^+]_{final}$ is 0-500 µM MPP^+ in the presence of Ca^{2+} (A) or 0-50 µM MPP^+ in the absence of Ca^{2+} (B) in KRB-HCO_3 for 12 h. Data represent mean ± S.D. of five samples. No Inhibitor (Blue), FFA (Red), MFA (Green), TFA (Purple).

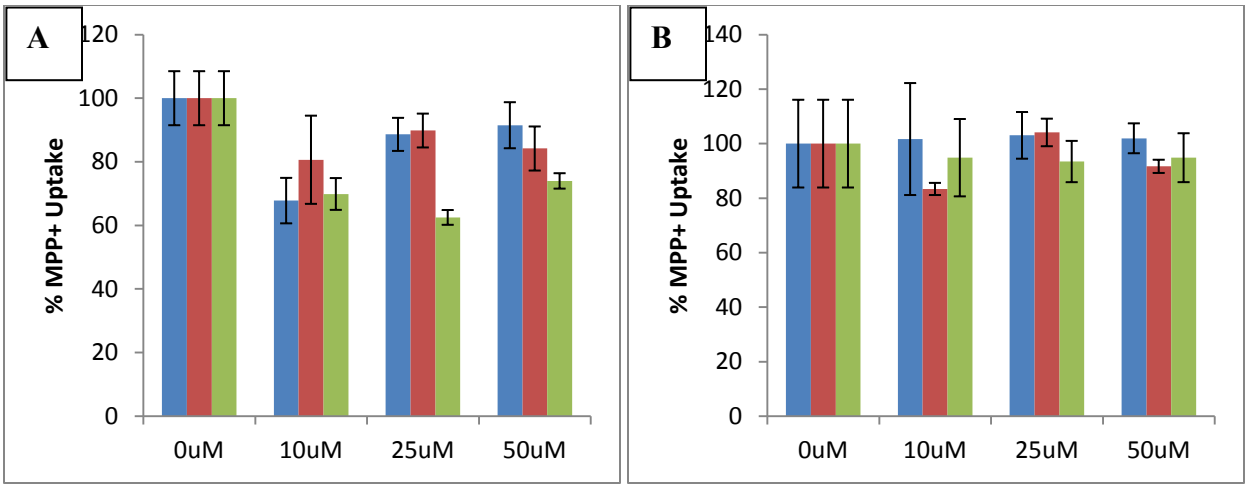

Figure 28- Inhibitory Effect of Flufenamic acid and its Analogs on MPP^+ Uptake in MN9D Cells. Cells were treated initially with 990 µL of 0-50 µM Inhibitor followed by addition 10 µL of MPP^+ in the presence (A) or absence (B) of extracellular Ca^{2+} in KRB-HCO_3 for 45 min. Final concentration of Inhibitor and MPP^+ are pre-determined. Cells were washed several times, collected, and intracellular MPP^+ concentrations were determined by reversed phase HPLC-UV. The intracellular MPP^+ concentrations were normalized to respective cellular protein concentrations. Data represent mean ± S.D. of triplicate samples. FFA (Blue), MFA (Red), TFA (Green).

In addition to flufenamic acid and its derivatives the mitochondrial calcium exchange inhibitors 2-APB and CGP37157 are also effective protective agents for the MPP^+ induced MN9D toxicity (Fig. 29)

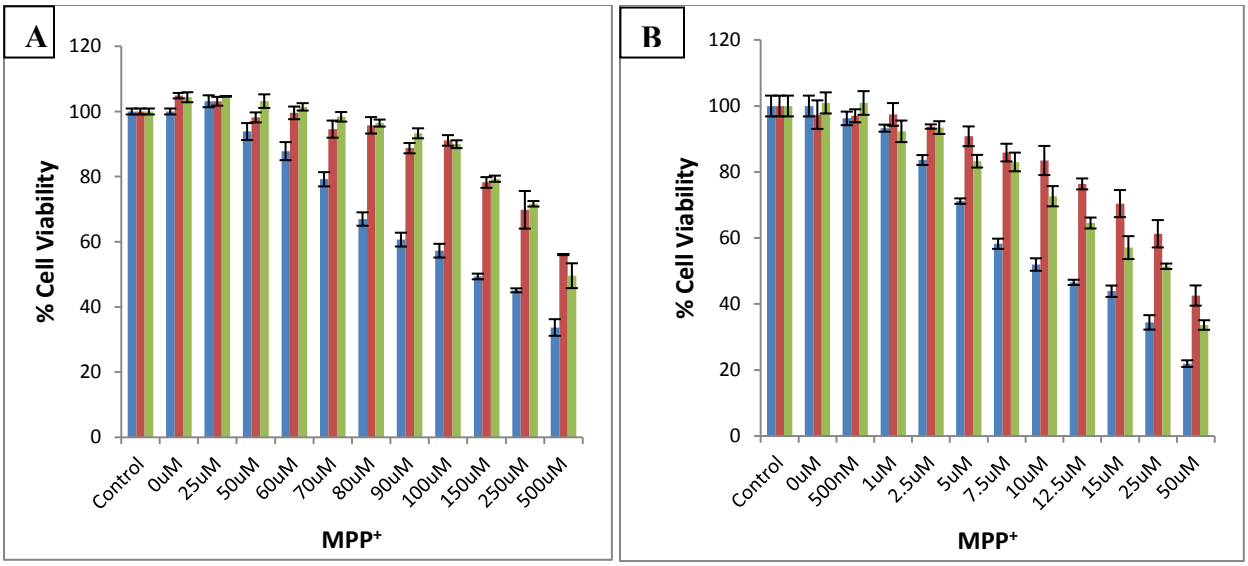

Figure 29- The Effect of 2-APB and CGP37157 on MPP^+ Toxicity in MN9D Cells. Cell were grown in 96-well plates and were pre-incubated with 40 µL of 50 µM 2-APB or CGP13757 ($[Inhibitor]_{final}$ is pre-determined) for 10 min followed by the addition 10 µL of MPP^+ where $[MPP^+]_{final}$ is 0-500 µM MPP^+ in the presence of Ca^{2+} (A) or 0-50 µM MPP^+ in the absence of Ca^{2+} (B) in KRB-HCO_3 for 12 h. Data represent mean ± S.D. of five samples. Ca^{2+} (A) and EGTA (B). No Inhibitor (Blue), 2-APB (Red), CGP13757 (Green).

4.7.4. MPP^+ uptake inhibitors increase the MPP^+ toxicity of MN9D cells

Although the most effective MPP^+ uptake inhibitors, benzamil, verapamil, GB12909, and SKF96365 were expected to protect MN9D cells from MPP^+, the toxicity studies with these show a significantly increase in toxicity. As found in Fig. 30 A&B, benzamil, verapamil, GB12909, and SKF96365 did not show significant cellular protection, but an unexpectedly increase the MPP^+ toxicity of MN9D cells.

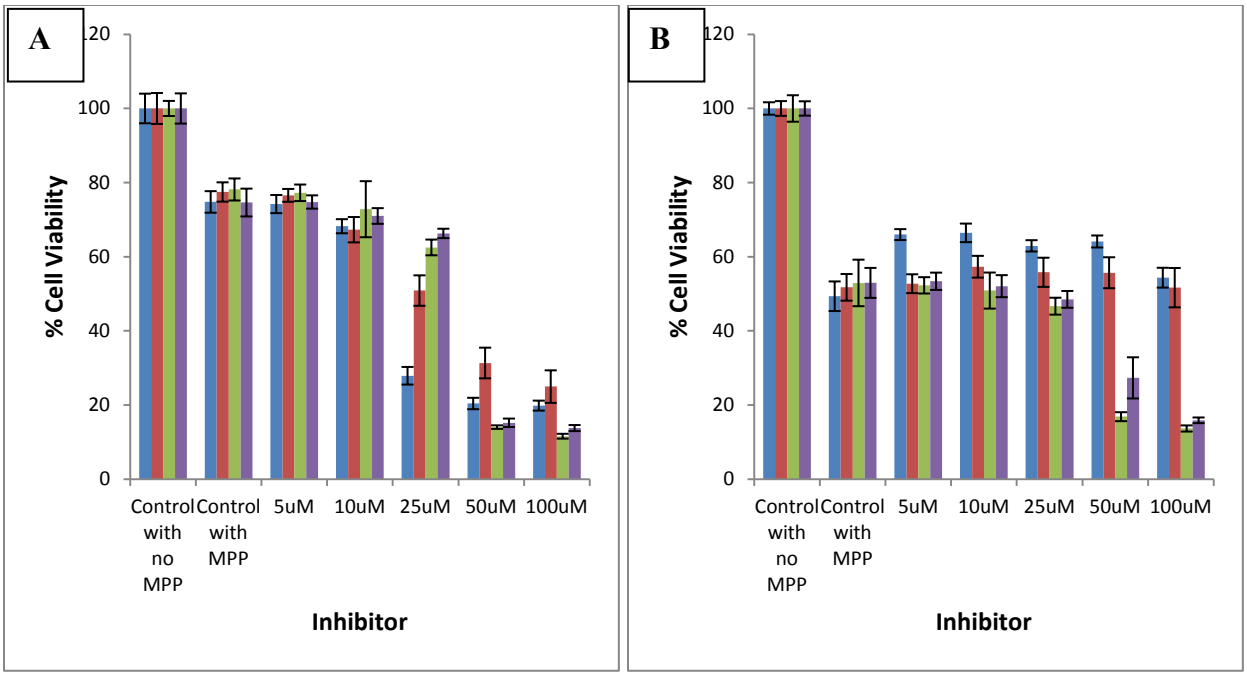

Figure 30 -The Effect of Inhibitors on MPP^+ Toxicity in MN9D Cells. Differentiated MN9D cells grown in 96-wells plate were initially treated with 40 µL of for 10 min followed by the addition 10 µL MPP^+ in the presence of Ca^{2+} (A) and absence of Ca^{2+} (B) in KRB-HCO_3 for 15 h. Final concentration of Inhibitor and MPP^+ are pre-determined. Cell viability was measured determined by the MTT assay as detailed in *"Experimental Methods"*. Data represent mean ± S.D. of five samples. Benzamil (Blue), Verapamil (Red), GBR12909 (Green), SKF96365 (Purple).

4.8 MPP^+ Uptake inhibitors are toxic to MN9D cells

MN9D toxicity of MPP^+ inhibitors uptake was determined by incubating cells with MPP^+ alone or MPP^+ uptake inhibitors for 15 h in the presence and absence of extracellular Ca^{2+} in KRB-HCO_3. As shown from Fig. 38, the most potent MPP^+ uptake inhibitors were highly toxic to MN9D cells both in the presence and absence of extracellular Ca^{2+} in the incubation medium. In the absence of extracellular Ca^{2+}, LD_{50} of MPP^+, Verapamil and Benzamil (Table 8; data were calculated from the data in Fig. 31) was significantly reduced. LD_{50} of GBR12909 and mibefradil was not changed significantly.

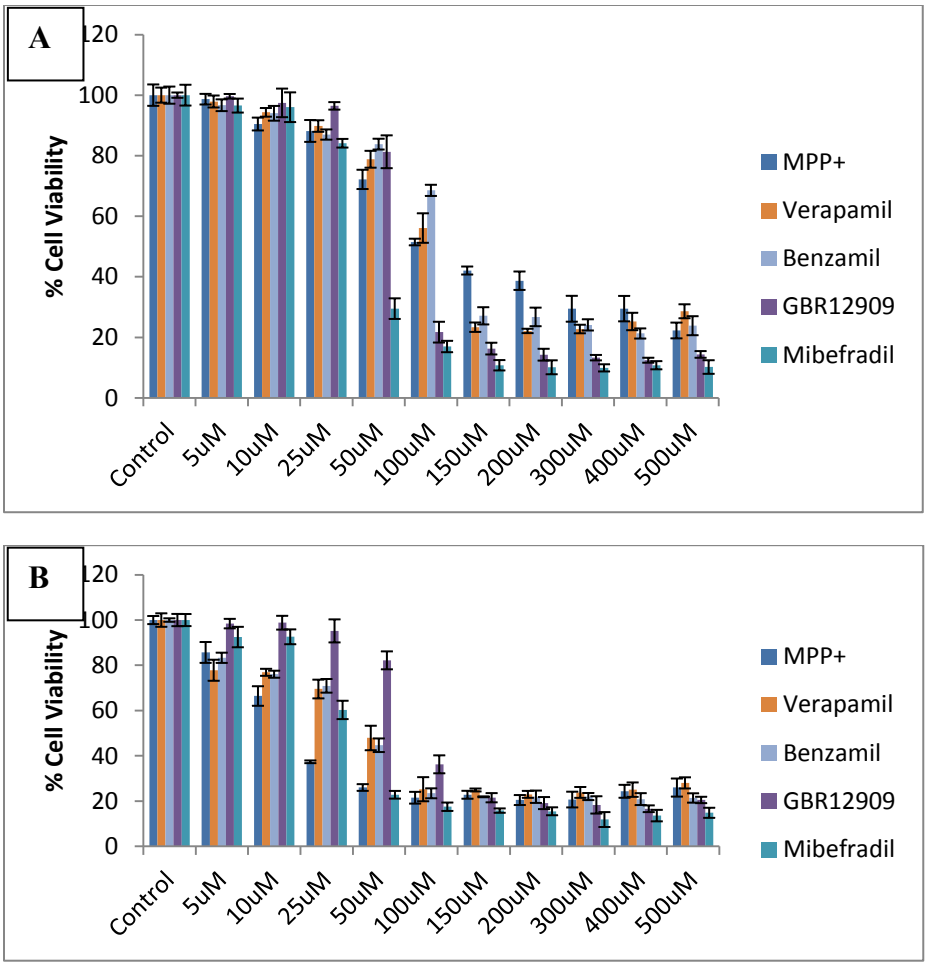

Figure 31- Toxicity of Inhibitors and MPP^+ in the Presence and Absence of Extracellular Ca^{2+} in MN9D Cells. MPP^+ was dissolved in water and inhibitors were dissolved in DMSO where the final DMSO concentration was kept to a minimum <0.5% v/v. Cells were grown in 96-well plates and were incubated with 50 µL of 0-500 µM MPP^+ or inhibitors in the presence (A) and absence (B) of extracellular Ca^{2+} in KRB-HCO_3 for 15 h and cell viability was determined by the MTT assay as detailed in "*Experimental Methods*". Data represent mean ± S.D. of 5 samples.

Table 8 - LD_{50} of MPP^+ and MPP^+ uptake Inhibitors of MN9D Cells in the Presence and Absence of Extracellular Ca^{2+}

Ca^{2+}	
	LD_{50} (µM)
MPP^+	118.28
GBR1209	74.43
Mibefradil	39.91
Verapamil	104.06
Benzamil	117.32

EGTA	
	LD_{50} (µM)
MPP^+	19.02
GBR1209	84.69
Mibefradil	39.91
Verapamil	54.06
Benzamil	52.29

4.9. The Effect of Extracellular Ca^{2+} on the viability of MPP^+ loaded MN9D Cells under Back-Transport conditions.

To investigate the toxicity of MPP^+ under back-transport conditions, MN9D cells are initially loaded with 0-500 μM MPP^+ in the absence of extracellular Ca^{2+} for 1 h, washed several times, and then incubated for 15 h in the presence or absence of 0-500 μM MPP^+ and extracellular Ca^{2+} (EGTA). The cell viabilities were determined using the MTT assay. As shown in Fig. 31A, cell viability did not decrease when cells were preloaded with MPP^+, and without MPP^+ in the presence of extracellular Ca^{2+}. However, cell viability decreased when cells were preloaded with MPP^+, and without MPP^+ in the absence of extracellular Ca^{2+} (Fig. 32B). On the other hand, GBR12909 had no effect on the cell viability in the presence and absence of extracellular Ca^{2+} (Fig. 31). However, when benzamil, verapamil, and SKF96365 were added, the cell viability decreased in the presence of extracellular Ca^{2+} (Fig. 32A), but there is no effect in the absence of extracellular Ca^{2+} (Fig. 32B).

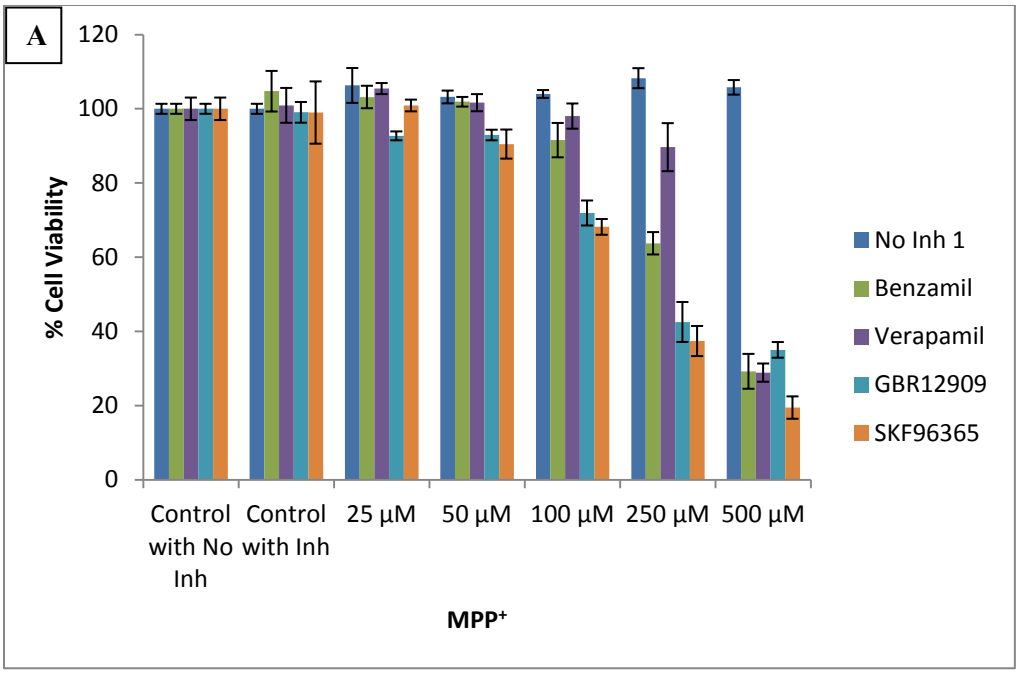

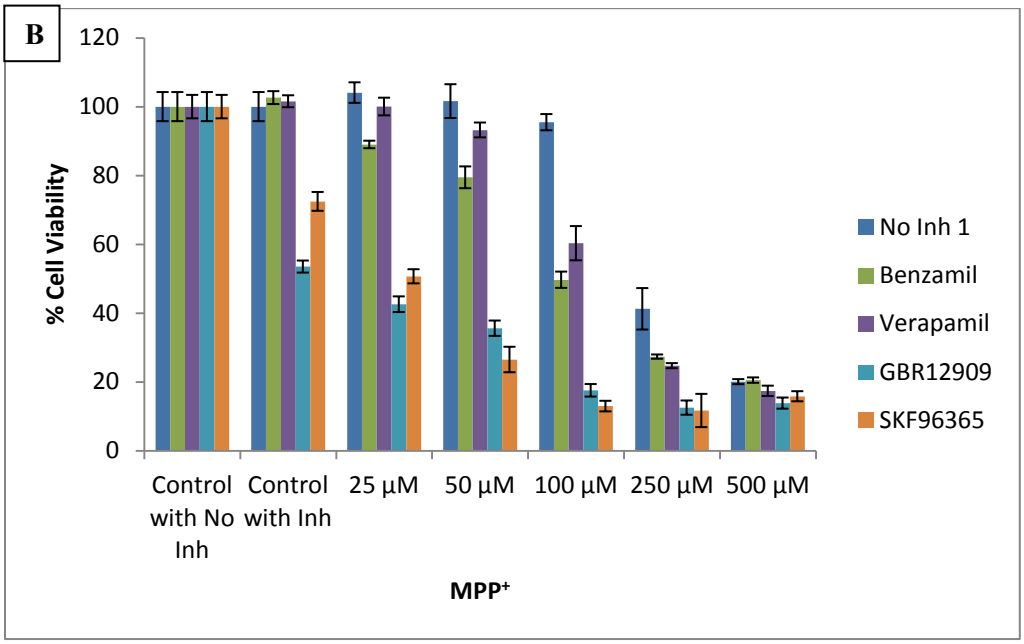

Figure 32- The Effect of Inhibitors on the Toxicity of Back-Transport of MPP^+ in the Presence and Absence of Extracellular Ca^{2+} in MN9D Cells. MN9D cells were grown in 48-well plates to about 70-80% confluence and were incubated with 100 µL of 100 µM MPP^+ in the absence of both $[Ca^{2+}]_o$ and $[EGTA]_o$ in KRB-HCO_3 buffer for 1 h at 37˚C. Cells were washed several times with appropriate buffer and incubate with 100 µL of 25 µM Inhibitor in KRB-HCO_3 for 15 h at 37˚C in the presence (A) or absence (B) of extracellular Ca^{2+}. The cell viabilities were

determined by MTT assay and results are expressed as % viability of untreated MPP^+ controls. Data are represented as mean ± SD (n=5).

4.10 Western Blotting Analysis of PMAT, NCX1, and OCT3.

As noted from Figure 33A, Western Blot experiments with polyclonical PMAT antibodies showed a band in the vicinity of 55-60 kDa for human liver HepG2 and neuroblastoma SH-SY5Y cells and also showed a band in the approximately 50-55 kDa for rat PC12 and mouse MN9D cells, which is characteristic of the PMAT protein (185,186). Although the number of the amino acids in the sequence for human and mouse/rat cell-lines are nearly identical, the difference in the molecular weight as shown in Fig. 33A may be due to the species specific. Similar experiments with rabbit polyclonal NCX1 (Fig. 33B) and OCT3 (data not shown) antibodies in rat PC12 and mouse MN9D cells extracts showed a characteristic band in the vicinity of ~70 kDa for the NCX1 protein (187), but no band corresponding to OCT3 was observed in either cell lines.

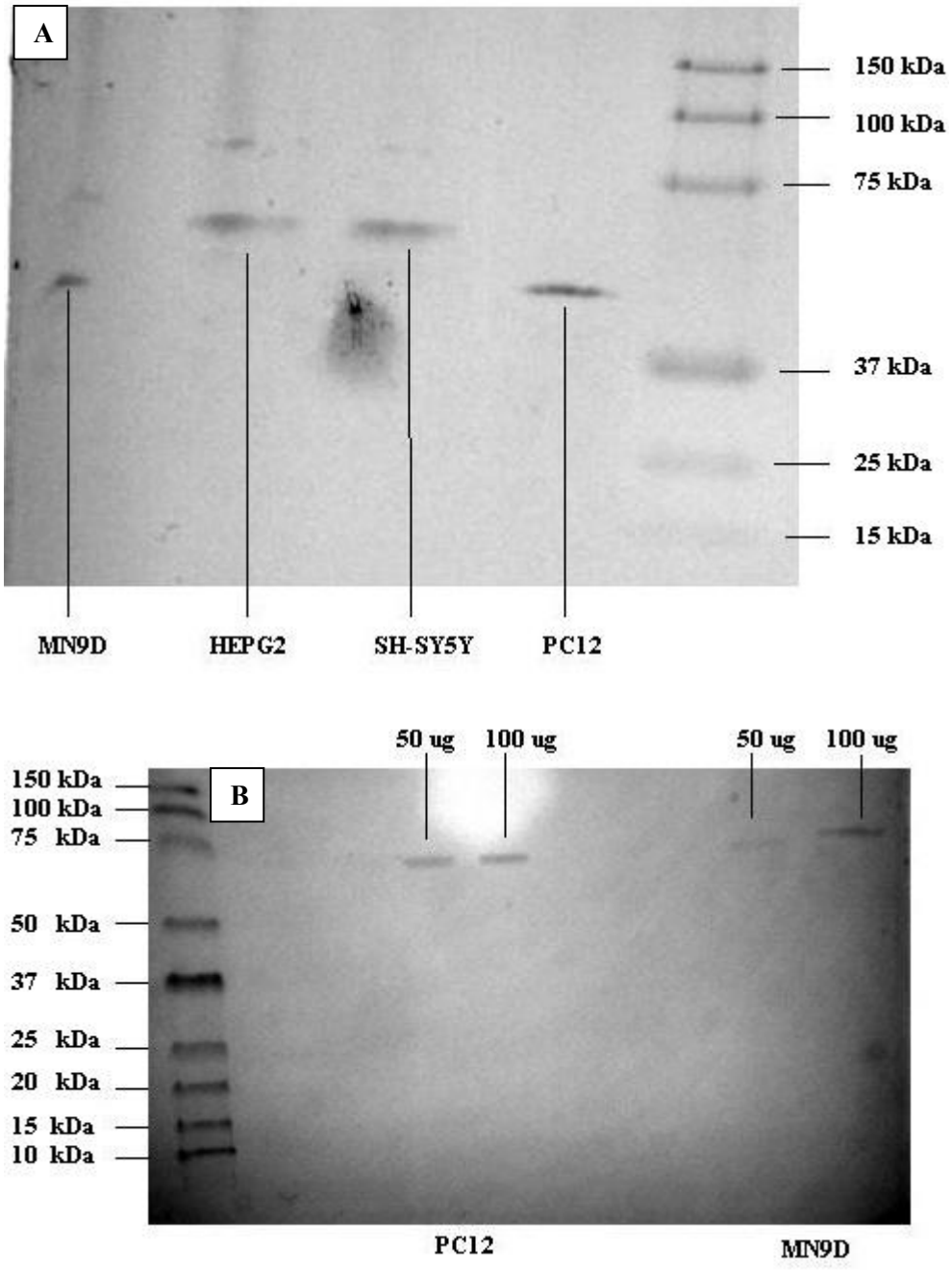

Figure 33- Western Blot Analysis of PMAT (A) present in HepG2, PC12, SH-SY5Y, and MN9D Cells and NCX1 (B) present in PC12 and MN9D Cells.

CHAPTER IV

DISCUSSION

5.1 Mechanism(s) of MPP^+ Uptake

Catecholaminergic MN9D, SHSY5Y, and PC12 and non-catecholaminergic HepG2 cells take up substantial amounts of MPP^+ under similar experimental conditions (Fig. 6). The analyses of the MPP^+ uptake regarding the effect of extracellular Na^+ and Ca^{2+} show that while 40-65% of MPP^+ uptake into dopaminergic cells (MN9D and SH-SY5Y) is effectively inhibited by extracellular Ca^{2+}, uptake into non-dopaminergic cells (PC12 and HepG2) is not affected by extracellular Ca^{2+} (Fig.7). In contrast to previous reports, MPP^+ uptake into dopaminergic cells is largely independent of extracellular Na^+, suggesting that this uptake process is distinct from the classical Na^+/Cl^- dependent monoamine transporters. Furthermore, 3'OH-MPP^+ and 4'I-MPP^+ show uptake characteristics similar to that of MPP^+ with all four types of cells (Fig. 8). Similarly, differentiated MN9D cells showed similar uptake characteristics as undifferentiated MN9D cells, further confirming that a Ca^{2+}_o sensitive Na^+/Cl^- independent MPP^+ uptake pathway is present in dopaminergic cells (Fig. 8E).

Careful analyses of the uptake of MPP^+ into HepG2 cells show that the uptake is primarily a Ca^{2+}_o or Na^+_o independent process (Scheme 1A). On the other hand, MPP^+ uptake into PC12 is comprised of at least two components both of which are Ca^{2+}_o insensitive and ~35% Na^+_o dependent and ~65% Na^+_o independent (Scheme 1B).

The uptake of MPP^+ into MN9D cells consist at least three components. The Na^+_o independent major component, which is about 65% of the total uptake, is inhibited by Ca^{2+}_o.

Interestingly, the Na^+ dependent component was minor, comprising only about 6% of the total uptake, and the remaining 29% is $Ca^{2+}{}_o$ insensitive and $Na^+{}_o$ independent similar to the major component of MPP^+ uptake into PC12 cells (Scheme 1D).

Parallel to MN9D cells, MPP^+ uptake into SH-SY5Y also has three components, consisting of 33% Na^+ dependent, 29% Na^+ independent, and 38% $Ca^{2+}{}_o$ dependent (Scheme 1C). These findings demonstrate that a major fraction of the MPP^+ uptake into MN9D cells and a significant portion into SH-SY5Y cells occurs through a $Ca^{2+}{}_o$ sensitive $Na^+{}_o/Cl^-$ independent pathway.

Scheme 1: Approximate contributions of various MPP^+ uptake in HepG2, PC12, SH-SY5Y, and MN9D Cells

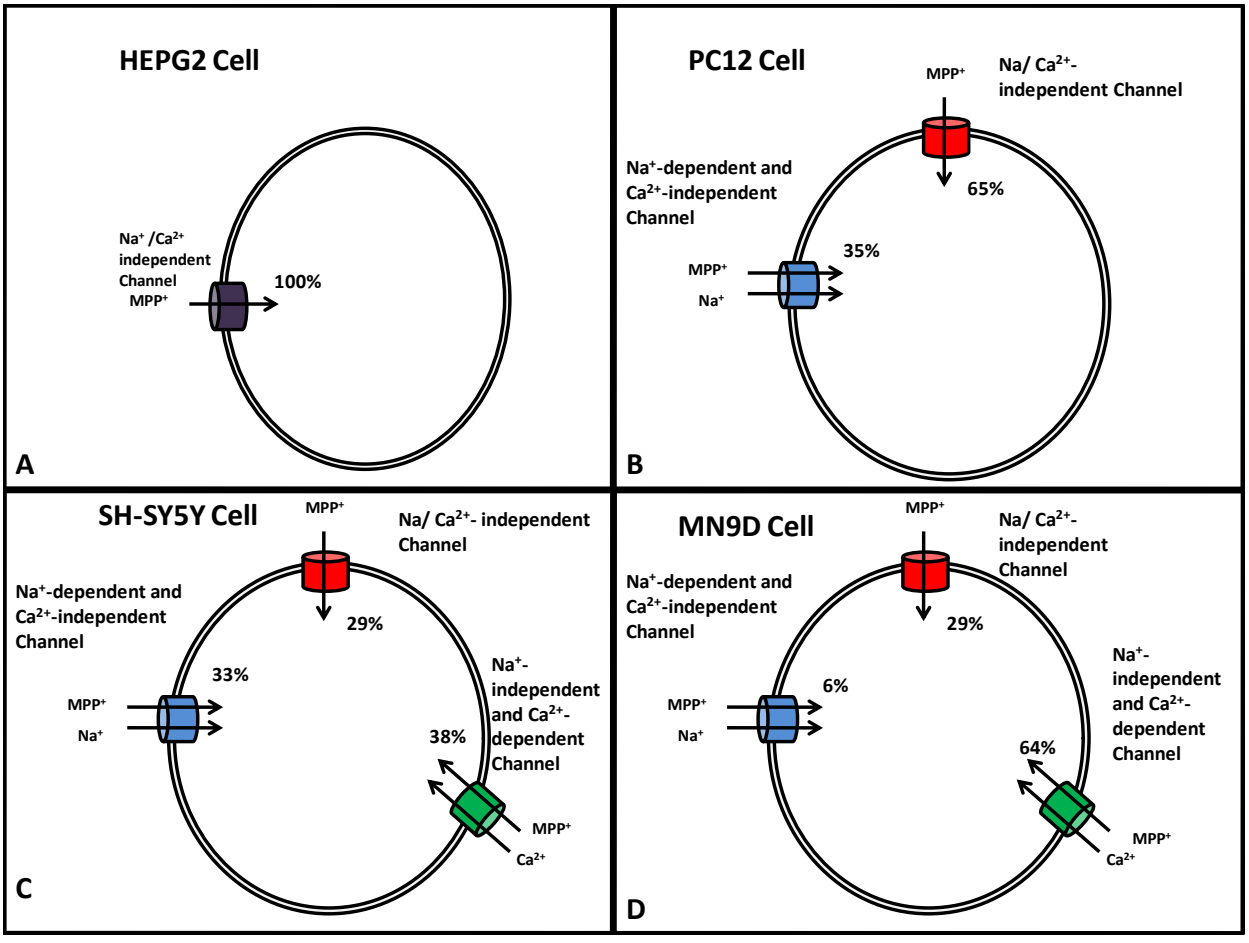

Kinetic analyses show extracellular Ca^{2+} behaves as a competitive inhibitor for MPP^+ uptake (K_m effect) with a K_i of 13.2 ± 1.5 μM and the V_{max} is not significantly affected by the extracellular Ca^{2+} (Fig. 10). If an exchange mechanism is operative and outward Ca^{2+} transport is coupled with MPP^+ uptake, then extracellular Ca^{2+} could not behave as a competitive inhibitor for MPP^+ uptake. Furthermore, undifferentiated and differentiated MN9D cells dramatically take up MPP^+ in the absence of extracellular Ca^{2+} after ~15 min whereas MPP^+ uptake is Ca^{2+}-independent for PC12 ells through time-course (Fig. 9).

Intracellular Ca^{2+}-perturbing agents including benzamil, mibefradil, verapamil, GBR12909, and SKF96365 have been shown to be competitive inhibitors for MPP^+ uptake into MN9D cells. However, while these are stronger inhibitors for the MPP^+ uptake into MN9D cells in the absence of extracellular Ca^{2+}, they are noticeably weaker inhibitors in the presence of extracellular Ca^{2+} (Fig. 15). Similarly, SH-SY5Y cells show similar inhibitory effect as undifferentiated MN9D cells suggesting that these are good inhibitors for the Ca^{2+}_o sensitive MPP^+ uptake pathway in dopaminergic cells (Fig. 15). In PC12 cells, these are even stronger inhibitors, but inhibition potency is not significantly affected by extracellular Ca^{2+} suggesting that these are also good inhibitors for the Ca^{2+}_o insensitive MPP^+ uptake pathways in PC12 cells (Fig. 15). Therefore, these inhibitors could be not used to differentiate between these pathways. On the other hand, MPP^+ uptake into liver HepG2 cells is not inhibited by these inhibitors except SKF96365 and benzamil confirming that the MPP^+ uptake pathway in HepG2 cells is different from that of catecholaminergic cells (Fig. 15).

The other pharmacological agents including non-specific dihydropyridine VGCC blockers, common cation channel blockers, or blockers of Ca^{2+} release from intracellular stores such as fenamates, Gd^{3+}, Ni^{2+}, 2-APB, and CGP37157 showed no or little effect on the MPP^+

uptake into MN9D in the presence or absence of extracellular Ca^{2+}, even at high concentrations (Fig. 11 and 12) suggesting that these channels are not responsible for the observed Ca^{2+}_o sensitivity of MPP^+ uptake. In addition, tetradotoxin (Fig. 12C) , Thapsigargin (Fig. 13), and BAPTA (Fig. 14) also had no significant effect on MPP^+ uptake demonstrating that the VGNC or the depletion of intracellular Ca^{2+} from the intracellular stores may not be directly associated with the Ca^{2+}_o sensitivity of MPP^+ uptake pathway.

In contrast to the inhibition of the MPP^+ uptake pathway by extracellular Ca^{2+}_o, the reverse transport of intracellular MPP^+ from MPP^+ loaded MN9D cells is accelerated by extracellular Ca^{2+} (Fig. 17). Extracellular Na^+ has no significant effect on the reverse transport of intracellular MPP^+ (Scheme 5D). In addition the reverse transport is also inhibited by benzamil, verapmil, and SKF96365, but in sharp contrast, GBR12909 did not inhibit the loss of intracellular MPP^+ (Fig. 18). A similar behavior, but less pronounced, is also observed with MPP^+ loaded SH-SY5Y cells (Scheme 5C). Interestingly, no loss of intracellular MPP^+ was observed with PC12 cells under similar experimental conditions in the presence or absence of extracellular Ca^{2+} or Na^+ as well as the above uptake inhibitors suggesting that MPP^+ uptake into PC12 cells is largely irreversible (Scheme 5B). Therefore, we conclude that Ca^{2+}_o-sensitive, Na^+_o-independent MPP^+ uptake into MN9D and SH-SY5Y cells is reversible in the presence of Ca^{2+}_o and the other Ca^{2+}_o insensitive pathways are irreversible under all conditions. On the other hand, complete loss of intracellular MPP^+ was observed with HepG2 cells under similar experimental conditions in the presence or absence of extracellular Ca^{2+}or Na^+ (Scheme 5A) and this process is moderately inhibited by benzamil which also inhibits the uptake of MPP^+ (Fig. 18).

Scheme 5: Pathway of back transport of MPP^+ from MPP^+ loaded HepG2, PC12, SH-SY5Y, and MN9D Cells

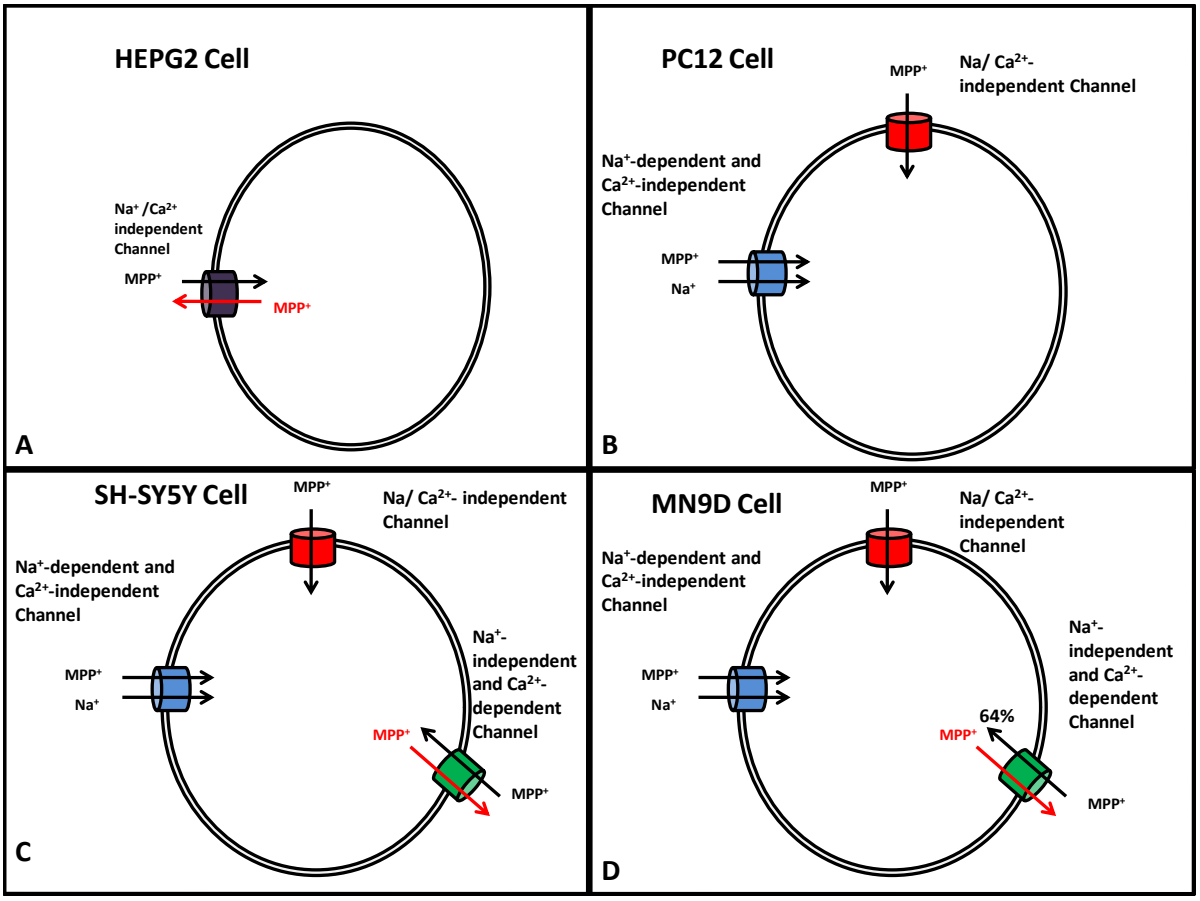

Based on the above findings, we propose that Ca^{2+}_o competitively inhibits the MPP^+ uptake into dopaminergic cells by directly interacting with the transporter. This proposal is supported by several key observations. First, Ca^{2+}_o acts as a competitive inhibitor for MPP^+ uptake (K_m effect) with a K_i of 13.2 ± 1.5 µM and Ca^{2+}_o did not significantly alter the V_{max}. If an exchange mechanism such as NCX is operative and extracellular MPP^+ is exchanged with intracellular Ca^{2+}, then Ca^{2+}_o could not behave as a competitive inhibitor for the MPP^+ uptake. In addition, such an exchange mechanism should decrease cytosolic Ca^{2+} levels in parallel to MPP^+ uptake and the reverse transport of MPP^+ from MPP^+ loaded cells should increase the

intracellular Ca^{2+}. However, we were not able to detect any changes in intracellular levels under MPP^+ uptake or reverse transport conditions (data not shown).

Overall, our findings confirm that MPP^+ is taken up into various cells through multiple pathways depending on the nature of the cells. Uptake of MPP^+ into non-neuronal HepG2 cells occurs through PMAT and/or OCT which are known to be expressed in these cells. These transporters are reported to be reversible and independent of both Na^+ and Ca^{2+}. On the other hand, uptake of MPP^+ into catecholaminergic PC12 cells occurs through two pathways, ~35% through classical Na^+ and Cl^- dependent monoamine transporters and the 65% through a Na^+ independent pathway which may involve PMAT. Both of which are not sensitive to extracellular Ca^{2+}. This proposal requires PMAT to be irreversible since Na^+ dependent monoamine transporters are known to be irreversible under normal conditions and MPP^+ is not back transported from PC12 cells. However, previous studies suggest that MPP^+ uptake into MSCK cells stably express human PMAT is reversible similar to OCTs (95). Regardless of these subtle differences, the above results demonstrate that, in addition to Na^+_o-dependent DAT and NET, a highly active Na^+_o-independent Ca^{2+}_o-insensitive apparently irreversible MPP^+ transporter similar to PMAT is present in PC12 cells. Uptake of MPP^+ into dopaminergic MN9D and SH-SY5Y cells occurs through three pathways in which two of them are similar to pathways of PC12 cells. The third Na^+ independent, Ca^{2+}_o sensitive pathway is a major MPP^+ uptake pathway in dopaminergic cells. Although Ca^{2+}_o sensitive reversibility of this pathway suggests that it may behave as a Ca^{2+}/MPP^+ antiporter. Ca^{2+}_o inhibition kinetics, intracellular Ca^{2+} measurements, and other experimental evidence clearly demonstrate that this transporter could not function as an antiporter, but as a novel Ca^{2+} sensitive monoamine/cation transporter.

5.2 Mechanism(s) of MPP^+ Toxicity

The specific dopaminergic toxicity of MPP^+ due to the specific uptake through DAT followed the inhibition of mitochondrial complex I of the energy chain transport. However, our studies show that MPP^+ is taken into not only dopaminergic cells but also into many other cells through a multitude of transporters with varying efficiencies. However, clearly MPP^+ is specifically and highly toxic to dopaminergic MN9D and SH-SY5Y cells and not significantly toxic to other cell types (Fig. 19). In addition cell specificity profiles similar to MPP^+ were observed for all the MPP^+ derivatives tested, with a noticeable increase of toxicity with the increasing hydrophobicity of the substituent as determined by the corresponding LD_{50} values. For example, MN9D toxicities of 4' halogenated derivatives gradually increase from 4'F (LC_{50} = 142 μM) to 4'I (LC_{50} = 81 μM) (Fig. 20A). This could be due to the increased uptake of more hydrophobic derivatives due to the passive diffusion through the plasma membrane in addition to the mediated transport. Interestingly, although MPP^+ uptake into MN9D and SH-SY5Y cells is partially inhibited by DAT blocker GBR12909 (Fig. 21-23), it failed to protect these cells from MPP^+ toxicity. Interestingly, more polar 3'OH-MPP^+ which is not expected to enter the cell through simple diffusion is also effectively taken up into all four cell types and DAT inhibitor GBR12909 again failed to protect dopaminergic cells from its toxicity (Fig. 21-23). These findings suggest that MPP^+ toxicity may be independent of DAT and some special characteristics of dopaminergic cells make them more vulnerable to MPP^+ toxicity present in these cells.

Exclusion of extracellular Ca^{2+} in the incubation medium increases the MPP^+ toxicities of MN9D and SH-SY5Y cells (Fig. 24), parallel to the increasing uptake of MPP^+. Under similar conditions, the effect of extracellular Ca^{2+} on the toxicity of MPP^+ is not observed in catecholaminergic PC12 and liver HepG2 cells, again parallel to the uptake (Fig. 24). While

benzamil, mibefradil, verapamil, and GBR12909 decrease the uptake of MPP^+ into MN9D cells, those inhibitors show no cellular protection from the exposure of MPP^+ (Fig. 25). In fact, these are toxic to MN9D cells (Fig. 30).

Flufenamic acid, 2-APB, CGP37157, BAPTA, and Thapsigargin have been reported to modulate intracellular Ca^{2+} levels. Thus, the toxicity of MPP^+ may be due to the perturbation of intracellular $Ca^{2+}$and the cellular protection could be due to the opposing effects of these agents to that of MPP^+ with respect to the intracellular Ca^{2+} level. Flufenamic acid has been shown to trigger a rise in intracellular Ca^{2+} concentration (156) by inducing the release of Ca^{2+} from the intracellular stores, mitochondria and ER (156,188). 2-APB is an IP_3-induced Ca^{2+} release inhibitor (141), but it increases cytosolic Ca^{2+} by activating other channels and SOCE at high concentrations similar to those used in our studies (189). CGP37157 is a mitochondrial Na^+/Ca^{2+} exchanger inhibitor that blocks the mitochondrial Ca^{2+} efflux which then stimulates the depletion of Ca^{2+} store from the ER into the cytosol (190). Thapsigargin is a SERCA pump inhibitor that raises cytosolic Ca^{2+} concentrations by preventing Ca^{2+} from being pumped into the ER causing this Ca^{2+} store to become depleted (191,192). BAPTA is an intracellular Ca^{2+} chelator that prevents the rises of intracellular Ca^{2+} concentration by chelating with the Ca^{2+} that leaks from the intracellular stores and hence prevents store refilling (193). Therefore, all of the above agents which protect dopaminergic cells from MPP^+ toxicity appear to deplete the intracellular Ca^{2+} stores. The activity of SOCE is responsible for maintaining the ER Ca^{2+} stores. Therefore, it is possible that the SOCE or SOCE-like mechanism is activated by the above neuroprotectants, allowing the refilling of the ER Ca^{2+} stores at the expense of extracellular Ca^{2+}, leading to the observed protection from MPP^+ toxicity (Fig.27 and 29). This hypothesis is further supported by the observation that the above compounds are ineffective as neuroprotectants in the absence of

extracellular Ca^{2+} (Fig. 27 and 29). In addition, the observed toxicity of MPP^+ uptake inhibitors benzamil, verapamil, and GBR12909 similar to MPP^+ is also consistent with this proposal. Based on these arguments we propose that MPP^+ toxicity is due to the depletion of ER and/or miotochondrial Ca^{2+} stores and simultaneous inhibition of a secondary unknown Ca^{2+} refilling pathway similar to SOCE (Scheme 6). Additional experimental evidence is certainly necessary to firmly establish these proposals.

Scheme 6: Toxicity Mechanism of MPP^+

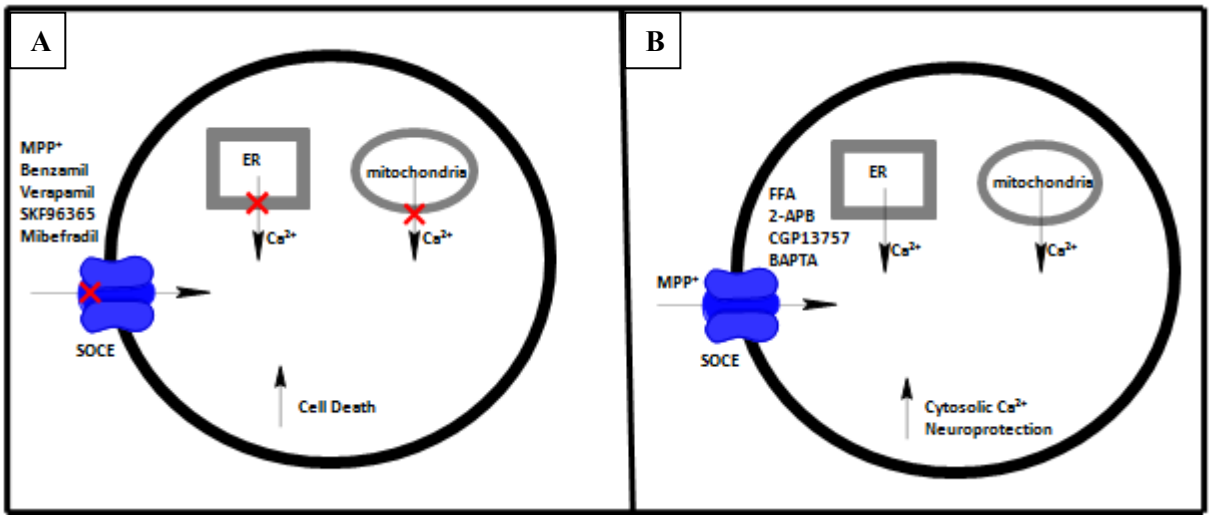

Our results show that the $Ca^{2+}{}_o$ sensitive, $Na^+{}_o$ independent MPP^+ uptake pathway into MN9D is reversible in the presence of $Ca^{2+}{}_o$. When MN9D cells are initially loaded with MPP^+ up to 500 µM in the absence of extracellular Ca^{2+}, then incubated in a Ca^{2+}-containing medium without MPP^+ for 15 h, nearly 100% of MN9D cells survived most likely due to the back transport of MPP^+ as observed in the uptake experiments (Fig. 32A). In contrast, when MN9D cells are initially loaded with MPP^+ up to 500 µM in the absence of extracellular Ca^{2+}, then incubated in a Ca^{2+}-free medium without MPP^+ for 15 h, significant cell death is observed most likely due to the inhibition of the back transport of MPP^+ (Fig. 32B). Benzamil, verapamil,

GBR12909, and SKF96365 increase the toxicity of MPP^+ in the presence of extracellular Ca^{2+} but have no significant effect in the absence of extracellular Ca^{2+} (Fig. 32) most likely due to the inhibition of the Ca^{2+} stimulated back transport of intracellular MPP^+. These findings appear to suggest that intracellular MPP^+ is responsible for the observed toxicity. In sharp contrast, MN9D toxicity experiments with uptake inhibitors under uptake conditions show that they do not protect against the toxicity of MPP^+ but exacerbate of it. Therefore, we conclude that MPP^+ may interfere with the above proposed ER Ca^{2+} refilling pathway from both external and internal phases of the membrane.

Our uptake and toxicity studies suggested that the cell death and a perturbed cellular Ca^{2+} homeostasis have an intimate relationship. Since MN9D cells are highly sensitive to MPP^+ toxicity similar to primary dopaminergic cultures, in comparison to other cell types, and this transporter is only present in dopaminergic cells, suggest the specific dopaminergic toxicity of MPP^+ may be closely associated with this $Ca^{2+}{}_o$ sensitive, $Na^+{}_o$ independent MPP^+ transporter. Therefore, the proper understanding of the functions of this transporter may not only reveal the details of the molecular mechanism of the specific dopaminergic MPP^+ toxicity, but also provide clues to the etiology of sporadic PD and potential targets for therapeutic development.

CHAPTER VI

CONCLUSION

The specific dopaminergic toxicity of MPP^+ has been widely studied to model the etiology of Parkinson's disease. The generally accepted mechanism of MPP^+ toxicity suggests that MPP^+ enters specifically into dopaminergic cells through the dopamine transporter followed by the inhibition of mitochondrial complex I of the electron transport chain that leads to excessive ROS production and decreases cellular energy production. However, experimental evidence from our laboratory strongly contradicts this proposal. We have used three catecholaminergic cell lines, MN9D and SH-SY5Y, PC12 and the non-catecholaminergic cell line HepG2 to further evaluate whether the exclusive uptake through a monoamine transporter followed by the inhibition of mitochondrial complex I is the major cause of specific dopaminergic toxicity of MPP^+. Our studies clearly show that while all the above cells take up substantial amounts of MPP^+ through various cell specific pathways under similar experimental conditions, MPP^+ is highly toxic only to dopaminergic cells, suggesting that cell specific uptake could not be the cause of specific dopaminergic toxicity. In addition, our studies show that although the DAT inhibitor, GBR12909, inhibits the MPP^+ uptake into PC12, MN9D, and SH-SY5Y cells, no significant protection from MPP^+ toxicity is observed with all these cells. In addition, non-catecholaminergic HepG2 cells, while taking up substantial amounts of MPP^+ under similar experimental conditions and rich in mitochondria and mitochondrial complex I, are not susceptible to MPP^+ toxicity. These findings strongly suggest that the MPP^+ toxicity could not primarily be due to the inhibition of mitochondrial complex I as proposed.

Uptake of MPP^+ into non-catecholaminergic HepG2 cells occurs through PMAT and/or OCT. Uptake of MPP^+ into catecholaminergic PC12 cells occurs through two pathways and about 1/3 through classical Na^+ and Cl^- dependent monoamine transporter which may be DAT or NET and about 2/3 through a Na^+ independent pathway which may be or similar to PMAT. Uptake of MPP^+ into dopaminergic MN9D and SH-SY5Y cells occurs through three pathways in which two of them are similar to those of PC12 cells. The third pathway is a novel pathway which is specifically present in dopaminergic cells, Na^+ independent, effectively inhibited by extracellular Ca^{2+} and distinct from the classical Na^+/Cl^- dependent monoamine transporters. This pathway is strongly inhibited by unrelated pharmacological agents such as benzamil, verapamil, GBR12909, and mibefradil. Based on these findings, we propose that a novel Ca^{2+} sensitive MPP^+ uptake system is specifically present in dopaminergic cells.

Parallel to the effect on uptake, the dopaminergic toxicity of MPP^+ is extracellular Ca^{2+}-dependent while the toxicities on adnergic PC12 and non-catecholaminergic HepG2 are independent of extracellular Ca^{2+}. However, while strong uptake inhibitors did not protect dopaminergic cells from MPP^+ toxicity, flufenamic acid, 2-APB, BAPTA, CGP13757, and thapsigargin showed good cellular protection with no effect on the MPP^+ uptake. All these agents are known to deplete the Ca^{2+} from the ER which would lead to the activation of SOCE. Therefore, we propose that the Na^+ independent, $Ca^{2+}{}_o$ sensitive pathway may be or be similar to SOCE and the interference of its physiological functions may lead to the depletion of ER Ca^{2+}, causing the perturbation of intracellular Ca^{2+} metabolism, and resulting in the cell death. However, experiments under reverse transport conditions show that under these conditions intracellular MPP^+ is responsible for the observed toxicity. In sharp contrast, MN9D toxicity experiments with uptake inhibitors under uptake conditions show that they do not protect against

the toxicity of MPP^+ but exacerbate it. Therefore, according to the above proposal MPP^+ may interfere with the above proposed ER Ca^{2+} refilling pathway from both external and internal phases of the membrane.

Further studies are certainly necessary to fully determine the specific uptake and toxicity of MPP^+. Future studies should directed towards the full characterization of the Ca^{2+} sensitive MPP^+ uptake pathway in dopaminergic cells and determining the physiological function of this transporter. In addition, it is necessary to test the proposal that MPP^+ toxicity is due to the depletion of Ca^{2+} in the ER by determining the effects of MPP^+ on the ER and mitochondrial Ca^{2+} levels using standard fluorescence techniques. In addition to further confirm the mechanism of the cell protection by flufenamic acid, BAPTA, CGP13757, Thapsigargin, and 2-APB from MPP^+ toxicity the effects of these agents on the ER Ca^{2+} level should be investigated. Finally, the findings with above transformed cell lines must be confirmed with dopaminergic primary cultures or physiologically more appropriate systems. The outcome of these studies will pave the way for further studies to identify the causes of dopaminergic cell death in PD and eventually lead to the development of effective novel preventive and therapeutic strategies.

REFERENCES

REFERENCES

1. Gibrat, C., Saint-Pierre, M., Bousquet, M., Levesque, D., Rouillard, C., and Cicchetti, F. (2009) Differences between subacute and chronic MPTP mice models: investigation of dopaminergic neuronal degeneration and alpha-synuclein inclusions. *J Neurochem***109**, 1469-1482

2. Kowal, S. L., Dall, T.M., Chakrabarti, R., Storm, M.V., and Jain, A. (2013) The Current and Projected Economic Burden of Parkinson's Disease in the United States. *Movement disorders***28**, 311-318

3. Berti, V., Pupi, A., and Mosconi, L. (2011) PET/CT in diagnosis of movement disorders. *Ann N Y Acad Sci***1228**, 93-108

4. George, J. L., Mok, S., Mosses, D., Wilkins, S., Bush, A. I., Cherny, R. A., and Finkelstein, D. I. (2009) Targeting the Progression of Parkinson's Disease. *Curr Neuropharmacol***7**, 9-36

5. Davie, C. A. (2008) A review of Parkinson's disease. *Br Med Bull***86**, 109-127

6. Inamdar, N. N., Arulmozhi, D. K., Tandon, A., and Bodhankar, S. L. (2007) Parkinson's Disease: Genetics and Beyond. *Curr Neuropharmacol***5**, 99-113

7. Blesa, J., Phani, S., Jackson-Lewis, V., and Przedborski, S. (2012) Classic and New Animal Models of Parkinson's Disease. *J Biomed Biotechnol***2012**, 845618

8. Brumback, R., and Claudet, R. R. (1996) *Neurology and Clinical Neuroscience*, 2nd ed., Springer New York

9. Freire, M. A., and Santos, J. R. (2010) Parkinson's disease: general features, effect of levodopa treatment and future directions. *Front Neuroanat***4**, 146

10. Parkinson, J. (2002) An essay on the shaking palsy. 1817. *J Neuropsychiatry Clin Neurosci***13**, 223-226

11. Korchounov, A. M. (2008) Role of D1 and D2 Receptors in the Regulation of Voluntary Movements. *Bull Exp Biol Med***146**, 14-17

12. Agnoli, A., Ruggieri, S., Del Roscio, S., Baldassarre, M., Bocola, V., and Denaro, A. (1983) Abnormal involuntary movements: a study of dopaminergic receptor interaction. *Adv Neurol***37**, 305-312

13. Nieoullon, A. (2002) Dopamine and the regulation of cognition and attention. *Prog Neurobiol***67**, 53-83

14. Clayton, D. F., and George, J. M. (1998) The synucleins: a family of proteins involved in synaptic function, plasticity, neurodegeneration and disease. *Trends Neurosci***21**, 249-254

15. Huang, Y., and Halliday, G. (2013) Can we clinically diagnose dementia with Lewy bodies yet? *Transl Neurodegener***2**, 1-9

16. Sagar, H. J. (1987) Clinical similarities and differences between Alzheimer's disease and Parkinson's disease. *J Neural Transm Suppl***24**, 87-99

17. Noe, E., Marder, K., Bell, K. L., Jacobs, D. M., Manly, J. J., and Stern, Y. (2004) Comparison of dementia with Lewy bodies to Alzheimer's disease and Parkinson's disease with dementia. *Mov Disord***19**, 60-67

18. Devanand, D. P., Pradhaban, G., Liu, X., Khandji, A., De Santi, S., Segal, S., Rusinek, H., Pelton, G. H., Honig, L. S., Mayeux, R., Stern, Y., Tabert, M. H., and de Leon, M. J. (2007) Hippocampal and entorhinal atrophy in mild cognitive imparement: prediction of Alzheimer disease. *Neurology***68**, 828-836

19. Izquierdo, I., and Medina, J. H. (1993) Role of the amygdala, hippocampus and entorhinal cortex in memory consolidation and expression. *Braz J Med Biol Res***26**, 573-589

20. Gais, S., and Born, J. (2003) Low acetylcholine during slow-wave sleep is critical for declarative memory consolidation. *Proc Natl Acad Sci U S A***101**, 2140-2144

21. Tolosa, E., Wenning, G., and Poewe, W. (2006) The diagnosis of Parkinson's disease. *Lancet Neurol***5**, 75-86

22. Brady, S. T., Siegel, G. J., Albers, R. W., Price, D. L., Benjamins, J., Fisher, S., Hall, A., Bazan, N., Coyle, J., and Sisodia, S. (2012) *Basic Neurochemistry: Principles of Molecular, Cellular, and Medical Neurobiology*, 8 ed., Elsevier Inc., Oxford

23. Lang, A. E. (2009) When and how should treatment be started in Parkinson disease? *Neurology***72**, 39-43

24. Chahine, L. M., and Stern, M. B. (2011) Diagnostic markers for Parkinson's disease. *Curr Opin Neurol***24**, 309-317

25. Pan-Montojo, F., Anichtchik, O., Dening, Y., Knels, L., Pursche, S., Jung, R., Jackson, S., Gille, G., Spillantini, M. G., Reichmann, H., and Funk, R. H. W. (2010) Progression of Parkinson's Disease Pathology is Reproduced by Intragastric Administration of Rotenone in Mice. *PLoS ONE***5**, e8762

26. Lobo, V., Patil, A., Phatak, A., and Chandra, N. (2010) Free radicals, antioxidants and functional foods: Impact on human health. *Pharmacogn Rev***4**, 118-126

27. Cadet, J. L., and Brannock, C. (1998) Free radicals and the pathobiology of brain dopamine systems. *Neurochem Int***32**, 117-131

28. Valko, M., Leibfritz, D., Moncol, J., Cronin, M. T., Mazur, M., and Telser, J. (2007) Free radicals and antioxidants in normal physiological functions and human disease. *Int J Biochem Cell Biol***39**, 44-84

29. Peng, X., Pigli, Y. Z., Rice, P. A., and Greenberg, M. M. (2008) Protein binding has a large effect on radical mediated DNA damage. *J Am Chem Soc***130**, 12890-12891

30. Ishikawa, K., Takenaga, K., Akimoto, M., Koshikawa, N., Yamaguchi, A., Imanish, H., Nakada, K., Honma, Y., and Hayashi, J. (2008) ROS-generating mitochondrial DNA mutations can regulate tumor cell metastasis. *Science***320**, 661-664

31. Stark, G. (2005) Functional consequences of oxidative membrane damage. *J Membr Biol***205**, 1-16

32. Abdel-Hamid, H. A., Fahmy, F. C., and Sharaf, I. A. (2001) Influence of free radicals on cardiovascular risk due to occupational exposure to mercury. *J Egypt Public Health Assoc***76**, 53-69

33. Bernhard, D., and Wang, X. L. (2007) Smoking, oxidative stress and cardiovascular diseases--do anti-oxidative therapies fail? *Curr Med Chem***14**, 1703-1712

34. Kumar, P., Devi, U., Ali, S., Upadhya, R., Pillai, S., Raja, A., Rao, S., and Rao, A. (2009) Plasma protein oxidation in patients with brain tumors. *Neurol Res***31**, 270-273

35. van Breeman, R. B., and Pajkovic, N. (2008) Multitargeted therapy of cancer by lycopene. *Cancer letters***269**, 339-351

36. Wells, P. G., McCallum, G. P., Chen, C. S., Henderson, J. T., Lee, C. J., Perstin, J., Preston, T. J., Wiley, M. J., and Wong, A. W. (2009) Oxidative stress in developmental origins of disease: teratogenesis, neurodevelopmental deficits, and cancer. *Toxicol Sci***108**, 4-18

37. Dwyer, B. E., Zacharski, L. R., Balestra, D. J., Lerner, A. M., Perry, G., Zhu, X., and Smith, M. A. (2009) Getting the iron out: Phlebotomy for Alzheimer's disease? *Med Hypotheses***72**, 504-509

38. Pratico, D. (2008) Evidence of oxidative stress in Alzheimer's disease brain and antioxidant therapy: lights and shadows. *Ann N Y Acad Sci***1147**, 70-78

39. Van Wijk, R., Van Wijk, E. P., Wiegant, F. A., and Ives, J. (2008) Free radicals and low-level photon emission in human pathogenesis: state of the art. *Indian J Exp Biol***46**, 273-309

40. Murphy, M. P. (2009) How mitochondria produce reactive oxygen species. *Biochem J***417**, 1-13

41. Lee, J., Koo, N., and Min, D. B. (2006) Reactive Oxygen Species, Aging, and Antioxidative Nutraceuticals. *COMPR REV FOOD SCI F***3**, 21-33

42. Uttara, B., Singh, A. V., Zamboni, P., and Mahajan, R. T. (2009) Oxidative Stress and Neurodegenerative Diseases: A Review of Upstream and Downstream Antioxidant Therapeutic Options. *Curr Neuropharmacol***7**, 65-74

43. Shah, A. M., and Channon, K. M. (2004) Free radicals and redox signalling in cardiovascular disease. *Heart***90**, 486-487

44. Staron, A., Makosa, G., and Koter-Michalak, M. (2010) Oxidative stress in erythrocytes from patients with rheumatoid arthritis. *Rheumatol Int***32**, 331-334

45. Wright, E., Scism-Bacon, J. L., and Glass, L. C. (2006) Oxidative stress in type 2 diabetes: the role of fasting and postprandial glycaemia. *Int J Clin Pract***60**, 308-314

46. Baynes, J. W. (1991) Role of oxidative stress in development of complications in diabetes. *Diabetes***40**, 405-412

47. Zhou, C., Huang, Y., and Przedborski, S. (2008) Oxidative Stress in Parkinson's Disease. A Mechanism of Pathogenic and Therapeutic Significance. *Ann N Y Acad Sci***1147**, 93-104

48. Medh, R. D., and Thompson, E. B. (2000) Hormonal regulation of physiological cell turnover and apoptosis. *Cell Tissue Res***301**, 101-124

49. Lodish, H., Berk, A., Zipursky, S. L., Matsudaira, P., Baltimore, D., and Darnell, J. (2000) *Molecular Cell Biology*, 4th ed., W.H. Freeman, New York

50. Elmore, S. (2007) Apoptosis: A Review of Programmed Cell Death. *Toxicol Pathol***35**, 495-516

51. Feng, Y., He, D., Yao, Z., and Klionsky, D. J. (2014) The machinery of macroautophagy. *Cell Research***24**, 24-41

52. Mattson, M. P. (2000) Apoptosis in neurodegenerative disorders. *Nat Rev Mol Cell Biol***1**, 120-129

53. Kothakota, S., Azuma, T., Reinhard, C., Klippel, A., Tang, J., Chu, K., McGarry, T. J., Kirschner, M. W., Koths, K., Kwiatkowski, D. J., and Williams, L. T. (1997) Capase-3-generated fragment of gelsolin: effector of morphological change in apoptosis. *Science***278**, 294-298

54. Yamada, M., Klda, K., Amutuhalre, W., Ichlnose, F., and Kanekl, M. (2010) Gene disruption of caspace-3 prevents MPTP-induced Parkinson's disease in mice. *Biochem Biophys Res Commun***402**, 312-318

55. Hartmann, A., Hunot, S., Michael, P. P., Muriel, M., Vyas, S., Faucheux, B. A., Mouatt-Prigent, A., Turmel, H., Srinivasan, A., Ruberg, M., Evan, G. I., Agid, Y., and Hirsch, E. C. (1999) Caspase-3: A vulerability factor and final effector in apoptotic death of dopaminergic neurons in Parkinson's disease. *Proc Natl Acad Sci U S A***97**, 2875-2880

56. Ioannou, Y. A., and Chen, F. W. (1996) Quantiation of DNA fragmentation in apoptosis. *Nucleic Acids Res***24**, 992-993

57. Sarkar, F. H., and Li, Y. (2006) Markers of apoptosis. *Methods Mol Med***120**, 147-160

58. Tieu, K. (2011) A Guide to Neurotoxic Animal Models of Parkinson's Disease. *Cold Spring Harb Perspect Med***1**, a009316

59. Bove, J., Prou, D., Perier, C., and Przedborski, S. (2005) Toxin-Induced Models of Parkinson's Disease. *NeuroRx***2**, 484-494

60. Cohen, G., and Heikkila, R. E. (1974) The Generation of Hydrogen Peroxide, Superoxide Radical, and Hydroxyl Radical by 6-Hydroxydopamine, Dialuric Acid, and Related Cytotoxic Agents. *J Biol Chem***249**, 2447-2452

61. Izumi, Y., Sawada, H., Sakka, N., Yamamoto, N., Kume, T., Katsuki, H., Shimohama, S., and Akaike, A. (2005) p-Quinone mediates 6-hydroxydopamine-induced dopaminergic neuronal death and ferrous iron accelerates the conversion of p-quinone into melanin extracellularly. *J Neurosci Res***79**, 849-860

62. Saito, Y., Nishio, K., Ogawa, Y., Kinumi, T., Yoshida, Y., Masuo, Y., and E., N. (2007) Molecular mechanisms of 6-hydroxydopamine-induced cytotoxicity in PC12 cells: involvement of hydrogen peroxide-dependent and -independent action. *Free Radic Biol Med***42**, 675-685

63. Rogers, D. C., Martel, F. L., and Dunnett, S. B. (1990) Nigral grafts in neonatal rats protect from aphagia induced by subsequent adult 6-OHDA lesions: the importance of striatal location. *Exp Brain Res***80**, 172-176

64. Weingarten, H. L. (1988) 1-Methyl-4-Phenyl-1,2,3,6-Tetrahydropyridine (MPTP): One Designer Drug and Serendipity. *J Forensic Sci***33**, 588-595

65. Langston, J. W., Ballard, P., Tetrud, J. W., and Irwin, I. (1983) Chronic Parkinsonism in humans due to a product of meperidine-analog synthesis. *Science***219**, 979-980

66. Davis, G. C., Williams, A. C., Markey, S. P., Ebert, M. H., Caine, E. D., Reichert, C. M., and Kopin, I. J. (1979) Chronic Parkinsonism secondary to intravenous injection of meperidine analogues. *Psychiatry Res***1**, 249-254

67. Schmidt, D. E., Ebert, M. H., Lynn, J. C., and Whetsell, W. J. (1997) Attenuation of 1-methyl-4-phenylpyridinium (MPP+) neurotoxicity by deprenyl in organotypic canine substantia nigra cultures. *J Neural Transm***104**, 875-885

68. Burns, R., Chiueh, C., Markey, S., Ebert, M., Jacobowitz, D., and Kopin, I. (1983) A primate model of parkinsonism: selective destruction of dopaminergic neurons in the pars compacta of the substantia nigra by N-methyl-4-phenyl-1,2,3,6-tetrahydropyridine. *Proc Natl Acad Sci U S A***80**, 4546-4550

69. Fritz, R. R., Abell, C. W., Patel, N. T., Gessner, W., and Brossi, A. (1985) Metabolism of the neurotoxin in MPTP by human liver monamine oxidase B. *FEBS Letters***186**, 224-228

70. Staal, R. G. W., Hogan, K. A., Liang, C., German, D. C., and Sonsalla, P. K. (2000) In Vitro Studies of Striatal Vesicles Containing the Vesicular Monoamine Transporter (VMAT2): Rat versus Mouse Differences in Sequestration of 1-Methyl-4-phenylpyridinium. *J Pharmacol Exp Ther***293**, 329-335

71. Lotharius, J., and O'Malley, K. L. (2000) The Parkinsonism-inducing drug 1-methyl-4-phenylpyridinium triggers intracellular dopamine oxidation. *J Biol Chem***275**, 38581-38588

72. Chen, Y., Ni, Y., Liu, J., Lu, J., Wang, F., Wu, X., Gu, M., Lu, Z., Wang, Z., and Ren, Z. (2013) Dopamine receptor 3 might be an essential molecule in 1-methyl-4-phenyl-1,2,3,6-tetrahydropyridine-induced neurotoxicity. *BMC Neuroscience***14**

73. Sherer, T. B., Trimmer, P. A., Borland, K., Parks, J. K., Bennett, J. P. J., and Tuttle, J. B. (2001) Chronic reduction in complex I function alters calcium signaling in SH-SY5Y neuroblastoma cells. *Brain Res***891**, 94-105

74. Sherer, T. B., Ranjita, B., Stout, A.K., Lund, S., Baptista, M., Panov, A.V., Cookson, M.R., and Greenamyre, J.T. (2002) An In Vitro Model of Parkinson's Disease: Linking Mitochondrial Impairment to Altered alpha-Synuclein Metabolism and Oxidative Damage. *The JOurnal of Neuroscience***22**, 7006-7015

75. Takeshige, K., and Minakami, S. (1979) NADH- and NADPH-dependent formation of superoxide anions by bovine heart submitochondrial particles and NADH-ubiquinone reductase preparation. *Biochem J***180**, 129-135

76. Li, N., Ragheb, K., Lawler, G., Sturgis, J., Rajwa, B., Melendez, J. A., and Robinson, J. P. (2003) Mitochondrial complex I inhibitor rotenone induces apoptosis through enhancing mitochondrial reactive oxygen species production. *J Biol Chem***278**, 8516-8525

77. Hasegawa, E., Kang, D., Sakamoto, K., Mitsumoto, A., Nagano, T., Minakami, S., and Takeshige, K. (1997) A dual effect of 1-methyl-4-phenylpyridinium (MPP+)-analogs on the respiratory chain of bovine heart mitochondria. *Arch Biochem Biophys***337**, 69-74

78. Calderbank, A., and Slade, P. (1976) Diquat and Paraquat. in *Herbicides- Chemistry, Degradation and Mode of Action* (Kearney, P. C., and Kaufmann, D.D. ed.), Marcel Dekker, Inc., New York. pp 501-540

79. Sagar, G. R. (1987) Uses and usefulness of paraquat. *Hum Toxicol***6**, 7-11

80. Miller, G. W. (2007) Paraquat: The Red Herring of Parkinson's Disease Research. *Toxicol Sci***100**, 1-2

81. McCormack, A. L., and Di Monte, D. A. (2003) Effects of L-dopa and other amino acids against paraquat-induced nigrostriatal degeneration. *J Neurochem***85**, 82-86

82. Ramachandiran, S., Hansen, J. M., Jones, D. P., Richardson, J. R., and Miller, G. W. (2007) Divergent mechanisms of paraquat, MPP+, and rotenone toxicity: Oxidation of thioredoxin and caspase-3 activation. *Toxicol Sci***95**, 163-171

83. Richardson, J. R., Quan, Y., Sherer, T. B., Greenamyre, J. T., and Miller, G. W. (2005) Paraquat neurotoxicity is distinct from that of MPTP and rotenone. *Toxicol Sci***88**, 193-201

84. Wagner, G. C., Carelli, R. M., and Jarvis, M. F. (1986) Ascorbic acid reduces the dopamine depletion induced by methamphetamine and the 1-methyl-4-phenyl pyridinium ion. *Neuropharamacology***25**, 559-561

85. Sundstrom, E., Goldstein, M., and Jonsson, G. (1986) Uptake inhibition protects nigro-striatal dopamine neurons from the neurotoxocity of 1-methyl-4-phenylpyridine (MPP+) in mice. *Eur J Pharmacol***131**, 289-292

86. Presgraves, S. P., Ahmed, T., Borwege, S., and Joyce, J. N. (2004) Terminally differentiated SH-SY5Y cells provide a model system for studying neuroprotective effects of dopamine agonists. *Neurotox Res***5**, 579-598

87. Kuhar, M. J., Couceyro, P. R., and Lambert, P. D. (1999) Catecholamines in Basic Neurochemistry: Molecular, Cellular and Medical Aspects. (Siegel, G. J., Agranoff, B. W., Albers, R. W., Fisher, S. K., and Uhler, M. D. eds.), 6th Ed., Lippincott-Raven Publishers, Philadelphia. pp 243-261

88. Giros, B., el Mestikawy, S., Godinot, N., Zheng, K., Han, H., Yang-Feng, T., and Carson, M. G. (1992) Cloning, pharmacological characterization, and chromosome assignment of the human dopamine transporter. *Mol Pharm***42**, 383-390

89. Fischer, J. F., and Cho, A. K. (1979) Chemical release of dopamine from striatal homogenates: evidence for an exchange diffusion model. *J Pharmacol Exp Ther***208**, 203-209

90. Giros, B., Jaber, M., Jones, S. R., Wightman, R. M., and Carson, M. G. (1996) Hyperlocomotion and indifference to cocaine and amphetamine in mice lacking dopamine transporter. *Nature***379**, 606-612

91. Inazu, M., Kubota, N., Takeda, H., Zhang, J., Kluchi, Y., Oquchi, K., and Matsumiya, T. (1999) Pharmacological characterization of dopamine transporter in cultured rat astrocytes. *Life Sci***64**, 2239-2245

92. Martel, F., Calhau, C., Soares-da-Silva, P., and Azevedo, I. (2001) Transporter of [3H]MPP+ in an immortalized rat brain microvessel endothelial cell line (RBE 4). *Naunyn Schmiedebergs Arch Pharmacol***363**, 1-10

93. Chemuturi, N. V., and Donovan, M. D. (2007) Role of organic cation transporters in dopamine uptake across olfactory and nasal respiratory tissues *Mol Pharm***4**, 936-942

94. Amphoux, A., Vialou, V., Drescher, E., Bruss, M., Mannoury La Cour, C., Rochat, C., Millan, M. J., Giros, B., Bonisch, H., and Gautron, S. (2006) Differential pharmacological in vitro properties of organic cation transporters and regional distribution in rat brain. *Neuropharamacology***50**, 941-952

95. Engel, K., and Wang, J. (2005) Interaction of Organic Cations with a Newly Identified Plasma Membrane Monoamine Transporter. *Mol Pharm***68**, 1397-1407

96. Sogawa, C., Kumagai, K., Sogawa, N., Morita, K., Dohi, T., and Kitayama, S. (2007) C-termini region regulates the functional expression of human noradrenaline transporter splice variants. *Biochem J***401**, 185-195

97. Wu, X., Kekuda, R., Huang, W., Fei, Y. J., Leibach, F. H., Chen, J., Conway, S. J., and Ganapathy, V. (1998) Identity of the Organic Cation Transporter OCT3 as the Extraneuronal Monoamine Transporter (uptake 2) and Evidence for the Expression of the Transporter in the Brain. *J Biol Chem***273**, 32776-32786

98. Engel, K., Zhou, M., and Wang, J. (2004) Identification and characterization of a novel monoamine transporter in the human brain. *J. Biol. Chem.***279**, 50042-50049

99. Koepsell, H., and Endou, H. (2004) The SLC22 drug transporter family. *Pflugers Arch***447**, 666-676

100. Jonker, J. W., Wagenaar, E., van Eijl, S., and Schinkel, A. H. (2003) Deficiency in the Organic Cation Transporters 1 and 2 (Oct1/Oct2 [Slc22a1/Slc22a2]) in Mice Abolishes Renal Secretion of Organic Cations. *Mol Cell Biol***23**, 7902-7908

101. Kekuda, R., Prasad, P. D., Wu, X., Wang, H., Fei, Y. J., Leiback, F. H., and Ganapathy, V. (1998) Cloning and Functional Characterization of a Potential-sensitive, Polyspecific Organic Cation Transporter (OCT3) Most Abundantly Expressed in Placenta. *J Biol Chem***273**, 15971-15979

102. Erickson, J. D., Eiden, L. E., and Hoffman, B. J. (1992) Expression cloning of a reserpine-sensitive vesicular monoamine transporter. *Proc Natl Acad Sci U S A***89**, 10993-10997

103. Liu, Y., Peter, D., Rogahani, A., Schuldiner, S., Prive, G. G., Eisenberg, D., Brecha, N., and Edwards, R. H. (1992) A cDNA That Suppresses MPP+ Toxicity Encodes a Vesicular Amine Transporter. *Cell***70**, 539-551

104. Reith, M. E. A. (1997) *Neurotransmitter Transporters: Structure, Function, and Regulation*, Humana Press, Totowa, NJ

105. Erickson, J. D., Schafer, M. K. H., Bonner, T. I., Eiden, L. E., and Weiher, E. (1996) Distinct Pharmacological Properties and Distribution in Neurons and Endocrine Cells of Two Isoforms of the Human Vesicular Monoamine Transporter. *Proc Natl Acad Sci U S A***93**, 5166-5171

106. Henry, J. P., Botton, D., Sagne, C., Isambert, M. F., Desnos, C., Blanchard, V., Raisman-Vozari, R., Krejci, E., Massoulie, J., and Gasnier, B. (1994) Biochemistry and Molecular Biology of the Vesicular Monoamine Transporter from Chromaffin Granules. *J Expt Biol***196**, 251-262

107. Lovinger, D. M. (2008) Communication networks in the brain: neurons, receptors, neurotransmitters, and alcohol. *Alcohol Res Health***31**, 196-214

108. Schapira, A. H. (2013) Calcium dysregulation in Parkinson's disease. *Brain***136**, 2015-2016

109. Marambaud, P., Dreses-Werringloer, U., and Vingtdeux, V. (2009) Calcium signaling in neurodegeneration. *Mol Neurodegener***4**

110. Zundorf, G., and Reiser, G. (2011) Calcium Dysregulation and Homeostasis of Neural Calcium in the Molecular Mechanisms of Neurodegenerative Dieases Provide Multiple Targets for Neuroprotection. *Antioxid Redox Signal***14**, 1275-1288

111. Chen, T. S., Koutsilieri, E., and Rausch, W. D. (1995) MPP+ selectively affects calcium homeostasis in mesencephalic cell cultures from embryonal C57/Bl6 mice. *J Neural Transm Gen Sect***100**, 153-163

112. Miller, R. J. (1991) The control of neuronal Ca2+ homeostasis. *Prog Neurobiol***37**, 255-285

113. Braunewell, K. H., and Gundelfinger, E. D. (1999) Intracellular neuronal calcium sensor proteins: a family of EF-hand calcium-binding proteins in search of a function. *Cell Tissue Res***295**, 1-12

114. Heizmann, C. W. (1999) Ca2+-binding S100 proteins in the central nervous system. *Neurochem Res***24**, 1097-1100

115. Lewit-Bentley, A., and Rety, S. (2000) EF-hand calcium-binding proteins. *Curr Opin Struct Biol***10**, 637-643

116. Burgoyne, R. D., O'Callaghan, D. W., Hasdemir, B., Haynes, L. P., and Tepikin, A. V. (2004) Neuronal Ca2+-sensor proteins: multitalented regulators of neuronal function. *Trends Neurosci***27**, 203-209

117. Schwaller, B. (2009) The continuing disappearance of "pure" Ca2+ buffers. *Cell Mol Life Sci***66**, 275-300

118. Hurley, M. J., Brandon, B., Gentleman, S. M., and Dexter, D. T. (2013) Parkinson's disease is associated with altered expression of Cav1 channels and calcium-binding proteins. *Brain***136**, 2077-2097

119. Ouh, I. O., Kim, Y. M., Gim, S. A., and Koh, P. O. (2013) Focal cerebral ischemic injury decreases calbindin expression in brain tissue and HT22 cells. *Lab Anim Res***29**, 156-161

120. Welling, A. (2009) Voltage-dependent calcium channels. *BIOTREND Reviews*

121. Nelson, D. L., and Cox, M. M. (2012) *Lehninger Principles of Biochemistry*, 6th ed., Worth Publishers, New York

122. Voet, D., Voet, J. G., and Pratt, C. W. (2002) *Fundamental of Biochemistry, upgraded edition ed.*, John Wiley & Sons, Inc., New York

123. Suryanarayanan, A., and Slaughter, M. M. (2006) Synaptic Transmission Mediated by Internal Calcium Stores in Rod Photoreceptors. *J Neurosci***26**, 1759-1766

124. Reuter, H. (1986) Voltage-dependent mechanisms for raising intracellular free calcium concentration: calcium channels. *Ciba Foundation symposium***122**, 5-22

125. Hess, P., Lansman, J. B., Nilius, B., and Tsien, R. W. (1986) Calcium Channel types in cardiac myocytes: modulation by dihydropyridines and beta-adrenergic stimulation. *J Cardiovasc Pharmacol***8 Suppl 9**, S11-21

126. Formisano, L., Saggese, M., Secondo, A., Sirabella, R., Vito, P., Valsecchi, V., Molinaro, P., Di Renzo, G., and Annunziato, L. (2008) The Two Isoforms of the Na+/Ca2+ Exchanger, NCX1 and NCX3, Constitute Novel Additional Targets for the Prosurvival Action of Akt/Protein Kinase B Pathway. *Mol Pharm***73**, 727-737

127. Canitano, A., Papa, M., Boscia, F., Castaldo, P., Sellitti, S., Taglialatela, M., and Annunziato, L. (2002) Brain distribution of the Na+/Ca2+ exchanger-encoding genes NCX1, NCX2, and NCX3 and their related proteins in the central nervous system. *Ann N Y Acad Sci***976**, 394-404

128. Pan, Z., Yang, H., and Reinach, P. S. (2011) Transient receptor potential (TRP) gene superfamily encoding cation channels. *Hum Genomics***5**, 108-116

129. Nilius, B., Owsianik, G., Voets, T., and Peters, J. A. (2007) Trasient Receptor Potential Cation Channels in Disease. *Physiol Rev***87**, 165–217

130. Clapham, D. E., Montell, C., Schultz, G., and Julius, D. (2003) International Union of Pharmacology. XLIII. Compendium of Voltage-Gated Ion Channels: Transient Receptor Potential Channels. *Pharmacol Rev***55**, 591-595

131. Selvaraj, S., Sun, Y., Watt, J. A., Wang, S., Lei, S., Bimbaumer, L., and Sigh, B. B. (2012) Neurotoxin-induced ER stress in mouse dopaminergic neurons involves downregulation of TRPC1 and inhibition of AKT/mTOR signaling. *J Clin Invest***122**, 1354-1367

132. Fan, Q., Huang, W. B., and Zhang, X. L. (2012) TRPC6: an underlying target for human glaucoma. *Int J Ophthalmol***5**, 523-526

133. Ong, H. L., Liu, X., Sharma, A., Hedge, R. S., and Ambudkar, I. S. (2007) Intracellular Ca(2+) release via the ER translocon activates store-operated calcium entry. *Pflugers Arch***453**, 797-808

134. Wehrens, X. H. T., Lehnart, S. E., and Marks, A. R. (2005) Intracellular Calcium Release and Cardiac Release. *Annu Rev Physiol***67**, 69-98

135. Giorgi, C., Agnoletto, C., Bononi, A., Bonora, M., De Marchi, E., Marchi, S., Missiroli, S., Patergnani, S., Poletti, F., Rimessi, A., Suski, J. M., Wieckowski, M. R., and Pinton, P. (2012) Mitochondrial calcium homeostasis as potential target for mitochondrial medicine. *Mitochondrion***12**, 77-85

136. Smyth, J. T., Hwang, S. Y., Tomlta, T., DeHaven, W. I., Mercer, J. C., and Putney, J. W. (2010) Activation and Regulation of Store-operated Calcium Entry. *J Cell Mol Med***14**, 2337-2349

137. Putney, J. W. (2010) Pharmacology of Store-operated Calcium Channels. *Mol Interv***10**, 209-218

138. Kodavanti, P. R. (1999) Measurement of calcium buffering by intracellular organelles in brain. *Methods Mol Biol***22**, 171-176

139. Reuter, N., Hinsen, K., and Lacapere, J. J. (2003) Transconformations of the SERCA1 Ca-ATPase: A Normal Mode Study. *Biophys J***85**, 2186-2197

140. Noble, D., and Herchuelz, A. (2007) Role of Na/Ca exchange and the plasma membrane Ca2+-ATPase in cell function. *EMBO reports***8**, 228-232

141. Maruyama, T., Kanaji, T., Nakade, S., Kanno, T., and Mikoshiba, K. (1997) 2APB, 2-aminoethoxydiphenyl borate, a membrane-penetrable modulator of Ins(1,4,5)P3-induced Ca2+ release. *J Biochem***122**, 498-505

142. Xu, S. Z., Zeng, F., Boulay, G., Grimm, C., Harteneck, C., and Beech, D. J. (2005) Block of TRPC5 channels by 2-aminoethoxydiphenyl borate: a differential, extracellular and voltage-dependent effect. *Br J Pharmacol***145**, 405-414

143. Bai, D., del Corsso, C., Srinivas, M., and Spray, D. C. (2006) Block of specific gap junction channel subtypes by 2-aminoethoxydiphenyl borate (2-APB). *J Pharmacol Exp Ther***319**, 1452-1458

144. Togashi, K., Inada, H., and Tominaga, M. (2008) Inhibition of the transient receptor potential cation channel TRPM2 by 2-aminoethoxydiphenyl borate (2-APB). *Br J Pharmacol***153**, 1324-1330

145. Varnai, P., Hunyady, L., and Balla, T. (2009) STIM and Orai: the long-awaited constituents of store-operated calcium entry. *Trends Pharmacol. Sci.***30**, 118-128

146. Tang, Q., Jin, M. W., Xiang, J. Z., Dong, M. Q., Sun, H. Y., Lau, C. P., and Li, G. R. (2007) The membrane permeable calcium chelator BAPTA-AM directly blocks human ether a-go-go-related gene potassium channels stably expressed in HEK 293 cells. *Biochem Pharmacol***74**, 1596-1607

147. Fischer, K. G., Jonas, N., Poschenrieder, F., Cohen, C., Kretzier, M., Greiber, S., and Pavenstadt, H. (2002) Characterization of a Na(+)-Ca(2+) exchanger in podocytes. *Nephrol Dial Transplant***17**, 1742-1750

148. Dai, X. Q., Ramji, A., Liu, Y., Li, Q., Karpinski, E., and Chen, X. Z. (2007) Inhibition of TRPP3 channel by amiloride and analogs. *Mol Pharmacol***72**, 1576-1585

149. Page, A. J., Brierley, S. M., Martin, C. M., Hughes, P. A., and Blackshaw, L. A. (2007) Acid sensing ion channels 2 and 3 are required for inhibition of visceral nociceptors by benzamil. *Pain***133**, 150-160

150. Cox, D. A., Conforti, L., Sperelakis, N., and Matlib, M. A. (1993) Selectivity of inhibition of Na(+)-Ca2+ exchange of heart mitochondria by benzothiazepine CGP-37157. *J Cardiovasc Pharmacol***21**, 595-599

151. Torres, G. E., Gainetdinov, R. R., and Caron, M. G. (2003) Plasma membrane monoamine transporters: structure, regulation and function. *Nat Rev Neurosci***4**, 13-25

152. Boullerne, A. I., Nedelkoska, L., and Benjamins, J. A. (2001) Role of calcium in nitric oxide-induced cytotoxicity: EGTA protects mouse oligodendrocytes. *J Neurosci Res***63**, 124-135

153. White, M. M., and Aylwin, M. (1990) Niflumic and flufenamic acids are potent reversible blockers of Ca2(+)-activated Cl- channels in Xenopus oocytes. *Mol Pharm***1990**, 5

154. Foster, R. R., Zadeh, M. A., Welsh, G. I., Satchell, S. C., Ye, Y., Mathieson, P. W., Bates, D. O., and Saleem, M. A. (2009) Flufenamic acid is a tool for investigating TRPC6-mediated calcium signalling in human conditionally immortalised podocytes and HEK293 cells. *Cell Calcium***45**, 384-390

155. Tu, P., Kunert-Keil, C., Lucke, S., Brinkmeier, H., and Bouron, A. (2009) Diacylglycerol analogues activate second messenger-operated calcium channels exhibiting TRPC-like properties in cortical neurons. *J Neurochem***108**, 126-138

156. Chi, Y., Li, K., Yan, Q., Koizumi, S., Shi, L., Takahashi, S., Zhu, Y., Matsue, H., Takeda, M., Kitamura, M., and Yao, J. (2011) Nonsteroidal anti-inflammatory drug flufenamic acid is a potent activator of AMP-activated protein kinase. *J Pharmacol Exp Ther***339**, 257-266

157. Milinar, B., and Enyeart, J. J. (1993) Block of current through T-type calcium channels by trivalent metal cations and nickel in neural rat and human cells. *J Physiol***469**, 639-652

158. Rothman, R. B., Baumann, M. H., Prisinzano, T. E., and Newman, A. H. (2008) Dopamine transport inhibitors based on GBR12909 and benztropine as potential medications to treat cocaine addiction. *Biochem Pharmacol***75**, 2-16

159. Keinanen, S., Simila, S., and Kouvalainen, K. (1978) Oral antipyretic therapy: evaluation of the N-aryl-anthranilic acid derivatives mefenamic acid, tolfenamic acid and flufenamic acid. *Eur J Clin Pharmacol***13**, 331-344

160. Mehrke, G., Zong, X. G., Flockerzi, V., and Hofmann, F. (1994) The Ca(++)-channel blocker Ro 40-5967 blocks differently T-type and L-type Ca++ channels. *J Pharmacol Exp Ther***271**, 1483-1488

161. Watanabe, H., Nishio, M., Miura, M., and Iijima, T. (1995) L-type Ca channel block by highly hydrophilic dihydropyridines in single ventricular cells of guinea-pig hearts. *J Mol Cell Cardiol***27**, 1271-1279

162. Lee, C. H., and Ruben, P. C. (2008) Interaction between voltage-gated sodium channels and the neurotoxin, tetrodotoxin. *Channels (Austin)***2**, 407-412

163. Yu, M., Zhong, L., Rishi, A. K., Khadeer, M., Inesi, G., and Hussain, A. (1998) Specific substitutions at amino acid 256 of the sarcoplasmic/endoplasmic reticulum Ca2+ transport ATPase mediate resistance to thapsigargin in thapsigargin-resistant hamster cells. *J Biol Chem***273**, 3542-3546

164. Davis, S. E., and Bauer, E. P. (2012) L-Type Voltage-Gated Calcium Channels in the Basolateral Amygdala Are Necessary for Fear Extinction. *J Neurosci***32**, 13582-13586

165. Hornof, M., Toropainen, E., and Urtti, A. (2005) Cell culture models of the ocular barriers. *Eur J Pharm Biopharm***60**, 207-225

166. Freshney, R. I. (2005) *Culture of Animal Cells: A Manual of Basic Technique*, 5th ed., John Wiley and Sons, Inc., Hoboken, New Jersey

167. Greene, L. A., and Tischler, A. S. (1976) Establishment of a noradrenergic clonal line of rat adrenal pheochromocytoma cells which respond to nerve growth factor. *Proc. Natl. Acad. Sci. U. S. A.***73**, 2424-2428

168. Chiasson, K., Daoust, B., Levesque, D., and Martinoli, M. G. (2006) Dopamine D2 agnoists, bromocriptine and quinpirole, increase MPP+-induced toxicity in PC12 cells. *Neurotox Res***10**, 31-42

169. Kadota, T., Yamaai, T., Saito, Y., Akita, Y., Kawashima, S., Moroi, K., Inagaki, N., and Kadota, K. (1996) Expression of dopamine transporter at the tips of growing neurites of PC12 cells. *J Histochem Cytochem***44**, 989-996

170. Klintworth, H., Newhouse, K., Li, T., Choi, W. S., Faigle, R., and Xia, Z. (2007) Activation of c-Jun N- Terminal Protein Kinase Is a Common Mechanism Underlying Paraquat- and Rotenone-Induced Dopaminergic Cell Apoptosis. *Toxicol Sci***97**, 149-162

171. Sai, Y., Wu, Q., Le, W., Ye, F., Li, Y., and Dong, Z. (2008) Rotenone-induced PC12 cell toxicity is caused by oxidative stress resulting from altered dopamine metabolism. *Toxicol In Vitro***22**, 1461-1468

172. Liu, H. Q., Zhu, X. Z., and Weng, E. Q. (2005) Intracellular dopamine oxidation mediates rotenone-induced apoptosis in PC12 cells. *Acta Pharmacol Sin***26**, 17-26

173. Rappoid, P. M., Cui, M., Chesser, A. S., Tibbett, J., Grima, J. C., Duan, L., Sen, N., Javitch, J. A., and Tieu, K. (2011) Paraquat neurotoxicity is mediated by the dopamine transporter and organic cation transporter-3. *Proc Natl Acad Sci U S A***108**, 20766-20771

174. Biedler, J., Roffler-Tarlov, S., Schachner, M., and Freedman, L. (1978) Mulitple neurotransmitter synthesis by human neuroblastoma cell lines and clones. *Cancer Res***38**, 3751-3757

175. Kalivendi, S. V., Cunningham, S., Kotamraju, S., Joseph, J., Hillard, C. J., and Kalyanaranman, B. (2004) Alpha-synuclein up-regulation and aggregation during MPP+-induced apoptosis in neuroblastoma cells: intermediacy of transferrin receptor iron and hydrogen peroxide. *J Biol Chem***279**, 15240-15247

176. Gomez-Santos, C., Ferrer, I., Reiriz, J., Vinals, F., Barrachina, M., and Ambrosio, S. (2002) MPP+ increases alpha-synuclein expression and ERK/MAP-kinase phosphorylation in human neuroblastoma SH-SY5Y cells. *Brain Res***935**, 32-39

177. Kakimura, J., Kitamura, Y., Takata, K., Kohno, Y., Nomura, Y., and Taniguchi, T. (2001) Release and aggregation of cytochrome c and alpha-synuclein are inhibited by the antiparkinsonian drugs, talipexole and pramipexole. *Eur J Pharm***417**, 59-67

178. Sorensen, I. F., Purup, S., and Ehrich, M. (2009) Modulation of neurotoxicant-induced increases in intracellular calcium by phytoestrogens differ for amyloid beta peptide (Abeta) and 1-methyl-4-phenyl-pyridine (MPP(+)). *J Appl Toxicol***29**, 84-89

179. Choi, H. K., Won, L. A., Kontur, P. J., Hammond, D. N., Fox, A. P., Wainer, B. H., Hoffmann, P. C., and Heller, A. (1991) Immortalization of embryonic mesencephalic dopaminergic neurons by somatic cell fusion. *Brain Res***552**, 67-76

180. Hermanson, E., Joseph, B., Castro, D., Lindqvist, E., Aanisalo, P., Wallen, A., Benoit, G., Hengerer, B., Olson, L., and Perlmann, T. (2003) Nurr1 regulates dopamine synthesis and storage in MN9D dopamine cells. *Exp Cell Res***288**, 324-334

181. Qi, H., Zhao, J., Han, Y., Lau, A. S. Y., and Rong, J. (2012) Z-Ligustilide Potentiates the Cytotoxicity of Dopamine in Rat Dopaminergic PC12 Cells. *Neurotox Res***22**, 345-354

182. Hayer-Zillgen, M., Bruss, M., and Bonisch, H. (2002) Expression and pharmacological profile of the human organic cation transporters hOCT1, hOCT2 and hOCT3. *Br J Pharmacol***136**, 829-836

183. Bradford, M. M. (1976) A rapid and sensitive method for the quantitation of microgram quantities of protein utilizing the principle of protein-dye binding. *Anal Biochem***72**, 248-254

184. Przedborski, S., Jackson-Lewis, V., Naini, A. B., Jakowec, M., Petzinger, G., Miller, R., and Akram, M. (2001) The parkinsonian toxin 1-methyl-4-phenyl-1,2,3,6-tetrahydropyridine (MPTP): A technical review of its utility and safety. *J Neurochem***76**, 1265-1274

185. Zhou, M., Xia, L., and Wang, J. (2007) Metformin Transport by a Newly Cloned Proton-Stimulated Organic Cation Transporter (Plasma Membrane Monoamine Transporter) Expressed in Human Intestine. *Drug Metab Dispos***35**, 1956-1962

186. Duan, H., and Joanne, W. (2013) Impaired Monoamine and Organic Cation Uptake in Choroid Plexus in Mice with Targeted Disruption of the Plasma Membrane Monoamine Transporter (Slc29a4) Gene. *J Biol Chem***288**, 3535-3544

187. Schulze, D. H., Muqhal, M., Lederer, W. J., and Ruknudin, A. M. (2003) Sodium/Calcium Exchanger (NCX1) Macromolecular Complex. *J Biol Chem***278**, 28849-28855

188. Gardam, K. E., Geiger, J. E., Hickey, C. M., Hung, A. Y., and Magoski, N. S. (2008) Flufenamic Acid Affects Multiple Currents and Causes Intracellular Ca2+ Release in Aplysia Bag Cell Neurons. *J Neurophysiol***100**, 38-49

189. Goto, J., Suzuki, A. Z., Ozaki, S., Matsumoto, N., Nakamura, T., Ebisui, E., Fleig, A., Penner, R., and Mikoshiba, K. (2010) Two novel 2-aminoethyl diphenylborinate (2-APB) analogues differently activate and inhibit store-operated Ca(2+) entry via STIM proteins. *Cell Calcium***47**, 1-10

190. Arnaudeau, S., Kelly, W. L., Walsh, J. V. J., and Demaurex, N. (2001) Mitochondria Recycle Ca2+ to the Endoplasmic Reticulum and Prevent the Depletion of Neighboring Endoplasmic Reticulum Regions. *J Biol Chem***276**

191. Paschen, W., Doutheil, J., Gissel, C., and Treiman, M. (1996) Depletion of Neuronal Endoplasmic Reticulum Calcium Stores by Thapsigargin: Effect on Protein Synthesis. *J Neurochem***67**, 1735-1743

192. Michelangeli, F., and East, J. M. (2011) A diversity of SERCA Ca2+ pump inhibitors. *Biochem Soc Trans***39**, 789-797

193. Parekh, A. B., and Putney, J. W. J. (2005) Store-Operated Calcium Channels. *Physiol Rev***85**, 757-810